March 2017

Humanoid Stereoscopic Vision System: A Systematic Redesign of the WPI Motor Eyes Mechanism

Ann Marie Votta
Worcester Polytechnic Institute

Jacob William Wennersten
Worcester Polytechnic Institute

Rodrigo Jose Rivas
Worcester Polytechnic Institute

Tyler C. Chaulk
Worcester Polytechnic Institute

Humanoid Stereoscopic Vision System
A Systematic Redesign of the WPI Motor Eyes Mechanism

A Major Qualifying Project Report
submitted to the Faculty
of the
WORCESTER POLYTECHNIC INSTITUTE

by
Tyler Chaulk
Rodrigo Rivas
Ann Marie Votta
Jacob Wennersten

Date: March 25, 2017

Professor Cagdas Onal, Advisor
Professor Holly Ault, Advisor

Abstract

In 2014, a group of Worcester Polytechnic Institute students completed a major qualifying project (MQP) on the design of a mechanical stereoscopic vision system, named WPI Motor Eyes Mechanism. In this project, they investigated the potential for creating a robotic system capable of mimicking the motion of human eyes through mechanical means. The Motor Eyes group created a functional prototype that was able to achieve the three different aspects of human eye movement: pan, tilt, and convergence.

The Motor Eyes mechanism used prismatic joints and a linear transmission to achieve coupled pan and convergence motion in the eyes. It used revolute joints to achieve the third desired motion, coupled tilt. The primary purpose of the design was to create a system that would be physically incapable of achieving inhuman eye movements. This means that the eyes would always be focused on a single point in space that was within a human's range of vision, and that the eyes would move in a coordinated manner, as human eyes do. By coupling the pan, convergence, and tilt, and allowing for only 3 degrees of freedom for the eyes together, the mechanism was successful in this goal. However, the movement was not optimal and had shortcomings, such as backlash caused by imprecise construction and reduced accuracy and repeatability due to a lack of closed loop feedback.

In this subsequent MQP, the original Motor Eyes system was evaluated and the sources of error were identified through static analysis and dynamic testing. These problem areas were redesigned to create an improved Humanoid Stereoscopic Vision System that better adheres to the original design constraints. Dynamic testing on both systems was performed to compare the original system to the new one and validate the changes made. Once the mechanism was completed, work focused on implementing image processing technology. Cameras were installed to add facial detection functionality and further increase the capabilities of the system. The final result is a robotic platform that is able to visually locate and track a moving human face.

The completed system can track a face at depths between 0.7 m and 2.5 m, horizontally 0.63 m to the left or right, and 45 deg up or down. It can change focus point positions with an angular velocity as high as 259 deg/s, and can follow a face in smooth pursuit with a speed of 31.2 deg/s. The system has a tilt resolution of 0.1 deg and a pan and convergence resolution of 0.35 cm. When driven to focus on a specific point the system is on average accurate to within 1.40 deg for tilt, 1.05 deg for convergence and pan for the left eye, and 2.01 deg for convergence and pan for the right eye.

Acknowledgements

First, we would like to thank our Advisors, Professor Cagdas Onal and Professor Holly Ault for providing guidance for this project and also for allowing us to improve on the previous project in order to create this MQP.

We would like to thank Professor Cagdas Onal for giving us technical guidance on this project and helping with troubleshooting of our mechanism. Thank you to Professor Holly Ault for providing invaluable feedback for the system analysis before it was built and also for encouraging thoroughness when documenting the flaws of the previous project in order to create a much more complete system.

We would like to thank Shou-Shan Chiang for providing invaluable advice and assistance that directly translated to a successful image recognition platform. We would like to thank Ming Luo for helping us setup the Motion Capture System in the Soft Robotics Lab which was used to complete the final testing of the HSV System.

We would like to thank Erica Stults from the Rapid Prototyping Lab for giving us advice for prints completed on the MarkForged 3D printer and for printing our parts in a timely manner. We would like to thank the lab monitors in the the CollabLab for allowing us to make last minute prints quickly for our mechanism. Finally, we would like to thank Barbara Furhman for helping us with part purchasing.

Table of Contents

List of Figures

1 Introduction

One of the biggest challenges of social robotics is achieving meaningful communication between humans and robots. A major shortcoming in the communication between humans and social robots currently is in the gaze of the robot itself. Many social robots are designed with an emphasis on other social behaviors, such as body language and voice recognition. As a result, humans often feel uneasy when interacting with robots because of the lack of a human-like gaze.

Many mechanical systems exist to emulate human eye movement or a shift in gaze. However, few do so with the speed, accuracy, and precision of human eyes. Those that do often use blind animatronics, and are unable to process what they are looking at; their gaze is simply a preprogrammed sequence of motions to give the appearance of human-like behavior. Another problem with existing systems is that they typically move each eye independently. This means that the eyes are decoupled from each other, which can allow for unnatural eye movements. This is undesirable in social robotics applications, as the goal of social robots is to interact with people in a way that makes them feel comfortable. When a robot's eyes move in a way that would be physically impossible for human eyes, it is likely to make the person interacting with the robot uncomfortable. Some systems use software to overcome this issue, but if there is an bug in the programming, the unnatural movements can still occur.

In 2014, a Major Qualifying Project (MQP) team at Worcester Polytechnic Institute (WPI) was formed to develop a mechanical solution to this problem. The team designed a mechanism to emulate human eye movement with coupled pan, convergence, and tilt movements. By coupling the eyes for each type of motion, the team ensured that the eyes would not be physically able to move in an unnatural or unexpected way. The design was further developed to ensure that it could achieve the velocities and accelerations of the human eye, as well as focus on any given point within a specified range of vision. The team built and tested a prototype of their design as the culmination of their project.

While the team's kinematic design had the potential to achieve all desired goals specifications, their physical system had many problems. The current MQP team was tasked with improving the mechanical design and implementation of the previously designed mechanism. It was also tasked with implementing closed loop control and the ability to track a moving face. The main objectives of this project include the following:

- Design a mechanism capable of accurately and repeatedly focusing on specific points within a realistic 3-D field of vision
- Design a mechanism capable of achieving eye speeds close to those of a human eye
- Develop a control system capable of smoothly tracking a moving face within a realistic 3-D field of vision

Overall, this project, called the Humanoid Stereoscopic Vision System (HSV System), took a "blind" system and enabled it to "see" human faces. In doing so it created a more robust system that can be used in the future for a variety of social robotics applications.

2 Background Research

Social robotics and robot vision are fields that are rapidly growing. The average person associates robotics with massive industrial robots, dangerous machinery that should be kept separate from humans. The idea of interacting or even communicating with a robot is still very unfamiliar. In order to develop the HSV System, it is necessary to review the basics of how people and robots interact, how robots can see the world, and what kinds of mechanical systems already exist to achieve the human-like eye motion.

2.1 Human Robot Interaction

One of the biggest challenges faced in social robotics is that of achieving meaningful human robot interaction (HRI). In addition to being able to sense a person and at the very least not collide with them, a social robot should be able to communicate with people in a way that does not make anyone uncomfortable. An important aspect of HRI in social robotics applications involves the ability of a robot to mimic human social behavior as closely as possible. In a one-on-one conversation, human facial expressions and movements, while subtle, are extremely important in conveying things like intent. For example, if someone is talking directly to another person or listening to them, they will most likely maintain direct eye contact with that person. On the other hand, if the person is thinking of a response to a question, they are more likely to look to the top-right or top-left of their field of vision (Ford, Bugmann, and Culverhouse, 2010).

It was found that even in non-conversational applications, such as when a robot is helping a person perform tasks around their home, the gaze of the robot is important (Dautenhahn, 2007). While performing tasks, or even while simply surveying the environment, a robot can either keep its camera stationary and only move it when absolutely necessary, or move its camera in the direction of whatever object it is looking at to indicate its gaze. In general, it was found that people preferred the latter, “socially interactive” robot over the “socially ignorant” one that appeared to stare blankly at its surroundings. In addition, in this study it was found that people find human-like communication to be more important than general human-like appearance in a robot (Dautenhahn, 2007). Because people communicate with their eyes in addition to spoken word, eye movement, eye contact, and gaze can be considered just as important to meaningful social human-robot interaction as the conversation itself.

2.2 Robot Vision

Robotic vision is a technology that involves the combination of cameras and computer algorithms to allow robots to receive and process visual data from their surroundings. More importantly, robotic vision differs from machine vision or computer vision because this input then allows the robot to interact with its surroundings, not simply extract information from them. Robotic vision is a rapidly developing field, and it can be used for a variety of applications including industrial automation, object detection, autonomous vehicle applications, and robotic navigation systems.

A robotic vision system requires two key hardware and software components in order to function properly. The first of these, discussed in Section 2.3, is a mechanism or device capable of receiving visual data and interacting with the environment. The second required component is the image processing software, discussed in Section 2.4.

2.3 Examples of Different Robot Vision Mechanisms

The kinematics of the HSV System are based primarily on the Motor Eyes Mechanism that was developed by a previous MQP group. The previous team designed their mechanism with the intent of adding cameras and making it a proper robotic vision system but never actually implemented the cameras, using lasers pointers to perform characterization experiments instead. Before making any designs to improve the Motor Eyes Mechanism, the HSVS team first had to determine whether to keep the same basic design as the Motor Eyes System, or to redesign the mechanism entirely. To make an informed decision, research was conducted on systems that have already been developed to achieve realistic eye motion. These systems were evaluated for feasibility and functionality, and compared with the Motor Eyes Mechanism before a final decision was made.

2.3.1 Gimbal Mechanism

The Affordable Compact Humanoid Robot (ACHR) project was completed in 2011 by Worcester Polytechnic Institute student Elizabeth Alexander (Alexander, 2011). The purpose of this robot was to interact with children with autism and to assist with their diagnosis and treatment. Although Alexander's robot was designed to resemble a penguin, the internal Head Gimbal Mechanism (shown in Figure 1 below) utilized a pair of gimbaled webcam eyes for a more

approachable and relatable appearance. The eyes were controlled by a single tilt servo and two independent pan servos. For visual feedback, the ACHR used the core camera board of disassembled commercial webcams. Complete object tracking was not implemented, but successful facial recognition was demonstrated using Microsoft's Face API.

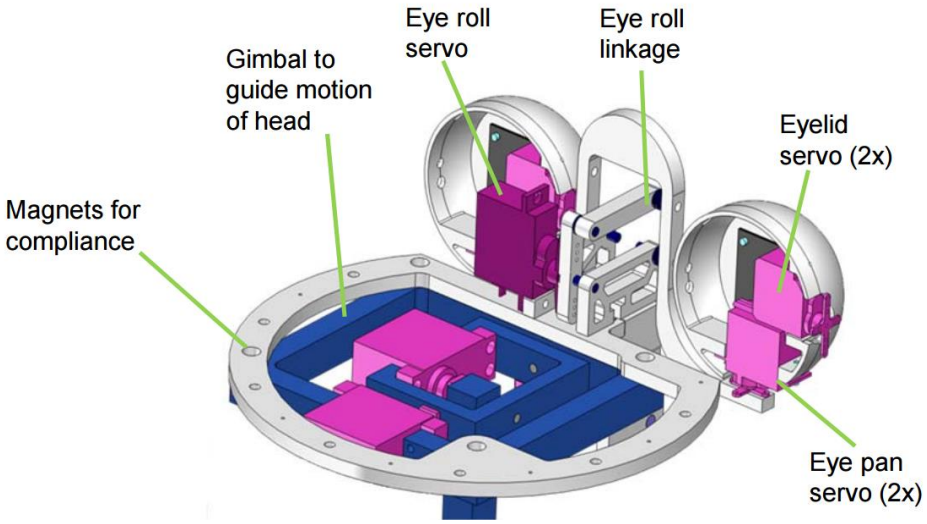

Figure 1: Solidworks model of the Head Gimbal Mechanism (Alexander, 2011).

Alexander also highlighted the importance of eye contact in HRI. Many early humanoid robots had no control over their eyes, resulting in a cold, inhuman stare. The focus of this project on HRI through eye contact, and its successful implementation, drew the HSVS team to examine it as a possible design. However, the mechanism was not ultimately used because it lacked some desired eye motions, such as coupled convergence.

2.3.2 Robotic Eye Mechanism

Chien-Pin Chen is a masters student at the University of California, Santa Cruz. He developed the mechanism shown in Figure 2 below with the purpose of simulating human eye movements (Chen, 2011). Although Chen did not mention any social purpose for the device, he expressed his desire to build a human friendly robot.

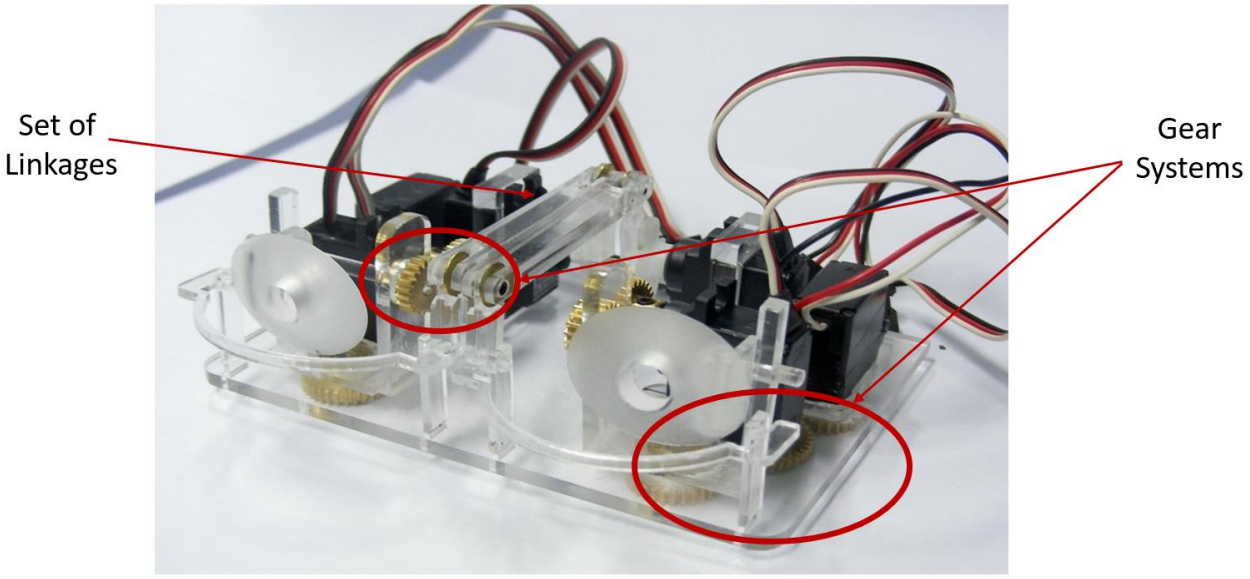

Figure 2: Chen's Robotic Eye Mechanism (Chen, 2011).

Chen freely provided CAD Files and a video of the image processing at work, useful for analyzing some of the capabilities and features of this mechanism. One of the advantages of Chen's mechanism is the use of linkages, as links can be easily and affordably manufactured using 3D printers or laser cutters. Also, having each type of motion controlled by a unique motor is beneficial, since it allows for simplified control. Since Chen did not provide any detailed specifications or results of his mechanism, the video only provides a conceptual alternative approach to eye actuation.

Chen's mechanism uses multiple motors to provide pan and tilt motion to the eyes. However, the design for the HSVS project should use a minimal number of motors in order to avoid unnatural eye motions. In addition, Chen's mechanism does not include a way to converge the eyes, which is one of the major characteristics desired in our project. Although a convergence motion can be added to Chen's mechanism, it would require to be redesigned to add an additional motor to provide such motion. Subsequently, this design was not used because it required more components to obtain the desired motions.

2.4 Image Processing Software

A key component of a robot vision system is the image processing software. One of the primary objectives of the HSVS project was the tracking of a moving face by using image

processing to control a pair of eyes. For this reason, it was necessary to obtain information about some of the various object detection and facial recognition software libraries and engines available. These include OpenCV, SwisTrack, Skilligent, SRI Stereo Engine, PTAM, TLD (Tracking-Learning-Detection), ARToolKit, CCTV Object Tracking, and RobotVision (IntoRobotics, 2013). In order to further the group's understanding of the scope of the project with regards to image processing, WPI graduate student Shou-Shan Chiang was interviewed. He provided a lot of insight that directly impacted many of the design specifications that are described in Section 3.5 (Camera/Image Tracking Design Specifications). Given that his work focuses on image processing, Chiang's insight was valuable through the project's duration.

The most commonly used method for locating a face of unknown size and position within an image is the weak classifier cascade, developed by Viola and Jones (2004). This algorithm scans a square window through the image at various scales and attempts to match the selection to the features described by a Haar Cascade classifier, which must first be trained on a set of faces. This algorithm is fast enough to allow for real-time face detection from video feeds. One common implementation of this algorithm is found within the OpenCV (Open source Computer Vision) programming library. The library is well documented and also contains pre-trained Haar cascades, making it the ideal choice for this project.

2.5 The Motor Eyes MQP

The design and testing of the Motor Eyes system is summarized below. The full Motor Eyes MQP report can be found in the bibliography (Kiely, Oo, Rappoli, Strobel, and Walcott, 2014).

2.5.1 Overview of Motor Eyes Mechanism

The original Motor Eyes team considered a number of different design concepts before finally choosing the Prismatic-Prismatic design shown in Figure 3 below.

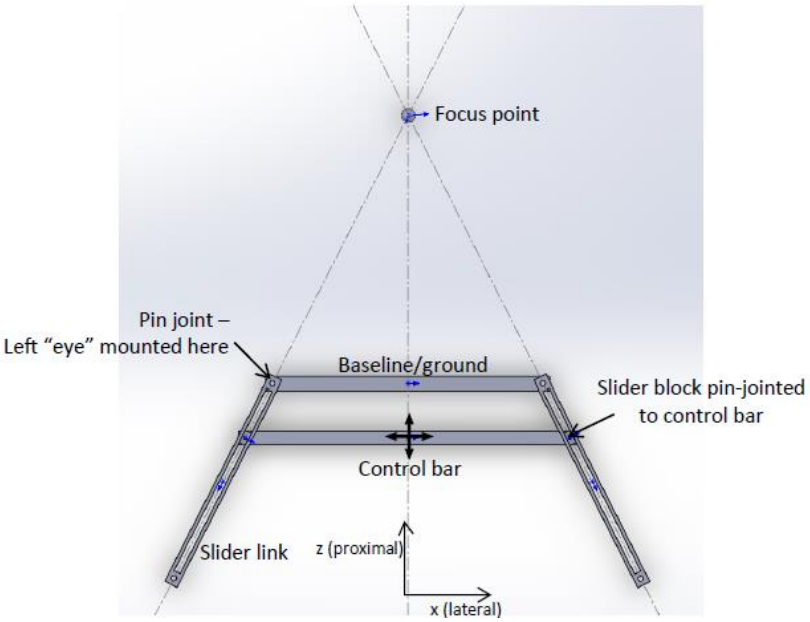

Figure 3: Simplified design of the eye mechanism (Kiely et al., 2014).

This mechanism has three independent types of motion: pan, tilt, and convergence. These motions were chosen to emulate the motion of a pair of human eyes. In the basic kinematic design (Figure 4), pan is achieved by moving the Control Bar in the x-direction, while convergence is achieved by moving the Control Bar in the y-direction. The Baseline/Ground link does not move, so when the Control Bar moves, so do the Slider Links, resulting in rotation of the pin joints connecting the Slider Links to Ground. The eyes are mounted on the slider links coinciding with the pin joints, and thus rotate as well. Figure 4 below illustrates how the pan and convergence of the eyes can be changed.

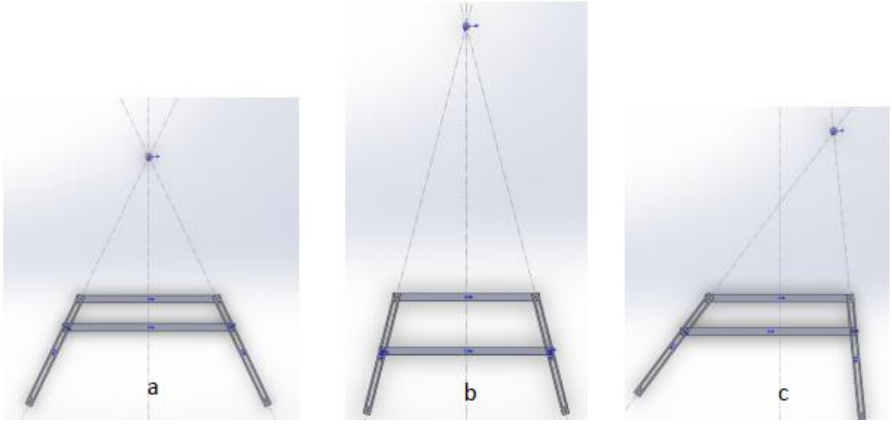

Figure 4: Examples of how the mechanism changes pan and convergence (Kiely et al., 2014).

Figure 4 (left) shows the mechanism at a small convergence depth, with zero pan; the control bar is relatively close to the baseline. Figure 4 (center) shows the mechanism at a larger convergence depth, still with zero pan; the control bar is moved farther away from the baseline. Figure 4 (right) shows the mechanism with a small convergence depth and panned to the right; the control bar is close to the baseline and is offset in the negative x-direction.

The Motor Eyes design went through a few iterations before reaching the final state, shown in Figure 5 below.

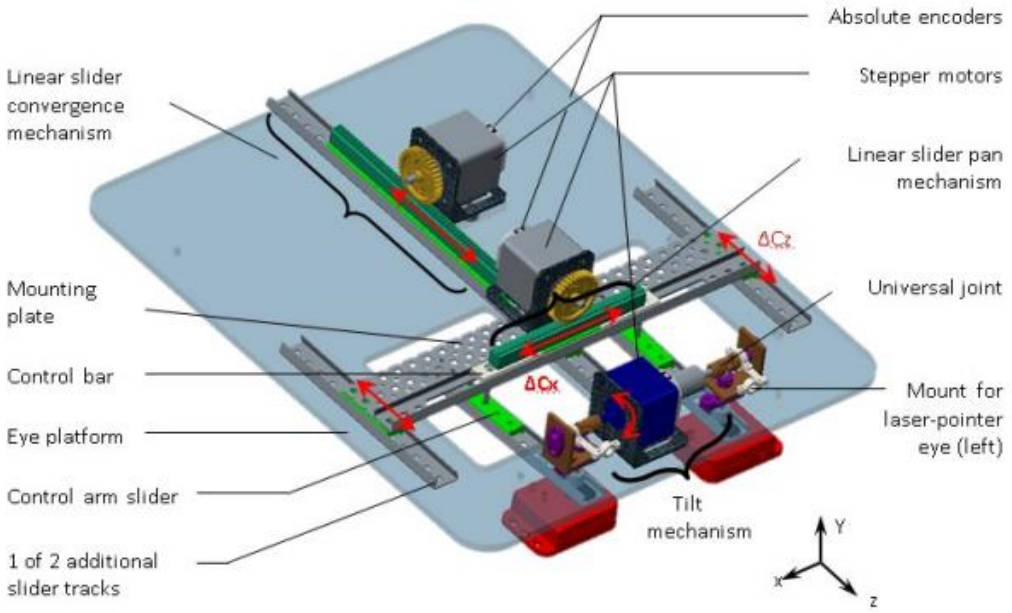

Figure 5: 3D model of the previous team's final design (Kiely et al., 2014).

In their final design, pan motion is controlled via the Linear Slider Pan Mechanism. This sub-mechanism is comprised of a stepper motor linked to a rack and pinion, which drives the Control Bar along the x-axis. This in turn rotates the Control Arm Sliders and the mounted eyes around the y-axis.

Convergence is controlled by a similar sub-mechanism, the Linear Slider Convergence Mechanism. A second stepper motor, driving another rack and pinion, is used to move the whole Linear Slider Pan Mechanism along the z-axis. As the Control Bar moves closer to or further from the eyes, the Control Arm Sliders rotate away from or towards each other, causing the eyes to converge or diverge.

The tilt of the eyes is controlled directly by the Tilt Mechanism. A third stepper motor rotates the eyes about the x-axis via a universal joint, so as to not interfere with the pan and convergence motions.

2.5.2 Overview of System Architecture

The Motor Eyes mechanism is controlled by an Arduino Uno microcontroller using an open loop control system. Each of the three stepper motors is driven a predetermined number of steps in order to achieve a desired pan, convergence, or tilt position. VEX encoders are mounted on the eye joints to measure eye rotation directly, but this data is only used for calculating maximum rotational velocity and acceleration (Kiely, Oo, Rappoli, Strobel, and Walcott, 2014). Characterizing the focus point position is achieved by using a laser diode in each eye, in place of a camera.

2.5.3 Motor Eyes Mechanism Evaluation

Although some possible mechanism alternatives were discussed before, it was decided that the HSV System would be based on the original Motor Eyes mechanism. One of the major reasons for this decision was the fact that the other mechanisms do not allow for coupled pan and convergence motion, which is the primary goal of the mechanism. In addition, some of the devices discussed before use multiple motors for each type of motion, but for this project it is intended to use only one for each motion. It was necessary to evaluate and test the Motor Eyes mechanism in detail and identify specific sources of error for redesign. In their report, the previous MQP team proved thorough kinematic analysis that their design could, in theory, meet all of the desired design specifications for size, pan and convergence values, resolution, and speed. They additionally proved that their physical mechanism, once built, could come close to meeting most of these specifications.

It was determined from the Motor Eyes MQP Report that specifications could be met after design improvements. Additional testing of the mechanism was performed to determine exactly what improvements were necessary. Given the mechanical advantages of the previous design, such as independent control of the three degrees of freedom and linear control of pan and convergence, it was ultimately decided that complete redesign would be unnecessary. By improving on an

already valid concept, more time and resources were made available for higher-level control and image processing work.

2.5.3.1 Motor Eyes Problems

Although the previous team's basic design concept was retained, there were a number of problems with the mechanism that were initially identified and corrected. Before completing the testing or in-depth analysis of the mechanism, a number of problems were identified based on the conclusions of the previous team and basic observations of the mechanism and its functionality.

When the previous MQP team tested their mechanism, they found that it had large amounts of position error in the focus point. They concluded that this error was due mainly to the fact that the mechanism is extremely sensitive to mechanical misalignment. One of the biggest issues noticed was in the L-Bracket used to secure each eye to its respective axle, as shown in Figure 6.

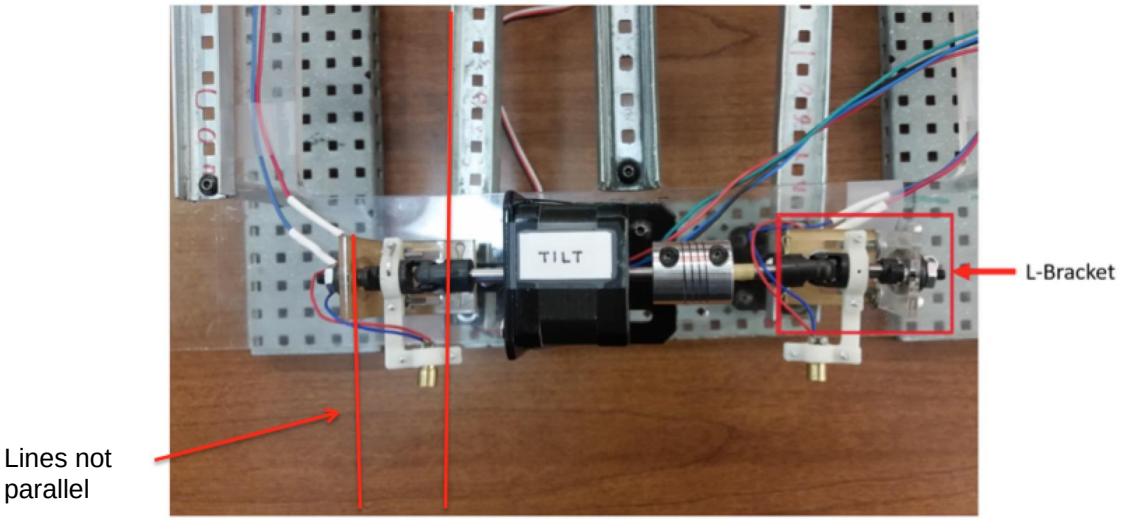

Figure 6: Misalignment of L-bracket component of laser mount.

These brackets are meant to keep the eyes aligned with the control arm sliders, but they are assembled from multiple laser cut components that are not securely joined. Another major issue was the use of a long screw to couple the control arm sliders with the pan slider, as shown in Figure 7.

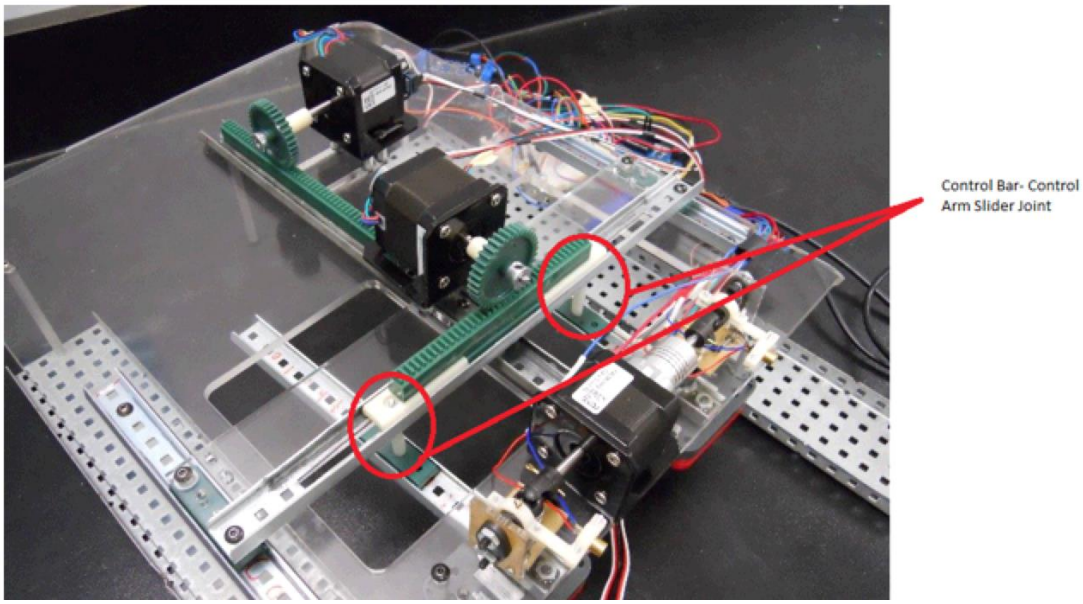

Figure 7: Control bar & control arm slider joints.

If these screws are tightened, the sliders are forced towards each other and the movement of the pan slider is hindered due to friction, since the screws are threaded through the slider blocks themselves. However, when the screws remain loose, they are able to move, allowing the control arm sliders to rotate several degrees even when the motors are fixed, creating a substantial error in the eye directions.

Another major source of error in the system stemmed from the lack of closed loop control. The system used by the previous MQP team was purely open loop, and as a result if the stepper motors skipped a step or if the eyes were not positioned as expected, the system could not self-correct. Once these initial observations were made, the mechanism was tested for focus point position, as described in the following section.

2.5.3.2 Motor Eyes Testing

Preliminary point-to-point testing on the existing mechanism was performed in order to determine additional sources of error or problems that would need to be addressed with the redesign of the mechanism.

For this testing, the eyes were placed 53 cm away from a whiteboard on a table. The origin was drawn on the board so that the x-axis was a horizontal line at the same height as the eyes' centers, and the y-axis was a vertical line halfway between the eyes as seen in Figure 8. The eyes were set to a zero pan and zero tilt position manually, and driven to the minimum convergence

depth using the convergence motor. The two points where the lasers met the whiteboard were marked using different colors for the left and right eyes.

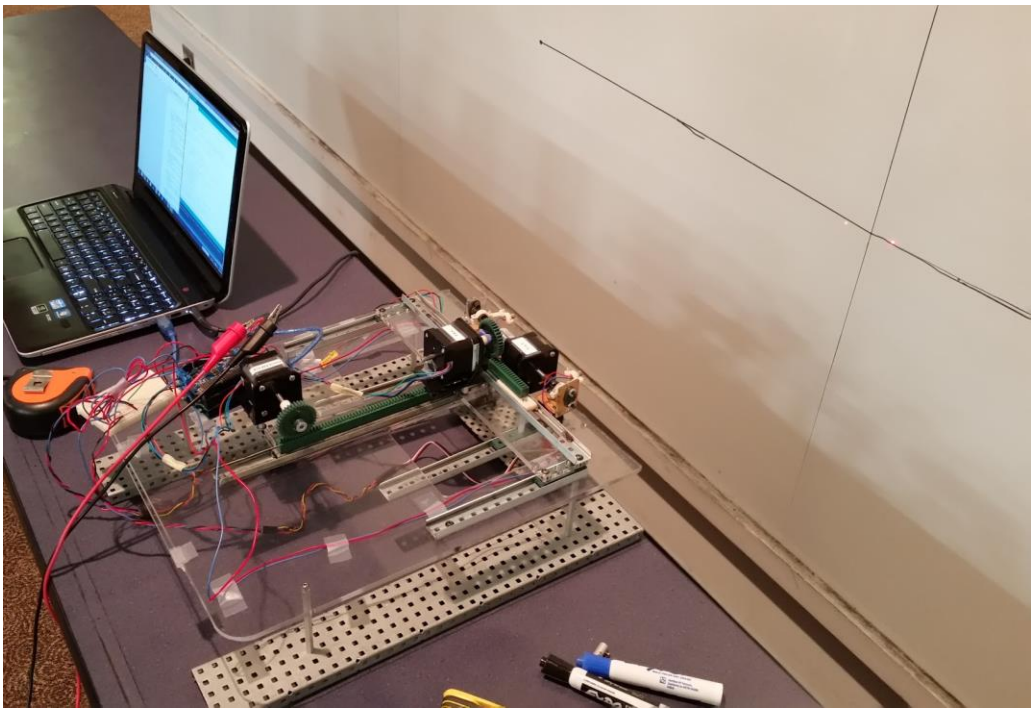

Figure 8: Motor Eyes Test Setup

The mechanism was then driven to 9 different points corresponding to various combinations of pan and tilt including minimum, maximum, and zero pan combined with minimum, maximum, and zero tilt. The laser points on the board were marked for each position, and the eyes were zeroed between each point using the points originally drawn on the board. After all 9 positions were tested for the specified convergence, the points were measured. The 9 points were then repeated and measured once more for the same convergence. Next, the 9 pan and tilt points were tested twice for the middle convergence and twice for the maximum convergence. The "zero" position marked on the board was updated for each new convergence. The actual pan, tilt and convergence of the eyes were calculated using the data gathered and equations determined by the previous MQP team, which are included in Appendix B: Motor Eyes Testing Results.

Figure 9 below shows the points where the lasers landed on the whiteboard compared to where they should have landed for a perfectly functioning mechanism. The "LEFT (or RIGHT) EYE (Ideal)" is where the left (right) "eye" laser point should have landed on the board, and the "LEFT (or RIGHT) EYE (Actual)" is where it was measured on the board relative to the origin.

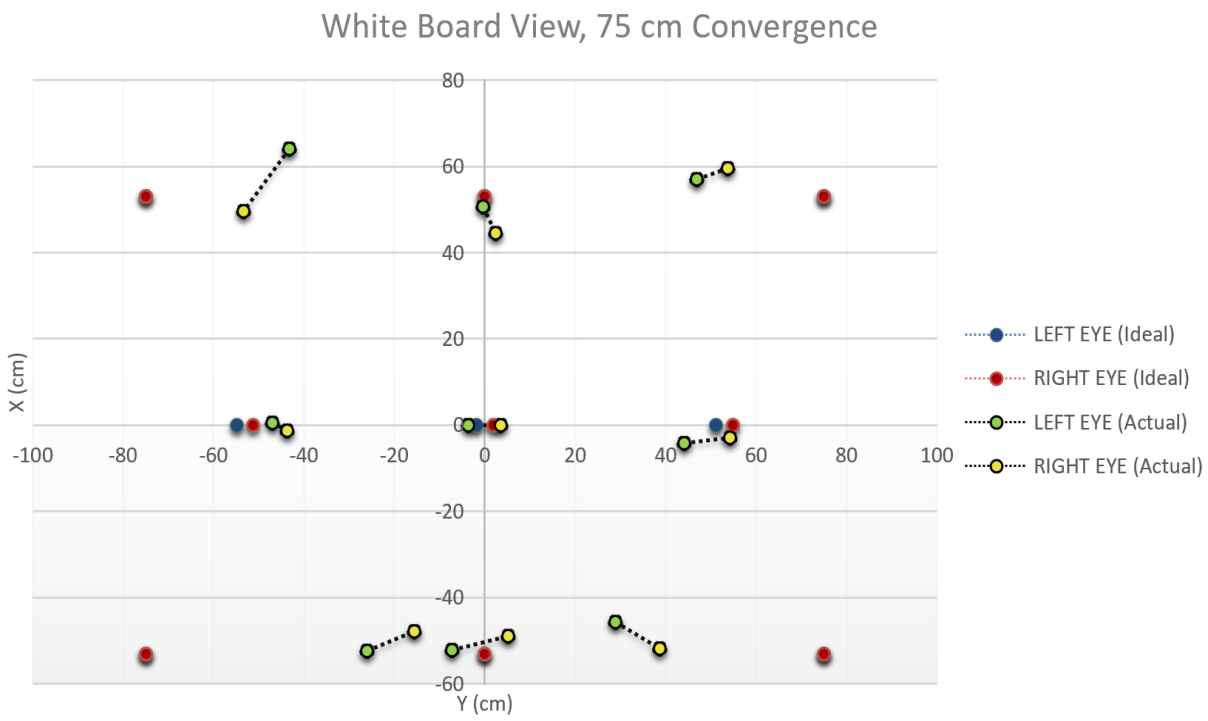

Figure 9: Plot of target (ideal) values vs tested (actual) values.

One problem discovered during testing was that the stepper motors used by the previous team require 24-48V at 3A, while the Arduino motor shields are only rated for 12V and 1.2A per motor. As a result, not enough power could be supplied to the motors, so there was not enough torque to move the sliders in some instances. This caused the motors to skip steps and the eyes to fail in reaching their desired positions.

Another issue encountered was that the 3D printed adapter used to connect the pan motor shaft to the pinion axle, shown in Figure 10, was damaged. The 3D printed part appeared to have been over-torqued at some point, and as a result the half that is supposed to be coupled with the pinion axle was loose, allowing the pinion to fall off occasionally. In addition, because the adapter was loose, it was possible to turn the motor shaft without the pinion actually rotating, which caused significant error in the system.

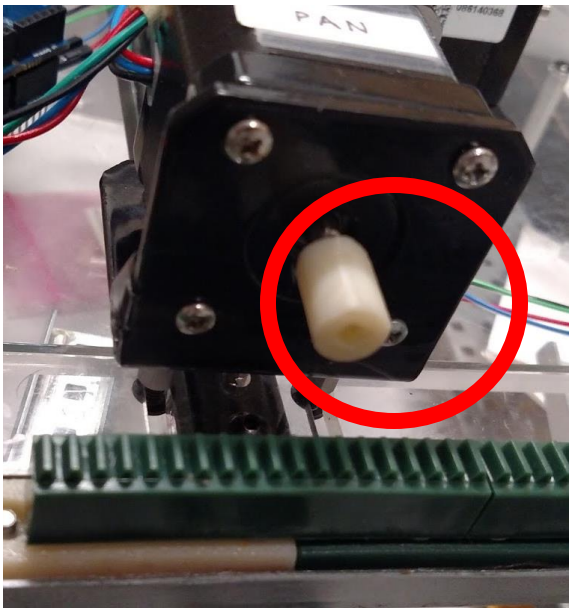

Figure 10: Pan Shaft Coupler

A major problem experienced during testing was the misalignment of the laser mounts, which was discussed briefly above. While testing, the mounts often became misaligned in relation to tilt and convergence. This resulted in extremely large amounts of error, and it was determined that the eyes would need to be properly mounted to the mechanism in order to achieve accurate focus point positioning.

Finally, it was discovered that the lasers experienced large amounts of vibration as they were moved to different focus points, which was caused primarily by the motion of the stepper motors. While this would not likely cause errors in the final focus point position, it would cause problems with the image processing, as the cameras would be unable to take clear images while the mechanism is in motion.

Testing the Motor Eyes mechanism provided the team valuable insight of what modifications needed to be made to the overall system in order to reduce error and increase accuracy. Using these testing results, design specifications were developed based on the design specifications of the previous mechanism and incorporating improvements that would be made.

3 Design Goals and Specifications

The goal of this MQP was to create a robotic vision system that is able to track and follow a face using a pair of mechanically linked cameras that are moved in a manner similar to human eyes. This system was created based on a previous MQP team's design, which has been analyzed, tested, and refined in order to achieve more accurate positioning. The new mechanism retains the functionality of the previous version, and also implements new features such as image processing and object tracking by utilizing cameras and associated software.

3.1 Social Robotics Aspect

1. The system must be capable of panning, tilting, and converging each eye about its respective center.
    - The system should be able to perform pan, tilt, and convergence movement for both eyes at the same time to avoid non-human movements. This is one of the most important design specifications of this project due to the fundamental movement needed in order to replicate a pair of human eyes from a kinematic standpoint.
2. The system must be able to focus two eyes on a single point within the defined range of vision as described in Section 3.3.
    - Convergence is needed in order to make the eye motion more human like, and also allows for the eye angles to be used to triangulate the focus point location. This information is used to simulate binocular vision or "vision created by two separate eyes working together to form a single image" (Rebuild Your Vision LLC, n.d.).
3. Each eye should have a peak angular velocity of 250 degrees/sec.
    - This speed is based on reflex saccadic movement of an average human eye, which "is triggered exogenously by the appearance of a peripheral stimulus, or by the disappearance of a fixation stimulus" (Rommelse, Van Der Stigchel, and Sergeant, 2008).

3.2 Kinematic & General Function

1. The pan, tilt, and convergence mechanisms must be capable of moving eyes with a maximum mass of 100 g or less each.

    - This weight limit is needed in order to minimize the inertia at the eye joints. This parameter is constrained in order to ensure the eye cameras do not overburden the system and decrease the possible acceleration and velocity of the system.
2. The overall system must be capable of tracking points with a pan resolution no greater than 2 cm, a convergence (depth) resolution no greater than 5 cm, and a tilt resolution no greater than 1 degree.
    - This is to allow for accurate positioning and smooth movements.
3. The control system must determine the directions the eyes are pointing relative to a predetermined initial position within 1 degree of accuracy on average.
    - When focusing on a given point, the system has an *average* error (meaning the system may occasionally have a larger error) of 1 deg for tilt and 1 deg for pan/ convergence. This is needed in order to obtain an accurate location of an object based on depth perception. Accuracy is key when designing this system due to the convergence sensitivity.
4. The system should be able to determine the velocity and acceleration of the eyes.
    - This is for testing purposes to ensure the system achieves the acceleration and velocity of human eyes.

3.3 Field of Vision

1. The tilt mechanism should be able to tilt the eyes 45 degrees above and below the horizontal plane.
    - The human eye can tilt 50 degrees above the horizontal and 70 degrees below (Buildmedia, n.d.). A range of -45 to 45 degrees was chosen based on how high or low the eyes would likely need to look to see a human face, depending on where the eyes were placed.
2. The convergence mechanism should be able to converge the eyes at depths of between 0.5 and 2.5 meters.
    - This is the range of distances between people for typical social interactions. When it comes to human interaction, 0.5 - 1.5 meters is known as the personal zone and 1.5 - 3 meters is known as the social zone (Social Distance, n.d.). These ranges

ensure that the robot is able to observe a person within a comfortable range of interaction.

3. The pan mechanism should be able to pan the eyes at least 45 degrees left or right of straight ahead while at the minimum convergence depth.
    - While the human range of view is 62 degrees left or right (Buildmedia, n.d.), most universal joints are limited to 45 degrees, which is still acceptable.

3.4 Manufacturing/Durability

1. Any additional material costs should not exceed $1000.
    - This is a limit to ensure the project does not become too expensive.
2. Any modifications made to the system should not result in an increase of the current 43.18 x 35.56 x 12.09 cm footprint of the system.
    - In order to make this a viable design for a social robotics system the system must not become bigger than it currently is.
    - It is important to keep the size as small as possible in order to work towards the end goal of making the system able to fit inside a robot head.

3.5 Camera/Image Tracking

1. The system should have a maximum smooth pursuit speed range of 30-100 degrees/sec
    - This is the average speed range of a human eye during smooth pursuit.
2. The system should track a face at a minimum refresh rate of 10 Hz.
    - A slower response time would result in noticeable lag.
3. The resolution of each camera should be at least 480p.
    - This is the minimum resolution needed to recognize a face at the maximum convergence depth. This is also a standard camera resolution.
    - A high quality image of the object being tracked is needed in order to capture enough detail to recognize if there is a face in frame.
4. The camera should be able to connect to a computer via a USB connection.
    - This is in order to ensure the system gets the fastest possible visual feedback from the camera.
    - A wireless camera of equal value would be a much lower quality product.

5. The camera must have optional autofocus.
    - This is used in order to increase the frame rate of the overall system by freeing up the additional resources needed to adjust the focus on the camera. This can be accomplished manually via programming or by modifying the lower level register codes to turn it off on the chip.

4 Final Component Decisions

All purchased parts for this project were chosen based on a number of considerations including functionality, convenience of use, cost, and size. Below is a description of many of the components, and how and why these specific parts were chosen.

4.1 Linear Transmission

One of the main redesign options considered for this project was the linear transmission system used to convert the rotational motion of the motors to the linear motion required for the mechanism's desired movement. The two options most seriously considered for this were a rack-and-pinion, which was used by the Motor Eyes Mechanism, and a lead screw.

The Motor Eyes Mechanism used Vex rack-and-pinions to produce the linear motion required by the mechanism. While being simplistic in functionality and efficient in power transmission, the rack & pinion is also good for prototyping linear motion for mechanisms. However, lead screws, while being less efficient, would allow us to drive the system with less torque as well as allowing for much more precise positioning of the eyes. After careful consideration, it was decided that the benefits to using a lead screw outweighed the drawbacks, and that a lead screw would be more effective in the system than a rack and pinion.

In choosing a specific lead screw, the primary consideration was the pan speed specification, which was 250 degrees/sec. The linear velocity required to achieve this when the eyes would be moving the slowest was determined, and it was used as the basis for calculating lead screw speed requirements. The desired linear speed to achieve an eye speed of 250 deg/s was calculated to be 61.1 cm/sec. The angular velocity of the motor required to achieve this linear velocity was calculated for a number of common leads, including 10, 15, 20, and 25 mm leads. The required motor speeds for the various leads were compared along with the efficiency and

approximate torque requirements for each lead length (torque calculations are described in greater detail in Appendix E: Determination of Dynamic Loads for Analysis).

In general, a smaller lead resulted in a motor speed that was infeasible given the cost and size constraints on the project. Larger leads required lower motor speeds but also higher torques, and additionally were less commonly manufactured by companies. The lead length ultimately chosen was a 15 mm lead that required a motor speed of 2,443 rpm, and which is a fairly common lead length. The speed of the convergence motor was not an important specification in the design process, so rather than buy a different sized screw for the convergence mechanism, it was decided that it would be more convenient to buy two different motors with different speeds rather than two lead screws with different leads. The lead screws and nuts were bought from Igus. The part numbers can be found in Appendix C: Final Parts List.

4.2 Linear Sliders

One of the main problems encountered with the Motor Eyes mechanism was the clearance between the VEX sliders and slider tracks, especially on the Control Arm Sliders. Different linear sliders were explored in order to find the best solution to this issue.

The VEX Linear Slider system is a simple track and slider system that is convenient for prototyping due to low cost and quick installation. However, due to their large coefficient of friction, large allowances, and ability to bend easily, it was decided that the VEX slider needed to be replaced.

Another method of linear motion transmission similar to the VEX linear slider is a rod & bearing linear slider. The main advantages of this system are miniscule clearances (~0.0007 in), rigidity (solid stainless steel rod), and a very low coefficient of friction (~.002). Bushings can also be used to achieve linear motion transmission. Bushings are more often used spacers than as alternatives to bearings, but they are usually created using a low friction material, making them viable for use in this type of application. In addition, bushings are generally cheaper than bearings. However, if reduced friction and a very precise fit are critical factors, ball bearings are more favorable.

After considering the pros and cons of the two sliders, it was decided to use linear rods with ball bearings for the linear motion within the mechanism. Due to the availability of 3D printers around the WPI campus, custom housings for the two rods were custom designed to be

printed, shown in Figure 11 below. The design of this part is described in greater detail in Section 6.6.1, Design of Linear Bearing Pan Slider Housing.

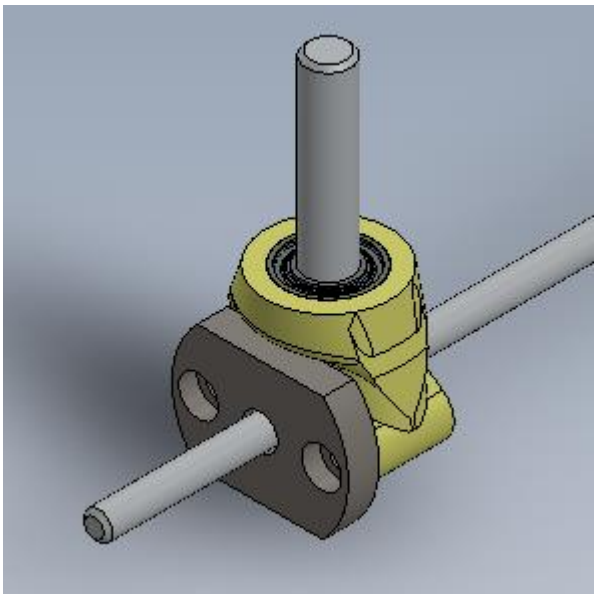

Figure 11: Linear bearing on rod with custom housing

4.3 Motors

One of the major issues identified during the Motor Eyes testing was vibration of the laser mounts, which was caused primarily by the stepper motors. This vibration would have caused problems with image tracking, as it would have prevented the cameras from obtaining a clear image. In addition, by replacing the racks and pinions with lead screws, a much higher angular velocity would be required from the motors than could be provided by stepper motors being used by the Motor Eyes Mechanism.

To achieve the high speeds required for the pan and convergence motions, a DC motor is the best option. In addition, a lead screw requires much less torque for the same load than a rack and pinion. DC motors typically have the highest efficiency when used for high-speed, low-torque applications, which fits the use of the pan and convergence motors with a lead screw.

The tilt motor was also replaced due to the vibration caused by the stepper motors. One replacement option was a DC motor used in conjunction with a potentiometer. Alternatively, a servo-motor with a built in potentiometer could be used. Rather than buying a DC motor and a potentiometer, then implementing controls for the angular position of the motor, it was decided that a servo would be used for tilt. This would provide direct, accurate drive for the tilt, and additionally will take up less space than the stepper motor.

The motors were chosen before the mechanism design was complete, since the design in part relied on the motor selection. As a result, torque had to be initially estimated for the pan and convergence motors so that specific motors could be chosen based on the speed and torque requirements for each. These torque estimations were calculated using an equation for lead screw motor torque as a function of lead, axial load, and linear acceleration. (See Appendix E: Determination of Dynamic Loads for Analysis for detailed calculations). Initially neither the load nor the acceleration could be determined since the system had not been fully designed and motors had not been chosen. To estimate the load for the pan motor, twice the weight of the previous team's pan mechanism, which is 0.5kg, was used. An acceleration of 25,000 deg/s^2 for the eyes was used (this value reflects the acceleration of human eyes during saccadic motion), which was the design goal set by the previous group. This translated to a linear acceleration of about 1.05 m/s^2 for the lead screw at minimum convergence (worst case).

Based on these initial calculations, it was determined that the torque required from the pan motor was about 2.74 oz-in. A number of motors from different companies were considered to meet the speed and torque specifications for the pan movement, and the motor eventually chosen was a planetary gear motor from ServoCity with a maximum speed of 2,737 rpm and a stall torque of 9.72 oz-in. The speed of the motor under the initially estimated torque load would be 2,000 rpm, which was determined to be sufficiently close to the 2,443 rpm required to achieve the desired eye speed. After the mechanism was fully designed, the actual required torque to move the pan mechanism was calculated to be 1.76 oz-in. Under this loading, the motor speed is 2,240 rpm, resulting in a peak eye rotation rate of 229 deg/s..

Figure 12: Pan motor, PN 638262

Although no specification was set for the convergence speed of the mechanism, an ideal motor speed was calculated based on the average walking speed of a person, the range of depth that the eyes "see," and the distance the convergence mechanism actually needs to move between the minimum and maximum convergence. A comfortable walking speed for a person is usually

between 1.4 and 1.8 m/s (British Heart Foundation, n.d.), and from this, a motor speed of 300 to 385 rpm was calculated. An estimate of required torque was determined using a similar method as for the pan motor. For this calculation, we used three times the weight used for pan, which is 1.5kg, and used the same linear acceleration, 1.05 m/s^2. This yielded an estimated torque requirement of 8.1 oz-in. Again, a number of different motors were considered, and finally a planetary gear motor was chosen from ServoCity with a maximum speed of 416 rpm and a stall torque of 36.12 oz-in. With the initially calculated torque requirement, the motor would have a speed of about 325 rpm, which falls within the range previously calculated. After the mechanism was fully designed, the actual torque requirement was calculated to be 6.9 oz-in, which results in a motor speed of 337 rpm.

Finally, the tilt motor was primarily chosen based on the required eye speed of 250 deg/s. Servo speed is defined as seconds per 60 degrees, and to achieve a speed of 250 deg/s, the required servo speed is 0.24s/60deg. This speed requirement was considered along with size and cost constraints, and the Servo ultimately chosen has a speed of between 0.14s/60deg and 0.11s/60deg. These speeds correspond to an eye tilt speed between 429 and 545 deg/s, assuming no load on the motor. The actual speed of the eye will be less than this, due to the moment of inertia of the eye and other components. In addition, the fact that this speed is greater than the design specification is not a concern because human saccadic eye speeds can reach upwards of 500 deg/s, so this high speed will not create a seemingly unnatural movement.

Figure 13: Tilt servo HS-225BB

Table 1 below shows a summary of the motors chosen and their specifications.

	Pan	Convergence	Tilt
No Load Speed	730 rpm	416 rpm	.11s / 60deg (@6V)
Stall Torque	27.8 oz-in	36.12 oz-in	66.65 oz-in (@6V)
Voltage Range	3-12 V	3-12 V	4.8-6 V
Current Range	.19 - 4.9 A	.12-3.1 A	8-340 mA
Weight	82 g	82 g	27 g

Table 1: Summary of motor specifications

4.4 Motor Shields

To simplify using an Arduino board to control multiple motors, additional hardware was necessary. While this could be made from scratch, purchasing a commercially available Arduino motor shield was simpler and more reliable. Most available projects are based on H-bridge chips, which are circuits that allow for switching the direction of electric current through a load.

The VNH2SP30 full-bridge driver is a relatively complex chip for driving a single DC motor, and can handle a continuous 14 amperes at 16 volts, or up to 30 amperes with supplemental cooling. Since this chip has a single output channel, two are included on most shields to allow for dual motor control, as shown in Figure 14 below. While more expensive than simpler shields, these ones are more robust and feature internal current and temperature shutoff circuits, which is of interest as one of the old H-bridges was burned out during testing of the Motor Eyes mechanism.

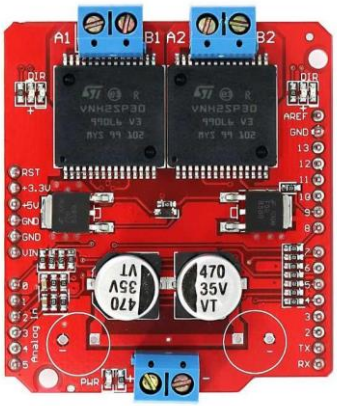

Figure 14: Motor shield, PN VNH2SP30

Given that the chosen motors had a combined stall current of over eight amperes, and only two motors were being used, the dual-VNH2SP30 shield was the clear choice.

4.5 Encoders

In order to effectively control the mechanism, absolute encoders were mounted to the drive motor shafts. This allowed for high-resolution measurement of the mechanism inputs, which for this mechanism are linearly proportional to the outputs (Kiely, Oo, Rappoli, Strobel, and Walcott, 2014). Using the feedback from the encoders, it was simple to calculate the theoretical output focus point based on the number of rotations of the convergence or pan shafts.

The previous team had identified, but not used, the CUI AMT20, shown in Figure 15 below, which features a center hole for fitting around a motor shaft and a 12 bit (4096 count) output via SPI (Serial Peripheral Interface). Upon further review this encoder was deemed optimal for the HSV System, as similar encoders are only slightly cheaper while requiring more work and additional hardware to mount and interface with.

Figure 15: Absolute encoder, PN AMT20

4.6 Cameras

The cameras were purchased according to the design specifications described in Section 3.5 (Camera/ Image Tracking Design Specifications). The reason for the small internal circuit board requirement is due to the fact that the eyes need to be small enough to be incorporated into the mechanism without interfering with any of the other components. One issue with this is that pictures of a camera's internal components are difficult to find. In order to be sure about the camera selection, further research was done on cameras that have been used for a similar purpose.

While doing research, the camera used by Elizabeth Alexander on her ACHR MQP seemed to be a very viable option for this project. Unfortunately, there was no information about the camera in her MQP report. However, based on the pictures in her report, a similar camera was found that satisfied all of the design requirements for the HSV System.

The camera chosen is the HDE USB 5 Megapixel Webcam, which was purchased from Amazon. This camera has a 1280x720 pixel sensor size, and a frame rate of up to 30 fps. It also plugs in via USB cable, as desired, and can be focused manually. The camera's circuit weighs about 11 grams, once the outer casing is removed, and is small enough to fit inside the "eyes," which makes it ideal for this project.

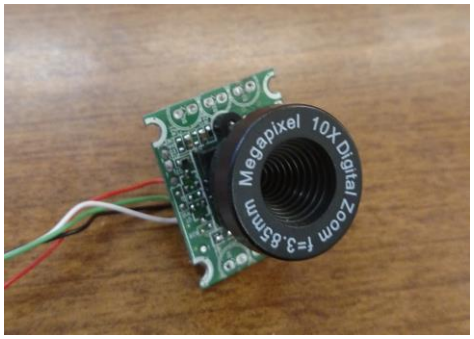

Figure 16: Webcam Internal Circuit

5 System Modifications

A number of changes were made in the design of the HSV System that remedy the problems found in the Motor Eyes System. In the following sections, figures are used to show the new parts and illustrate the differences between the two designs.

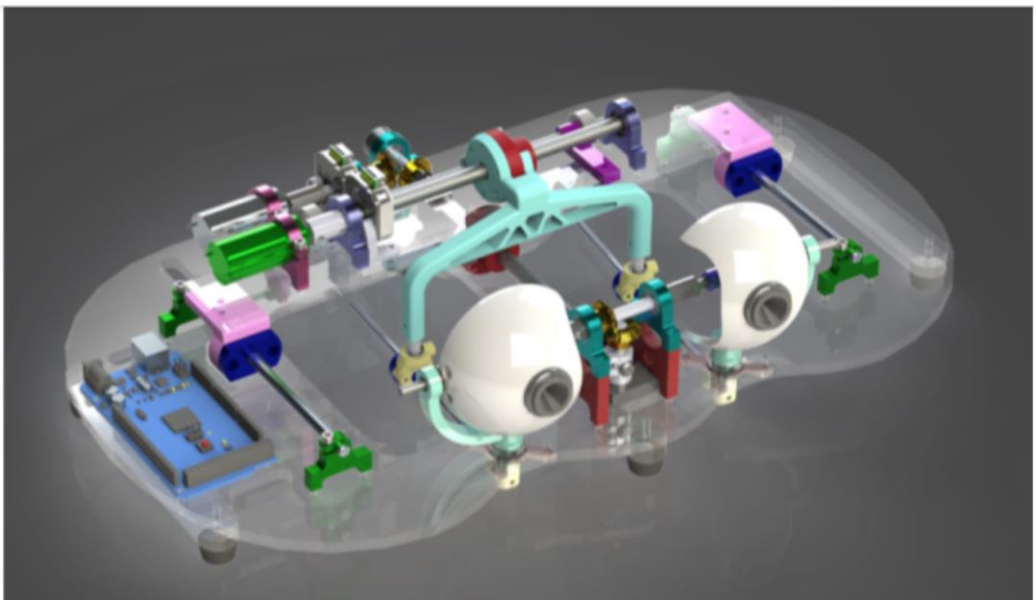

Figure 17: Final rendering of HSV System

The pictures below are the two systems that are going to be compared: the Motor Eyes design from 2014 and the HSV System.

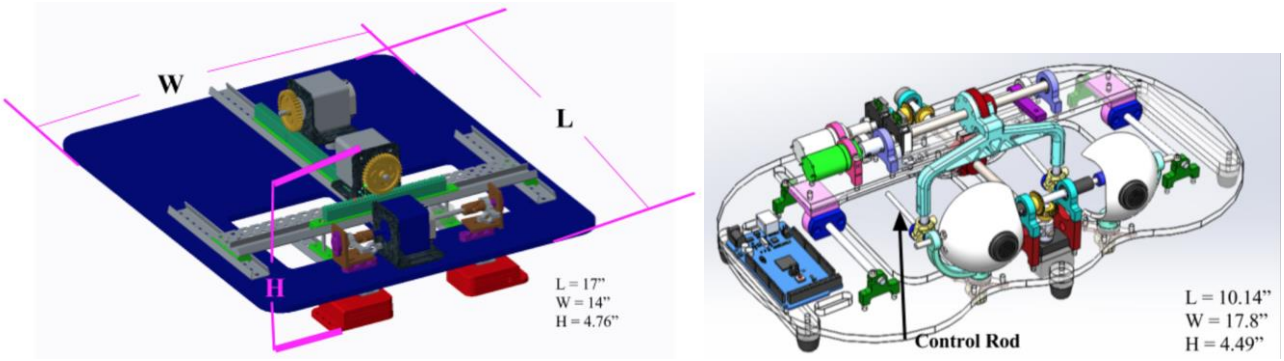

Figure 18: Motor Eyes System with dimensions

One of the goals of the HSV System was to reduce the size of the overall mechanism. In Figure 18, the dimensions of the Motor Eyes and HSV System are shown. The length and height were both successfully reduced. However, the system needed to be wider to allow the Arduino to be mounted to the platform and to prevent the control rods from extending past the acrylic platform.

5.1 Electrical Modifications Overview

In the Motor Eyes System, there was no consideration for placement of the electrical components apart from the stepper motors. The wires and connectors were held down by tape,

which resulted in occasional electrical issues. In the HSVS, wire slots in the acrylic and wire ties were used in order to ensure the wires were organized and secured more permanently, resulting in a refined electromechanical prototype. All of the wires were routed beneath the acrylic base and are secured using wire ties connected to wire tie mounts. This ensured that the wires stayed organized and nothing got caught in the moving components. Figure 19 below shows the slots put into the base plate for wire management.

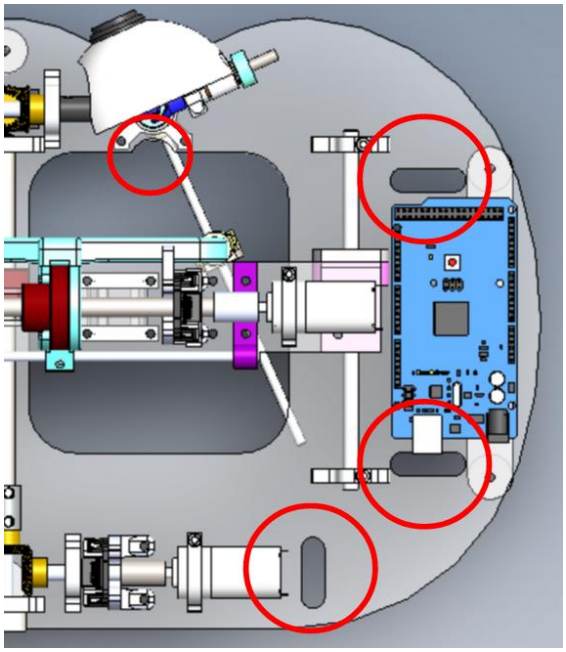

Figure 19: Slots and cutaways for cable organization on HSV System

To control the mechanism, an Arduino Mega2650 was used instead of the Arduino Uno because it has more memory and more pins, so was more convenient for this project, especially with the motor shield taking up so many pins. The Mega has 54 digital I/O pins and 16 analog input pins. To control the pan and convergence motors, since the 12V DC motors cannot be controlled directly by the 5V Arduino, a motor shield was necessary. In addition to the Arduino and motor shield, an encoder was needed on each DC motor to keep track of the motor's rotational position. The encoders chosen were AMT203-V absolute encoders made by CUI Inc and sold by DigiKey, with 4096 pulses per revolution. They require a 5V input voltage, so they can be powered directly from the Arduino, and have a number of interchangeable shaft size options, which means they fit directly on the pan lead screw and convergence shaft.

5.2 Convergence Mechanism Modifications

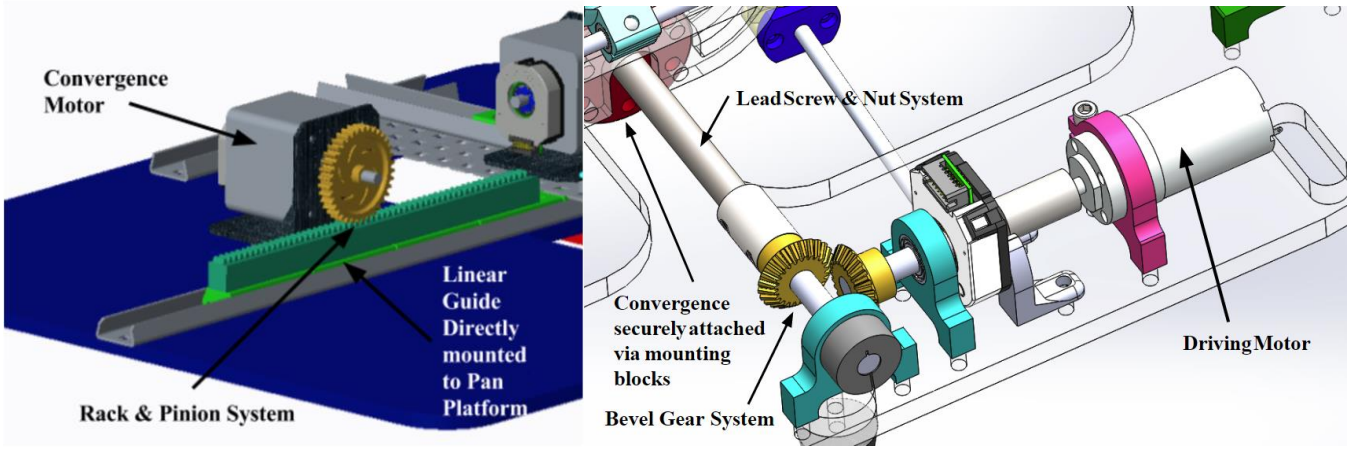

Figure 20: Old convergence mechanism on Motor Eyes System

The convergence drive changed almost entirely from the original Motor Eyes design. To start, the motor was changed from a stepper to a DC motor to reduce the vibrations. The rack and pinion drive was replaced by a lead screw drive connected to the motor with bevel gears. The use of a lead screw allowed for much more precise control. The bevel gear system was used so that the motor could be perpendicular to the lead screw, which reduced the length of the system.

In order to attach the convergence nut to the pan mounting plate, two acrylic plates and mounting blocks were used to securely drive the pan platform to its desired location. While the encoder was accounted for on the old design, it was never actually mounted and used. For the HSV System a mounting bracket was designed in order to secure the encoder in place.

5.3 Tilt Mechanism Modifications

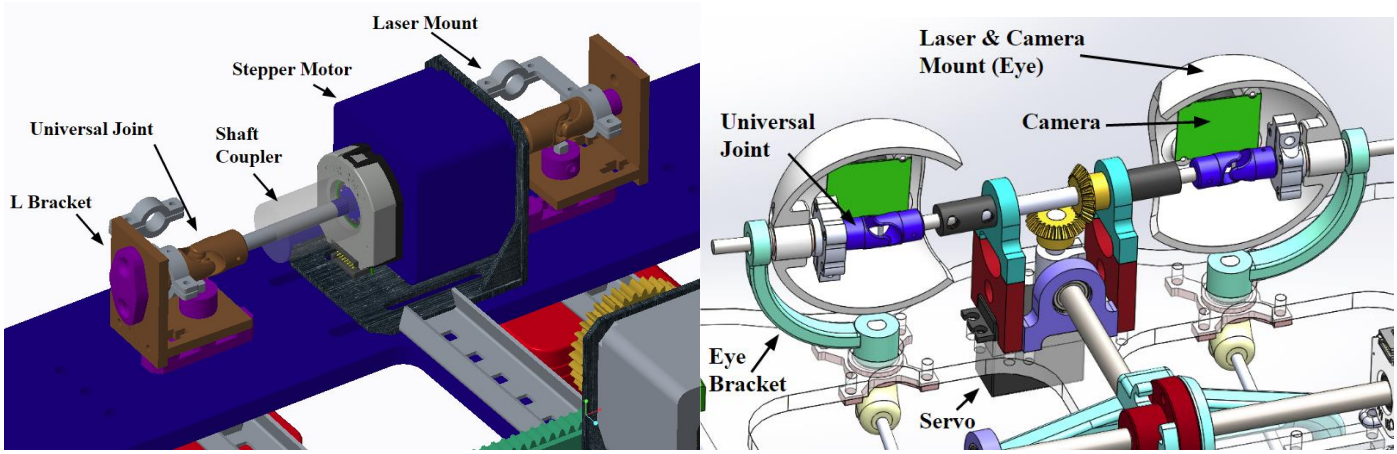

Figure 21: New tilt mechanism on HSV System

The new tilt mechanism design was fundamentally similar to the old one, but included many improvements to make it more human-like and less error prone. It was also modified to allow for the cameras to be mounted to the system. The two universal joints are the only components that remain from the previous system. The stepper motor was replaced with a servo in order to reduce the vibration of the eyes and to allow for simpler control of angular position. However, because the servo did not have a drive shaft in the front and the back of the system, as the stepper motor did, the eyes were designed to be driven using bevel gears. The acrylic L-bracket used in the previous design failed, and had to be redesigned to have the same functionality while being more robust. The new eye bracket is small, lightweight, and reinforced with fiberglass to sustain potential applied forces.

5.4 Pan Motion Rotary Connection Modifications

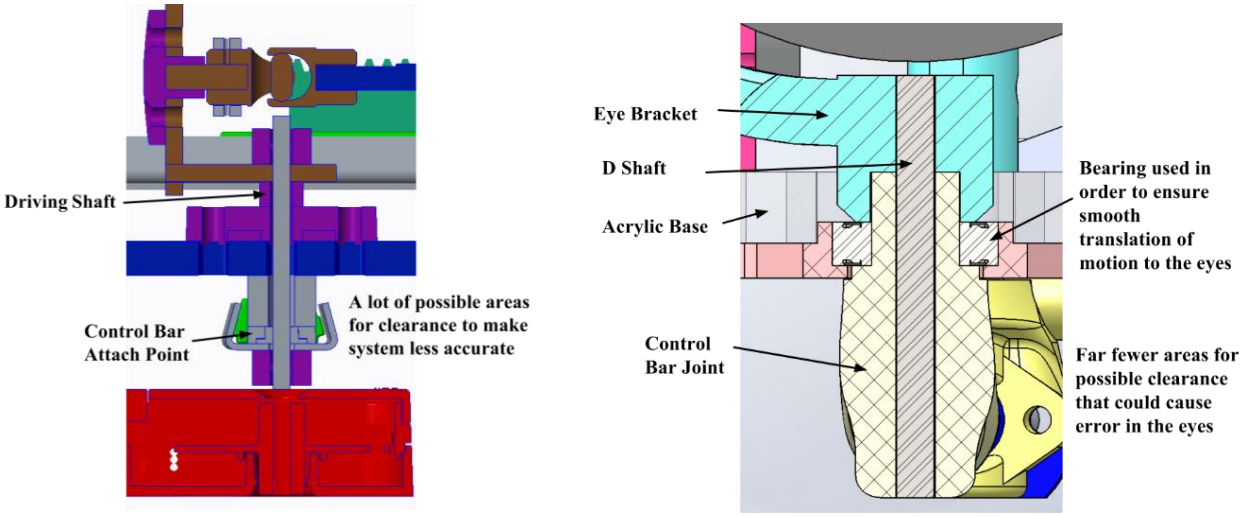

Figure 22: New section view of eye attached to control bar slider on HSV System

In order to reduce the possible sources of error, the number of components in this joint was minimized to reduce clearance buildup. The less clearance there is in the joint, the more accurate and consistent the pan motion is. The Eye Bracket and the Control Bar Joint were custom made to fit together without the need for extra spacers and keyed components. The bearing pillow block was used to hold the joint in place and to ensure smooth rotational motion. A D-Shaft was used to keep the control bar joint and the eye bracket aligned. Both the control bar joint and the eye bracket had a D channel running the length of the hole in order to reduce the chance of hole deformation that might cause backlash in the design. Along with this, a set-screw was used in both eye brackets to ensure the 1:1 ratio of rotation from the control bar joint to the eye bracket.

5.5 Pan Mechanism Modifications

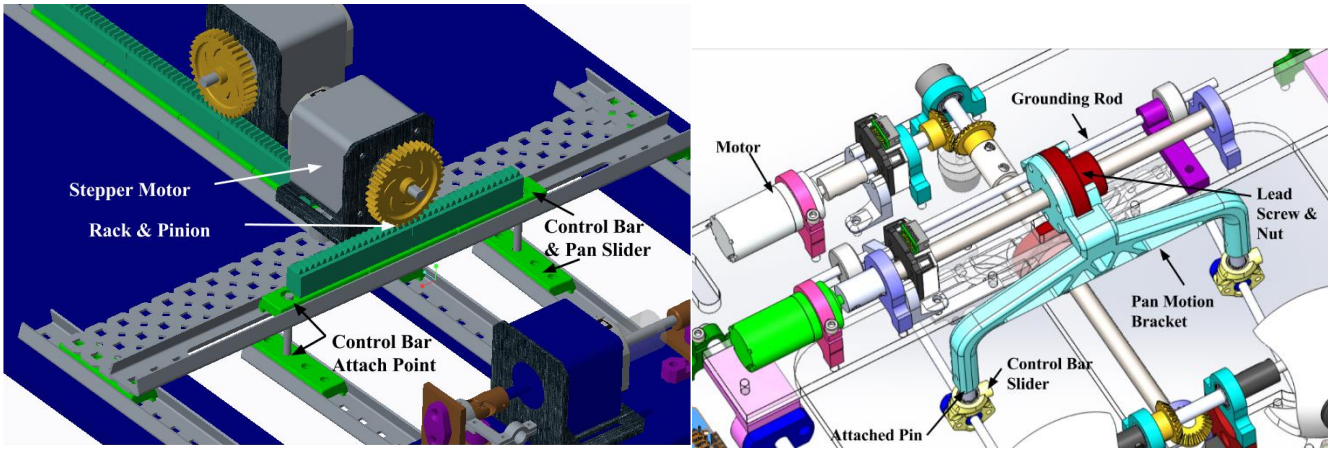

Figure 23: Old pan mechanism on Motor Eyes System

In the redesigned pan mechanism, some of the main points of error were remedied. The Control Bar attachment point is more rigid to significantly reduce the amount of motion allowed in the pan mechanism. The lead screw and nut were used to increase the accuracy and resolution of the system. A grounding rod was used to ensure the nut and pan motion bracket did not rotate and apply a force on the control rod. This force could have damaged the control bar joint or other components, and could have caused inaccuracies in the system. The standoff was inserted in the control bar slider bearing and held onto it via a screw. The other side of the standoff was held in place by the pan motion bracket and a setscrew. The control bar slider consisted of a rotary bearing as well as a linear bearing. This was done in order to ensure the pan & convergence motion translated to the control rod did not bind and cause deformation in the system.

6 Design and Analysis of Custom Parts

The majority of components used for this new mechanism were purchased by selecting parts that satisfy our design specifications. However, many other components of this new mechanism were designed to fit the specific functions required for them, and were fabricated using 3D printing or laser cutting. Since these parts were custom made, it was important to perform stress analyses to confirm their functionality in the new system.

As a first step, it was necessary to select the materials that were going to be used for every component. Next, Creo Parametric and ANSYS Workbench were used to determine the forces acting on different components by performing dynamic analyses on specific components. Due to

the complexity of the designed mechanism, a full dynamic analysis could not be performed in Creo, and hand calculations were performed to estimate loads on certain components. ANSYS Workbench was again utilized to perform static structural stress analyses using the applied loads that had been previously determined.

The failure criteria used for these analyses were the equivalent stress, or Von Mises Stress, and the total of deformation in the material. The Von Mises Stress (VMS) was used to determine whether the maximum stress in the part exceeds the yield stress of the material used to fabricate it. This would indicate the potential for part failure. The total deformation indicates the amount the part will move or deform under operation. If the deformation is high, the accuracy of the system could be compromised, as all kinematic calculations assume perfectly rigid bodies. A detailed explanation of the analysis done for each part is presented below.

6.1 Analysis of Pan Mounting Plate

The first component to be analyzed was the pan mounting plate, shown in Figure 24. The purpose of this part is to support all the components that make up the pan assembly. This plate is connected to the convergence lead screw and therefore is responsible for moving the pan assembly either forward or backward when the convergence motor is in operation. As an initial step, the material and manufacturing process to be used for fabrication was determined. Since the mounting plate was a fairly simple 2-dimensional part, it was decided to make it out of laser cut acrylic. This allows the part to be very strong and very exact. A complete summary of the acrylic material properties used in analysis can be found in Appendix D: Material Properties used for Analysis.

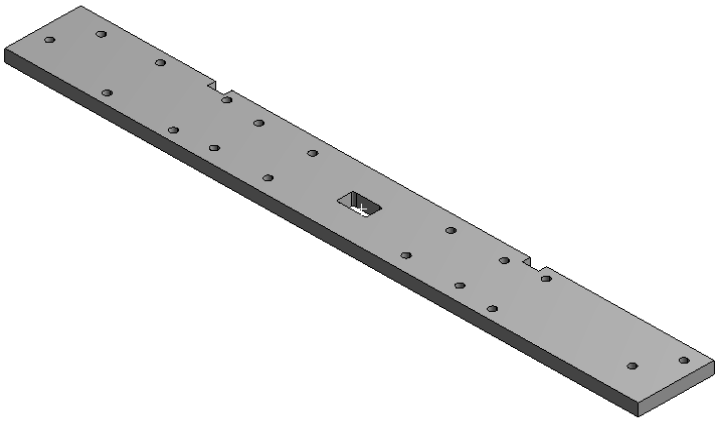

Figure 24: Acrylic mounting plate

In order to perform a stress analysis for this part, it was necessary to determine all the forces and moments acting on the part. SOLIDWORKS was used to obtain the forces that were acting on this element. The initial approach taken for this analysis was to consider the worst case scenario for the part when it is under operation. By doing this, it was possible to see if the part would fail in operation under the worst circumstances, and if not, then the part would not fail at all. It was found from SOLIDWORKS that a total of 10 forces in the negative "y" direction (see Figure 26) were acting on this plate. The magnitudes of these forces were not higher than 1 N individually. This result was expected, as the whole assembly is not very heavy.

ANSYS was used to perform stress analysis. To start a static analysis, it was necessary to input the fixed supports, the forces acting on the component, and material properties for acrylic. The fixed supports were selected at the points at which the plate is connected to other components in the mechanism, as shown in Figure 25. There were 6 fixed supports in total, 2 of which being on the bottom of the plate. The supports located on the bottom face were selected to obtain the reaction forces at those sections in order to use those results in the analysis for other components. The forces previously determined in SOLIDWORKS were applied as appropriate, as shown in Figure 25.

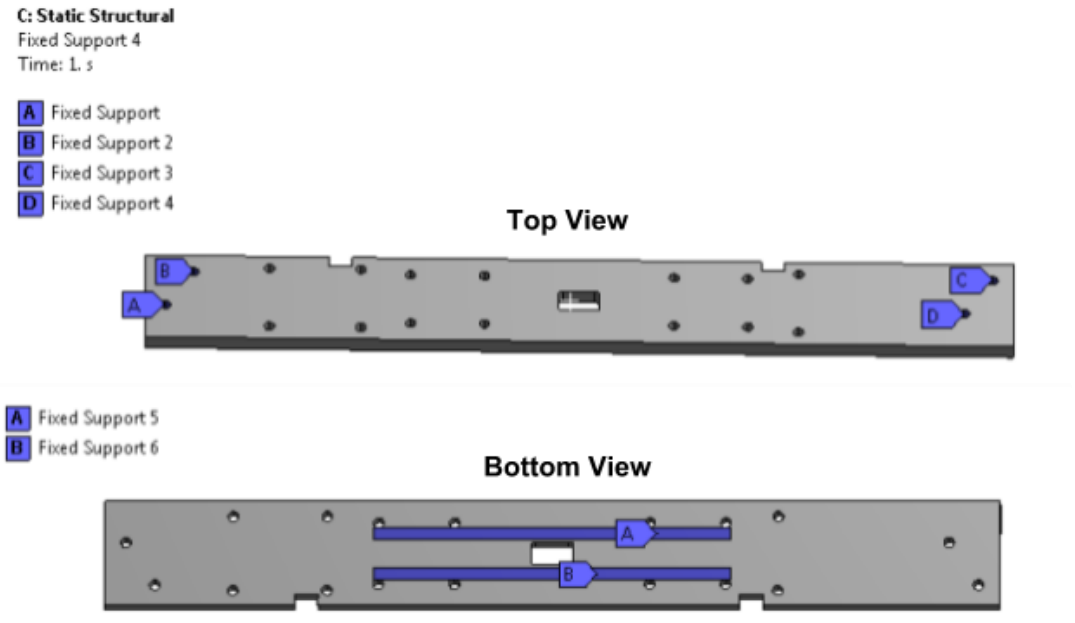

Figure 25: Mounting plate analysis fixed support setup

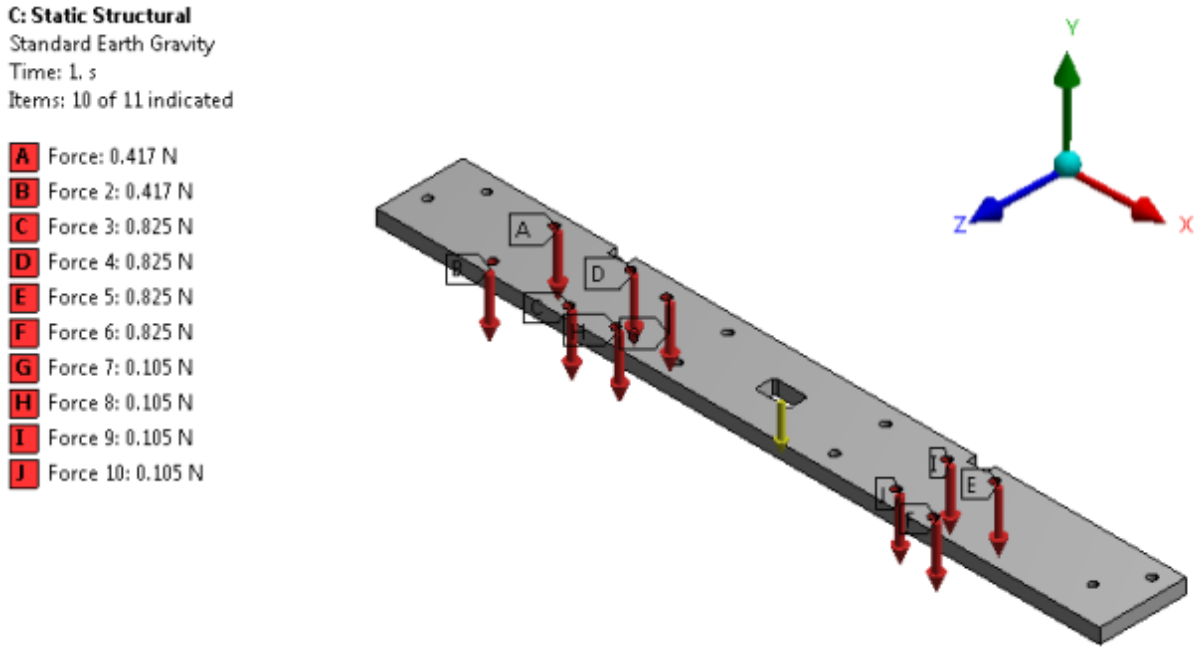

Figure 26: Mounting plate stress analysis forces setup

Once the setup was complete, analysis results were obtained. The values of interest were the maximum equivalent stress (von Mises), shear stress, and deformation on the part. The maximum equivalent stress on the component was 0.22 MPa. This low value is reasonable, since all applied forces are small. The tensile strength of acrylic is approximately 69 MPa, which gives a very high safety factor for this component. The maximum shear stress on this component was 0.117 MPa. The shear strength for this material is approximately 34 MPa. Once again, this result was expected given the small values of applied loads, and the safety factor is extremely high. The maximum deformation on the material was 0.003 mm, which was not anticipated to cause any significant error in the system. The results obtained are shown in Figures 27 and 28.

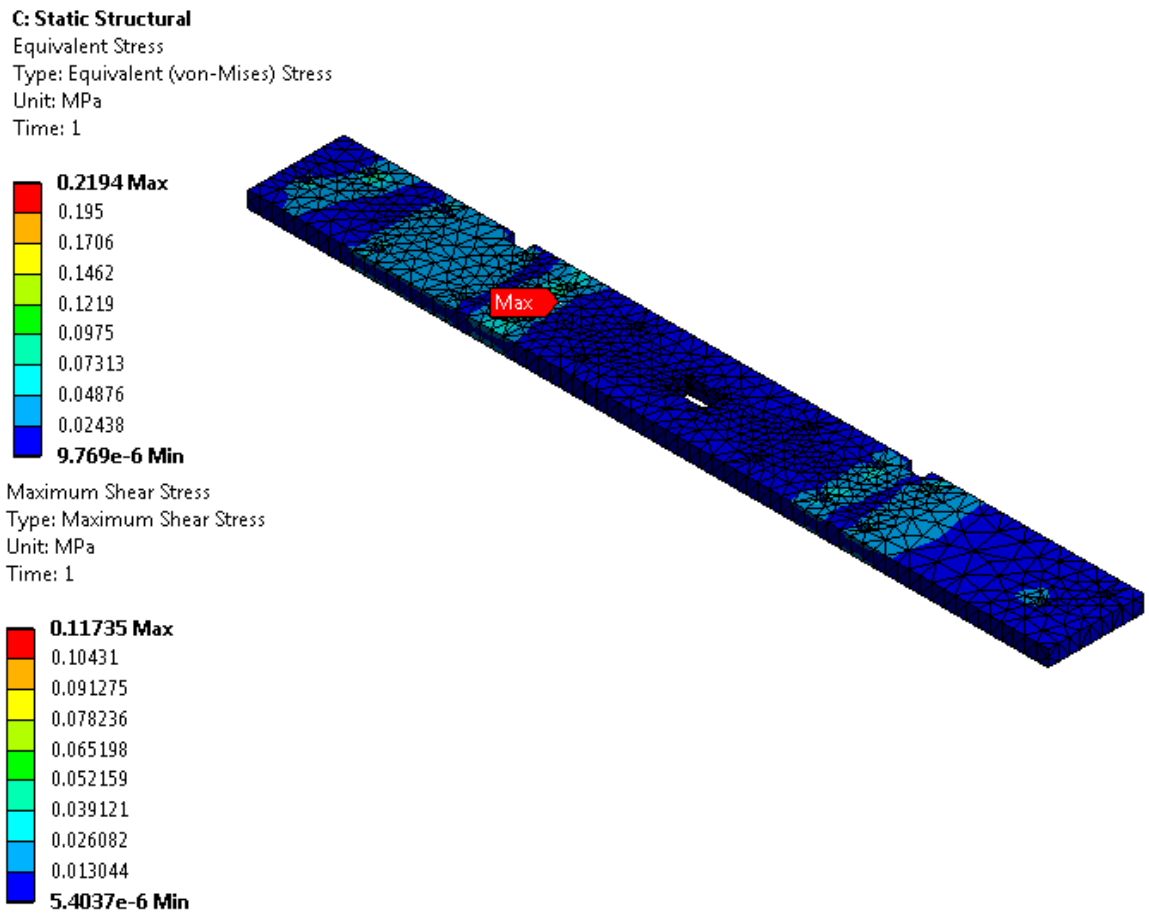

Figure 27: Mounting plate stress analysis maximum equivalent stress and shear stress

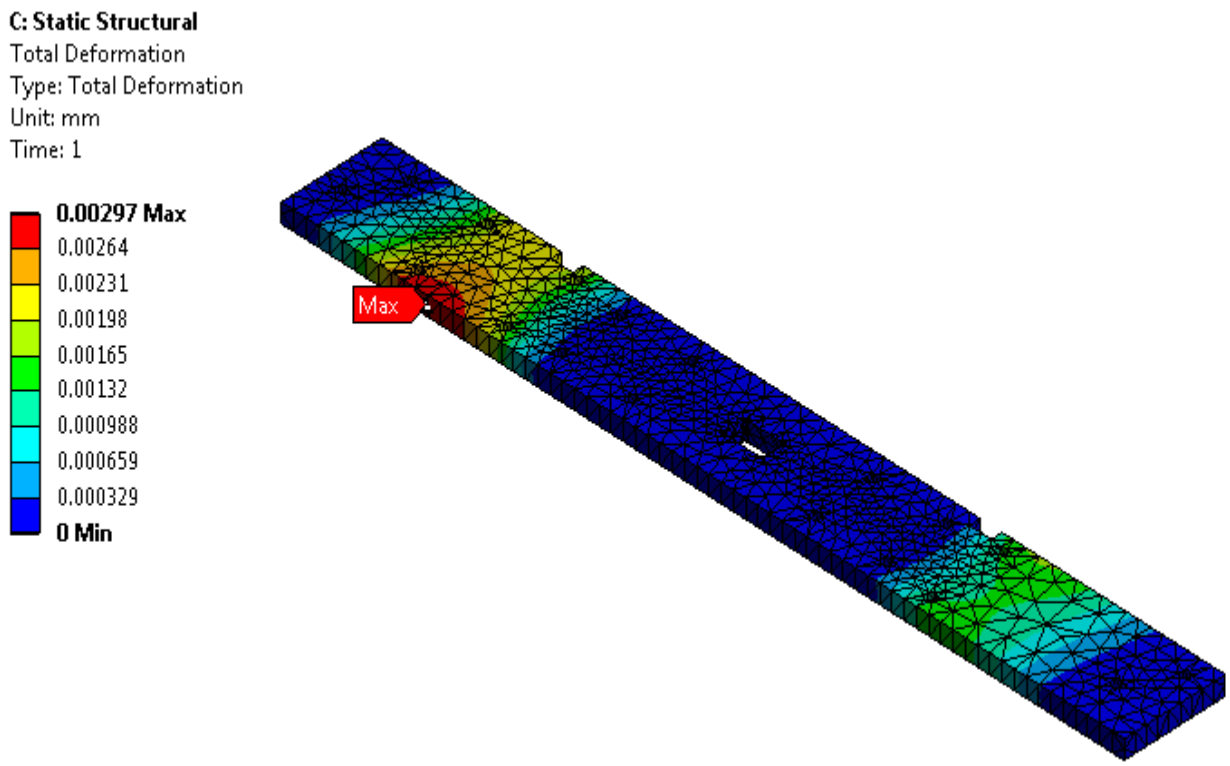

Figure 28: Mounting plate stress analysis maximum deformation

The results obtained for this component provided enough confidence that it would not fail during operation. The safety factors obtained for equivalent stress and shear stress were extremely high.

6.2 Analysis of Convergence-Pan Support

The next component to be analyzed was the convergence-pan support. This part is used to translate the motion from the convergence nut to the pan assembly. This component was divided into two similarly shaped parts that perform the same objective. These parts were connected to the front and back faces of the convergence nut. Taking advantage of symmetry, it was sufficient to perform a complete analysis on only one of them. This part was made of laser-cut acrylic. As with the previous part, the worst-case scenario loading conditions were analyzed.

The first step taken for this analysis was to identify the locations of fixed supports . The fixed supports were ultimately placed at points where the part connects to the mounting plate. Locations for fixed supports are shown in Figure 29.

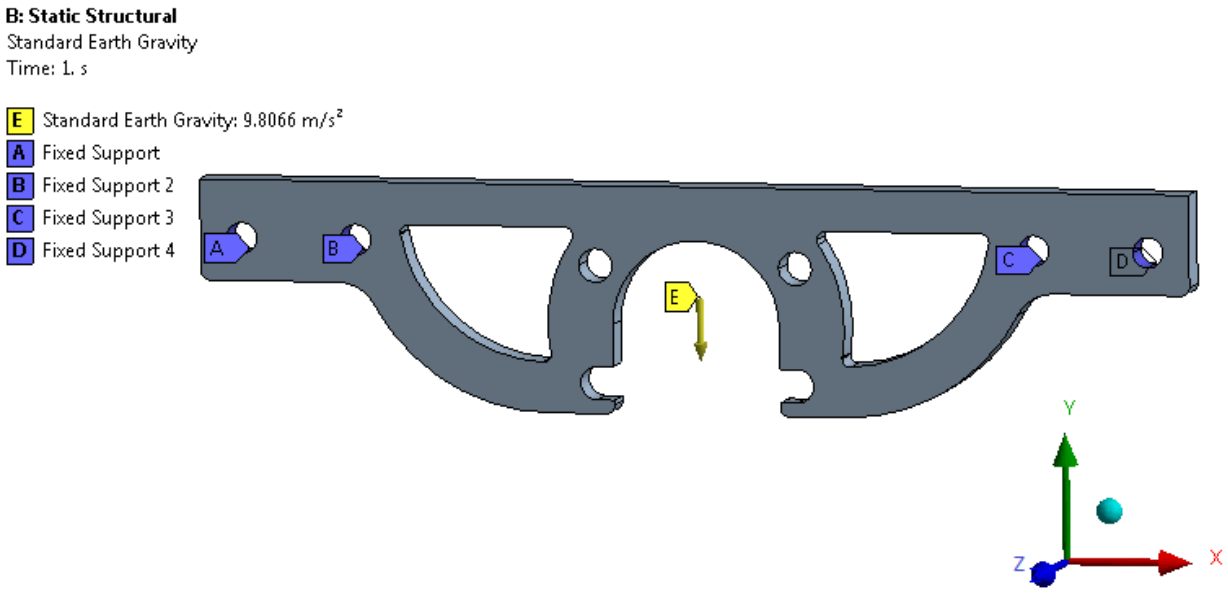

Figure 29: Convergence-Pan support stress analysis fixed support setup

When performing the previous analysis for the mounting plate, the reaction forces on the bottom of the plate were obtained. These forces are equal and opposite to the forces applied to the top face of the convergence-pan support. Because there were two forces, and only one analysis was being performed, the higher of the two forces was applied. The magnitude of that force was 2.007 N. It was also necessary to determine how much linear force the motor was providing the lead screw and nut, and thus to the convergence-pan support. This force was approximated by multiplying the mass of the pan mechanism by its maximum possible linear acceleration. Once this force was known, it was possible to set up an analysis in order to determine the maximum equivalent stress, or Von Mises Stress, and the maximum deformation on the part. The final set up for this analysis including the forces acting on the part are shown in Figure 30.

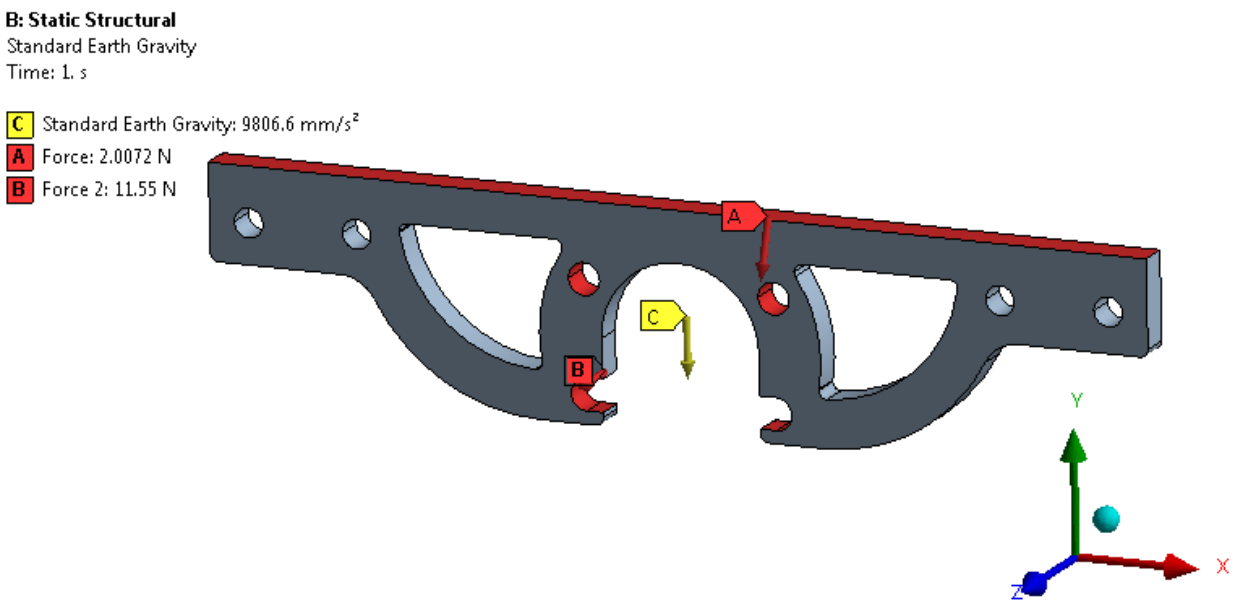

Figure 30: Convergence-Pan support stress analysis force setup

Once the results from the analysis were obtained, it was possible to determine if this part was going to fail in operation. The maximum equivalent stress on the part was 5.996 MPa, the maximum shear stress was 3.292 MPa, and the maximum deformation was 0.3 mm. This results in a safety factor of approximately 10 for both von Mises and shear stress. In addition, the maximum total deformation is not enough to cause error in the system. The results obtained from this analysis are shown in Figures 31 and 32 below.

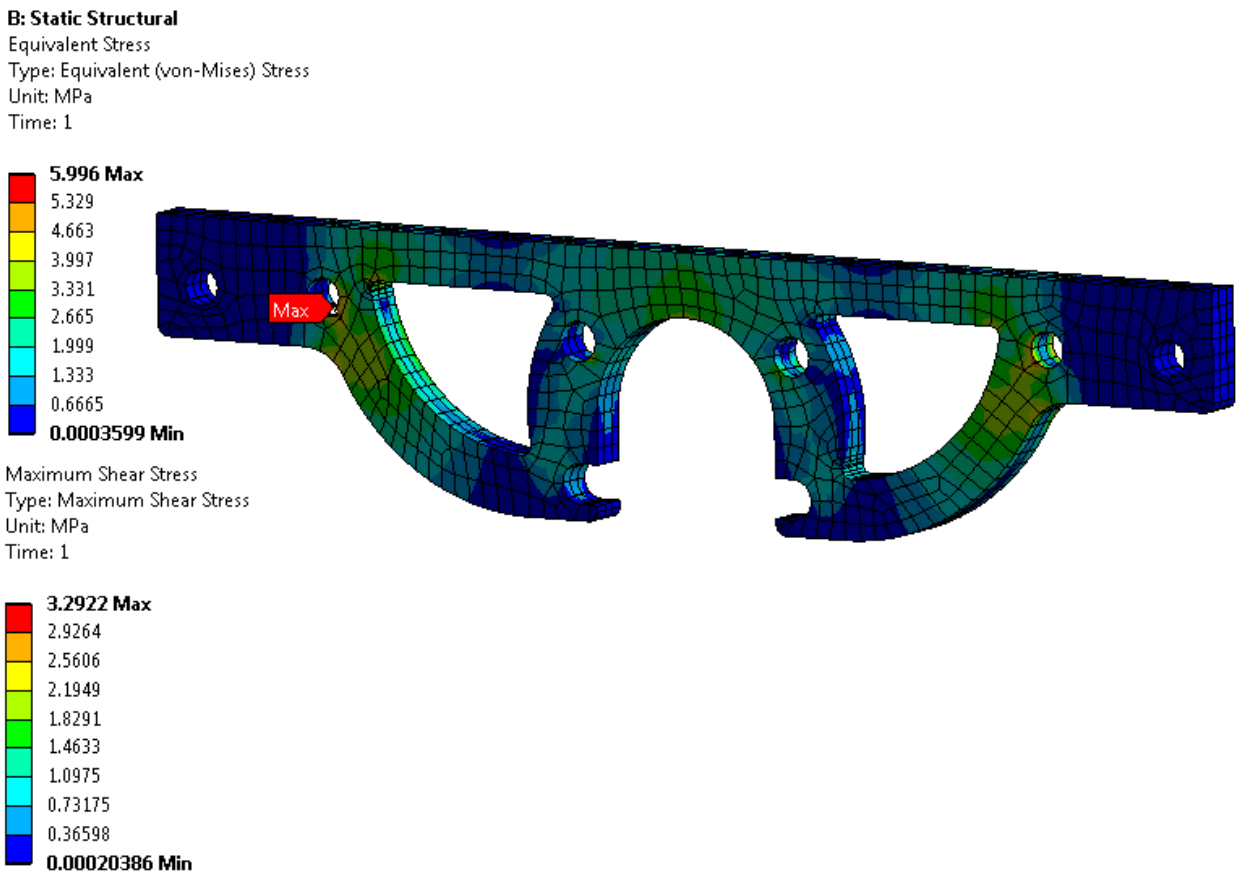

Figure 31: Convergence-Pan stress analysis maximum equivalent stress and shear stress

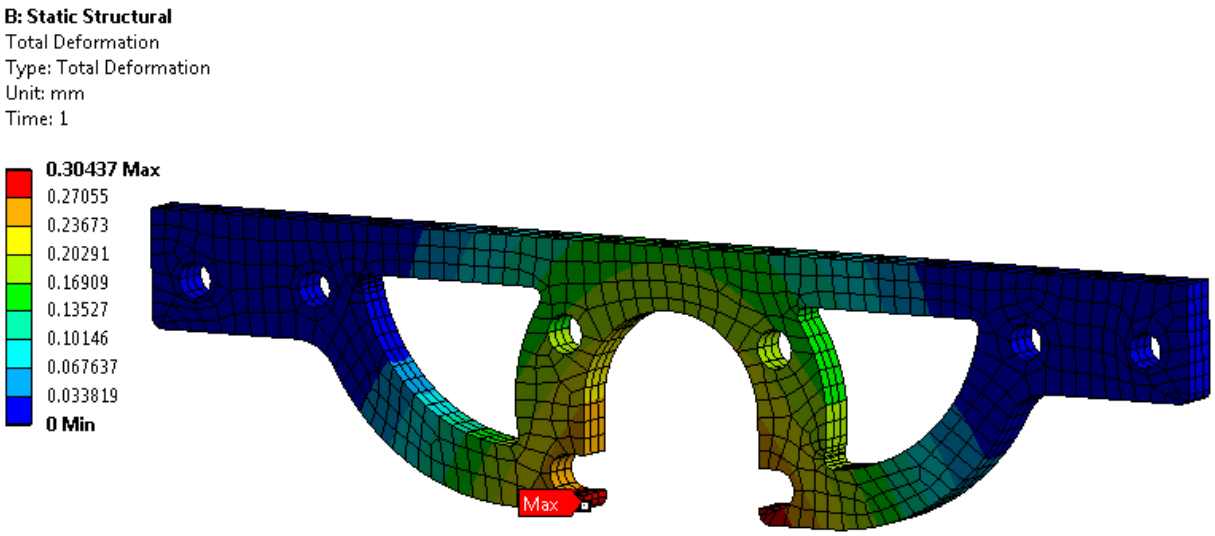

Figure 32: Convergence-Pan support stress analysis maximum deformation

Given the very high safety factors for von Mises and shear stress, and the small total deformation, it was determined that this component would be safe from failing during operation.

6.3 Analysis of Pan Movement Bracket

The purpose of the pan movement bracket is to translate the linear motion of the pan lead screw nut to the control arm slider bearings, causing the rotation of the eyes for pan movement. There were a few iterations of this part throughout the design process, and the final design is shown in Figure 33.

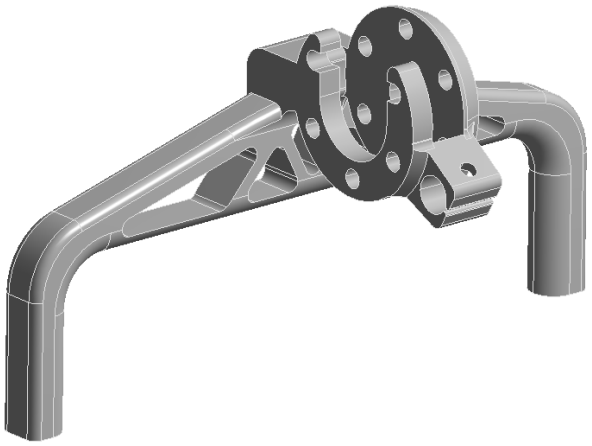

Figure 33: Pan movement bracket

The majority of changes to the part were made simply to make sure it fit with other parts. For example, in the first few design iterations, there was no consideration for the possible rotation about the pan lead screw. This led to the need for a part on the bracket that could hold a linear bearing. This did not change any of the other parts of the design, and was simply added to the existing design. During the design process, it was decided that this part would be printed on the Dimension SST 1200es using Acrylonitrile Butadiene Styrene (ABS). The Dimension SST 1200es was chosen because it provides an acceptable tolerance of approximately 0.006in, and can print small enough features for this part. In addition, printing on this machine is much cheaper than other available options. For a summary of 3D printer options and specifications that were available to the project team, see Appendix D: 3D Printer Specification Table.

For the last couple of design iterations, static structural stress analysis was performed in ANSYS to ensure that the part would not fail, and that deflections were not large enough to affect the accuracy of the mechanism. When an analysis was performed on the second to last design

iteration, the safety factor was extremely high, and some additional material was removed from the design in order to decrease the weight and cost of the part.

Because this part will be 3D printed with a low fill density, an analysis of the part as modeled would not provide an accurate reflection of the stresses and deformations occurring in the part. In order to perform a more conservative analysis, the part was shelled to a 1 mm wall thickness before being imported to ANSYS. The model was fixed using three frictionless supports, and loaded using force reactions from the slider bearings below and accelerations in the x and z directions from the pan and convergence motion. (See Appendix E: Determination of Dynamic Loads for Analysis for dynamic load calculations.)

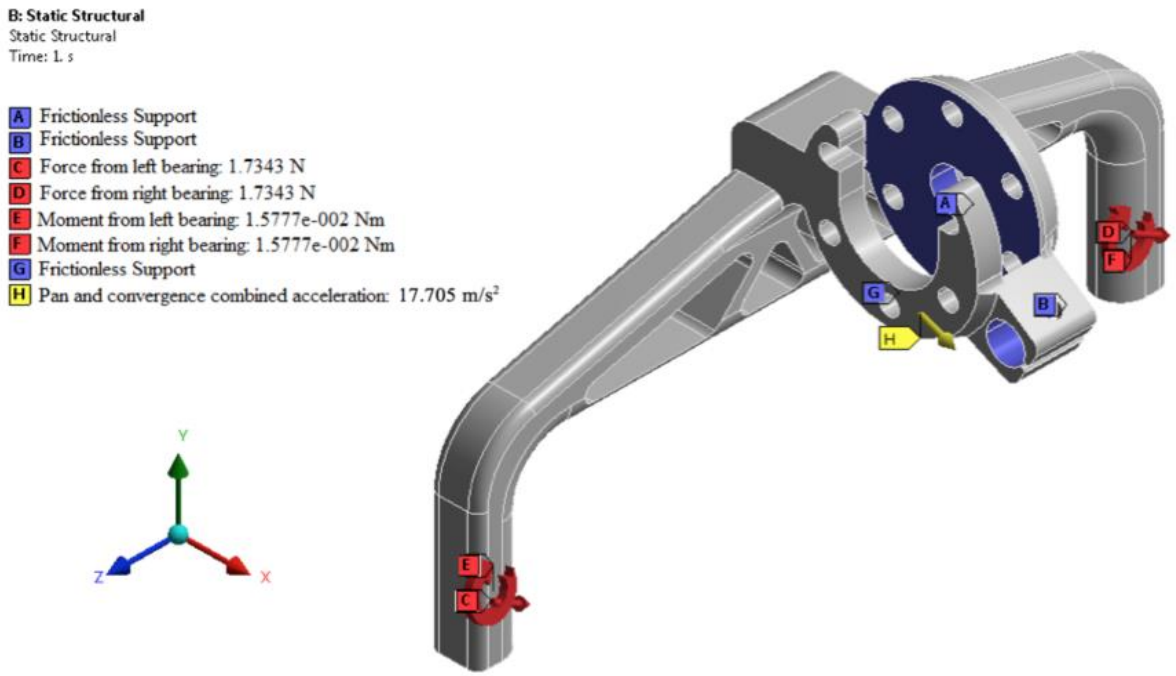

Figure 34: Analysis setup for pan movement bracket in ANSYS

A new material, ABS, was created using mechanical properties of ABS found in the SOLIDWORKS material library. The relevant properties used in the ANSYS analysis are shown in Table 6 in Appendix F: Material Properties used for Analysis.

When the analysis was run, equivalent (von Mises) stress and total deformation were plotted, shown in Figures 35 and 36.

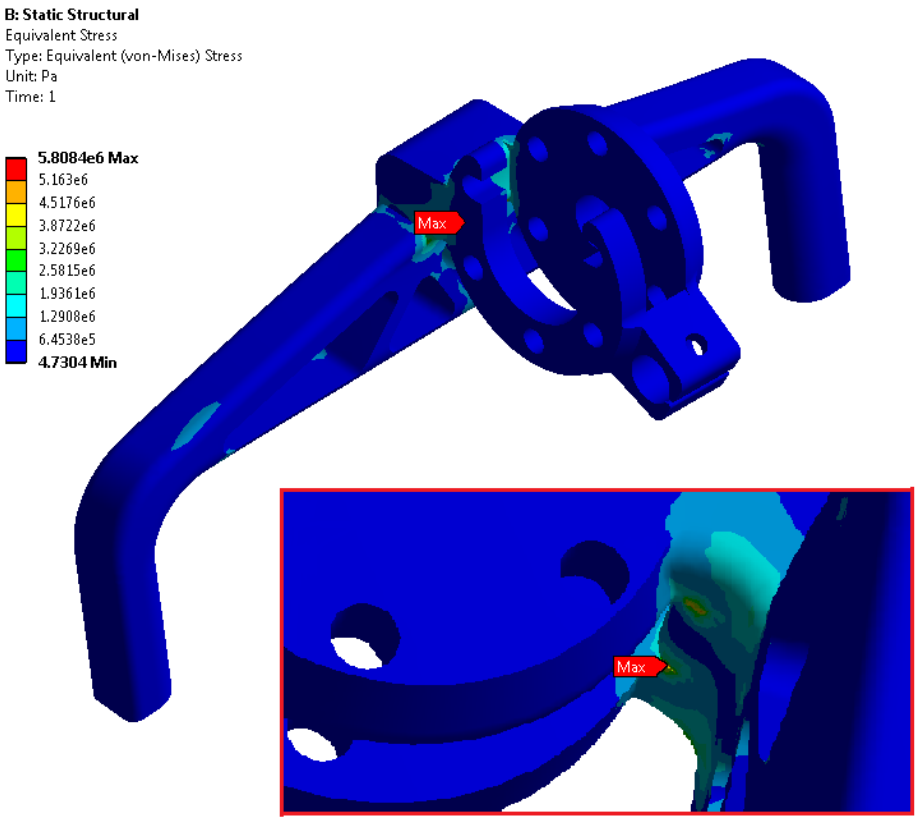

Figure 35: Von mises stress on pan movement bracket

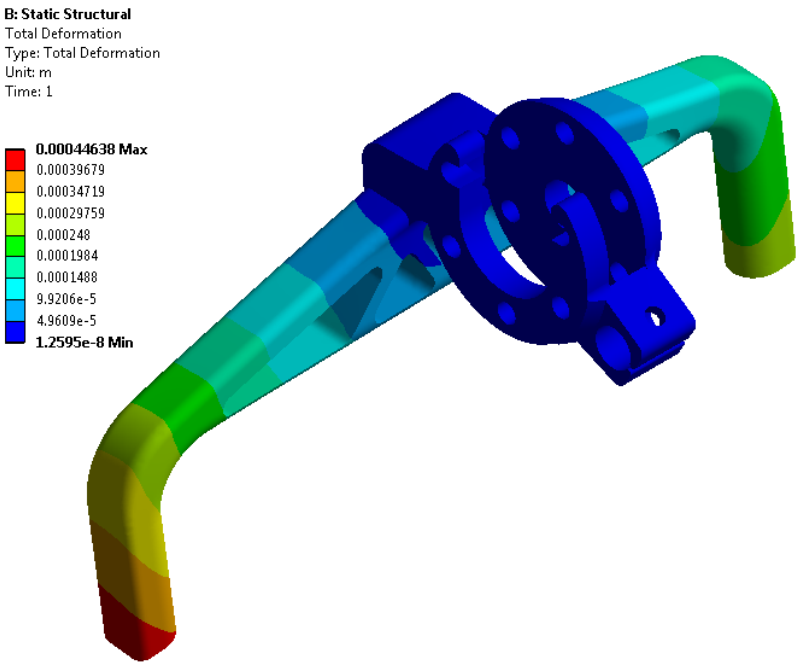

Figure 36: Total deformation of pan movement bracket

The maximum equivalent stress in the part, under the maximum applied loading conditions, was 5.8 MPa, which means the part has a safety factor of 3.18 when compared with the yield strength of ABS (18.5 MPa). The maximum deformation of the part was 0.45 mm, which was not enough to affect the functionality of the mechanism. In addition, the stress and deformation would realistically be lower in the physical part, because there would be some material inside to support it, whereas this analysis was performed on a shelled part. From this analysis, it was concluded that this part would not fail during operation, and thus no further redesign was needed.

6.4 Analysis of Eye Brackets

The purpose of the eye brackets is to translate the rotational motion from the control bar and control bar joint to the eyes themselves. Due to geometric and space constraints, this part had to be considerably small and thin, and as a result is the most likely to fail during operation. A number of different design changes were made to this part, as analysis was completed to determine failure and weak points. Initially, the Dimension SST 1200es was going to be used to 3D print the part. In an analysis performed on one of the earlier designs (Figure 37, left) using material properties of ABS, the part failed. A rib was added to the part (Figure 37, right), to provide additional support and make the part stronger, and analysis was performed again (still using ABS). In this case, the maximum equivalent stress was lower than the yield stress, but there was a large deflection, which is undesirable for this application. To prevent this deflection, the MarkForged 3D printer was considered, which can print composite parts such as nylon with fiberglass reinforcement. Using this printer would minimize the deflection of the part, because the fiberglass reinforcement has a high modulus of elasticity (20 GPa) compared with ABS (2 GPa), making the part stiffer. When the part was run through the 3D printing software for the MarkForged, it was found that the part was too thin to have reinforcement through the entire cross section, so the part was widened further to allow for more reinforcement. The final design of the part is shown in Figure 38.

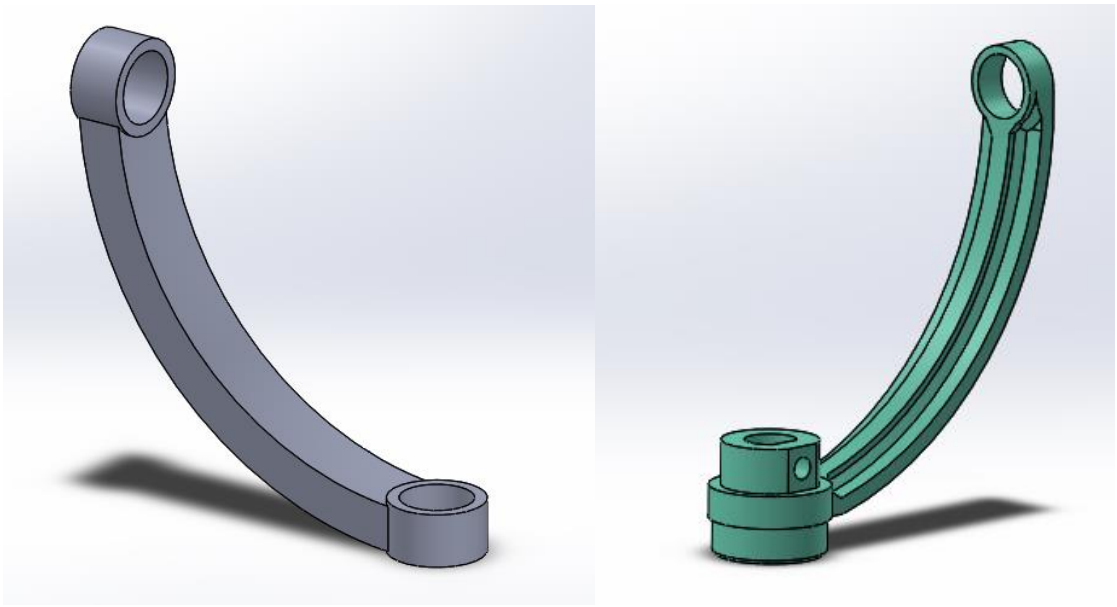

Figure 37: Two earlier revisions of the eye bracket

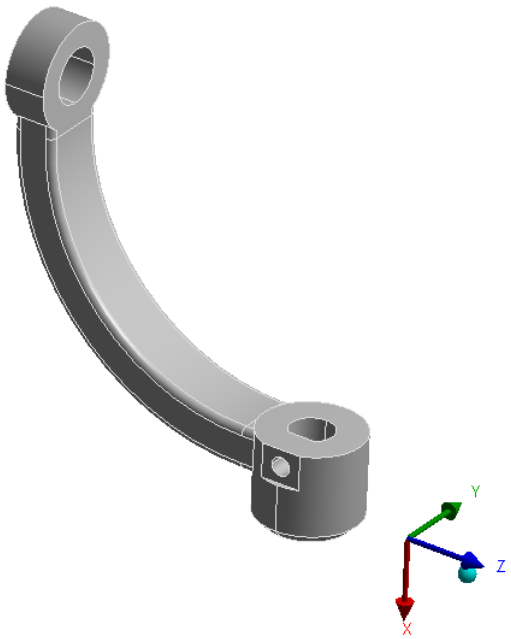

Figure 38: Final design of eye bracket

When the part was printed, it was printed with the y-axis as the build direction. Figure 39 shows the build direction of the part and the fiberglass reinforcement layers, in yellow, for the right eye bracket.

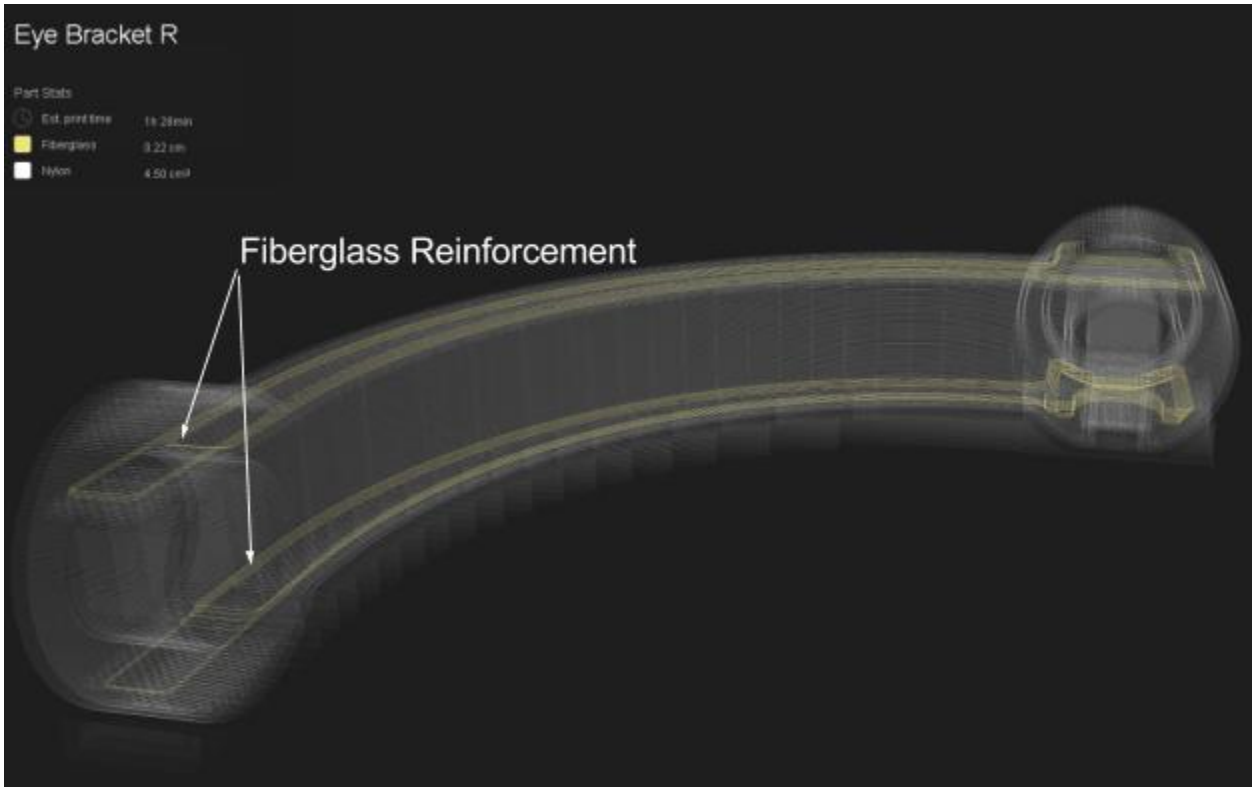

Figure 39: Eye bracket showing layers of fiberglass

From here, a stress analysis was completed in ANSYS to determine the maximum stress and deflection of the part, to determine whether the part would fail. For this analysis, material properties of nylon were used, because the part is over 95% nylon and because doing so would result in a more conservative analysis. Earlier in the design process, Creo had been used to determine the loads at the top hole of the bracket, and these loads were used for the analysis performed in ANSYS. The setup and results of the Creo analysis can be found in Appendix E: Determination of Dynamic Loads for Analysis. The material properties used for nylon were found on the MarkForged website, shown in Table 6 in Appendix F: Material Properties used for analysis.

Figure 40 shows the locations and magnitudes of the external loads applied to the bracket for the final analysis, as well as the location of the fixed support on the bracket.

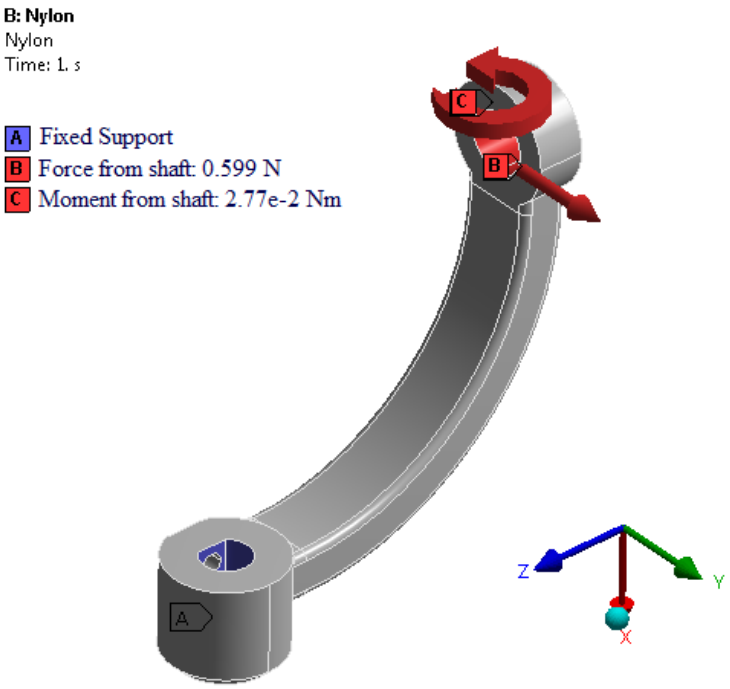

Figure 40: Analysis setup for bracket in ANSYS

Once the analysis was complete, the von Mises stress and the total deformation were plotted. In addition, the directional deformation was plotted for all three axes, to determine what the direction of the highest deformation was, which was the y-direction. These three plots are shown in Figures 41 and 42.

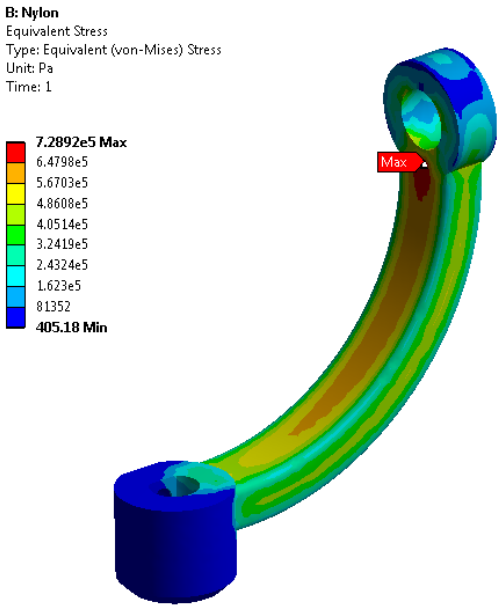

Figure 41: Von mises stress on eye bracket

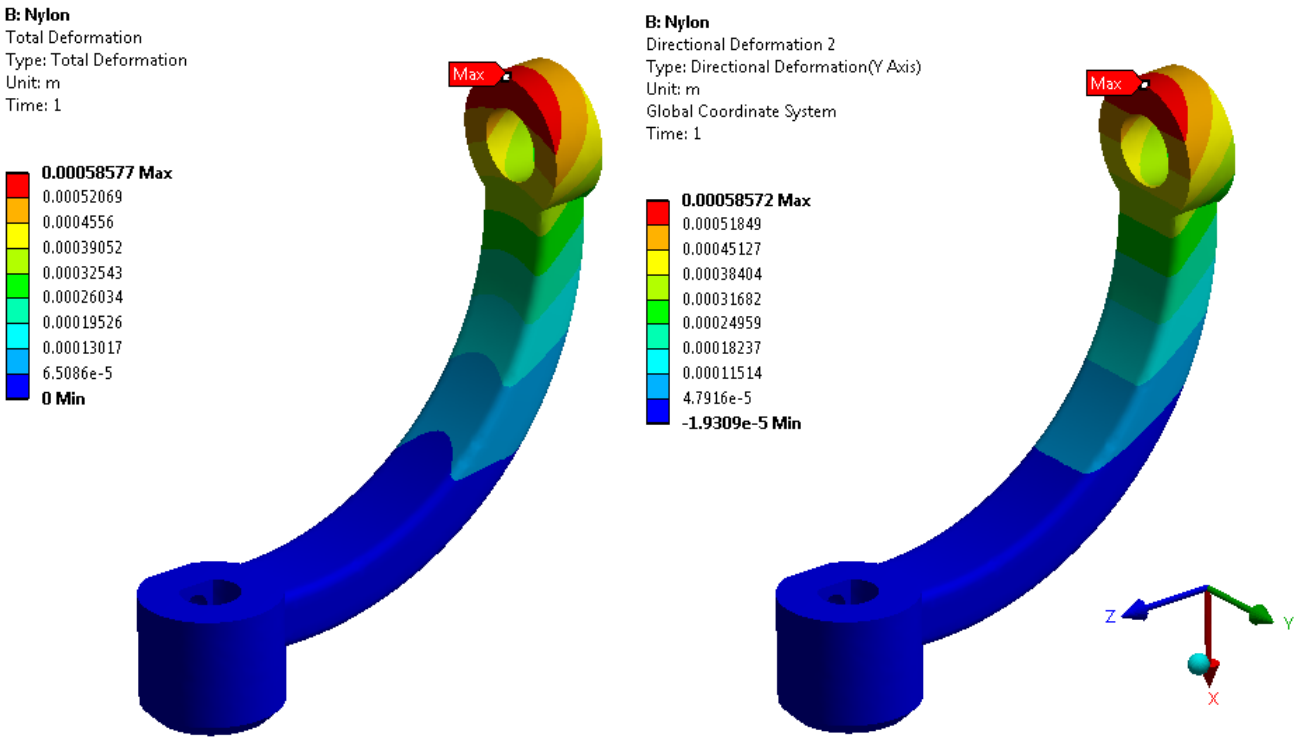

Figure 42: (a)Total deformation of eye bracket (b) Directional deformation of eye bracket in y-direction

The maximum von Mises stress determined in ANSYS was 0.73 MPa, which when compared with the yield strength of nylon (45 MPa) gives a safety factor of 61.6. Because the part was 3D printed, the yield strength will realistically be less than 45 MPa. However the fiberglass reinforcement adds strength to the material, and because the safety factor was so high there was no concern about the part breaking. The maximum total deformation of the part was 0.59 mm, which is not enough to cause any significant or noticeable error in the system. In addition, this was the deflection of the part if it had been made of pure nylon, so in reality the fiberglass reinforcement would strengthen and stiffen the part, resulting in an even smaller deflection. Overall, based on the results of this analysis, it was concluded that the part would not fail during operation, so no further design changes were made.

6.5 Design of Camera Mount and Laser Adapter

The Camera & Laser Mount (the Eye) was designed in order to make the system appear more human-like while also providing sufficient space for the camera and avoiding any interference. As seen in Figure 43, the hub of the eye was the only major point where any significant forces could cause the Eye to fail. The hub had a sufficient amount of material to ensure

this problem did not occur during the mechanism movement. Due to this, the only major design consideration dealt with the geometry. Bushings were inserted into both ends of the hub in order to make sure the eye stayed concentric on the shaft.

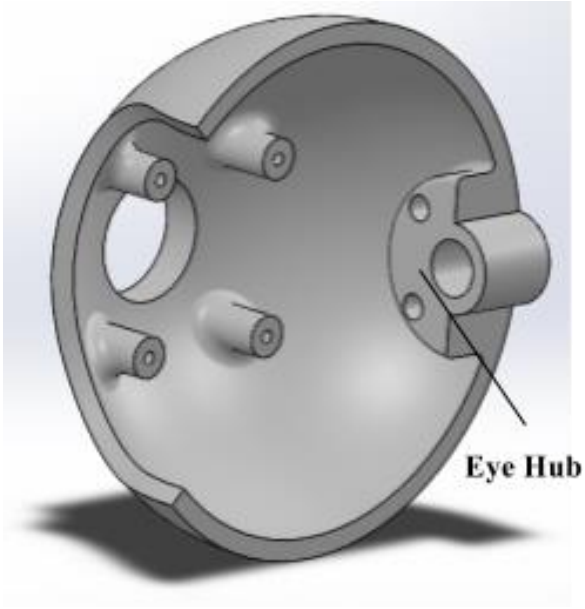

Figure 43: Eye, camera mount

The laser mount was designed in order to hold the laser in place as firmly as possible using the same holes that were to be used for the camera. The section that holds the laser diode was press fit into the eye hole and would squeeze the laser in place with enough force to remove any clearance but not enough to damage the laser itself.

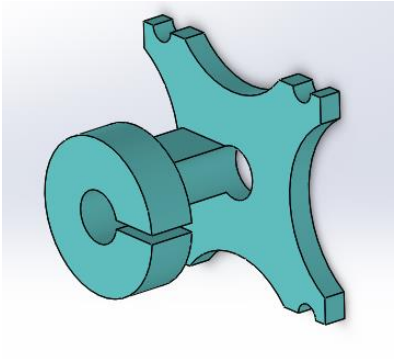

Figure 44: Laser adapter

6.6 Design of Additional Parts

The following sections describe the design of additional parts that were custom made for the HSV System.

6.6.1 Linear Bearing Pan Slider Housing

The goal of the linear bearing pan slider housing was to remove the problem areas caused by the original design. This housing held a linear bearing that rode along the control rod and a rotary bearing that allowed for any and all rotational movement caused by pan and convergence movement. In order to avoid the possibility of components being over tightened, the housing was created in a way that allowed minimal friction in order to avoid binding in the system.

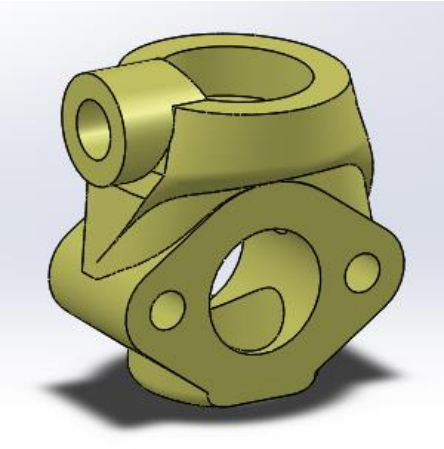

Figure 45: Linear Bearing Pan Slider Housing

6.6.2 Encoder Mounts

The encoder mounts' primary goal was to hold the encoder in place and ensure accurate readings by preventing any unwanted rotation about the lead screw. The pan encoder mount, however, was slightly different and also supported the grounding rod that fixed the rotation of the pan movement bracket. Due to the minimal forces that could have been applied to the mount, no other reinforcement was used to strengthen the design.

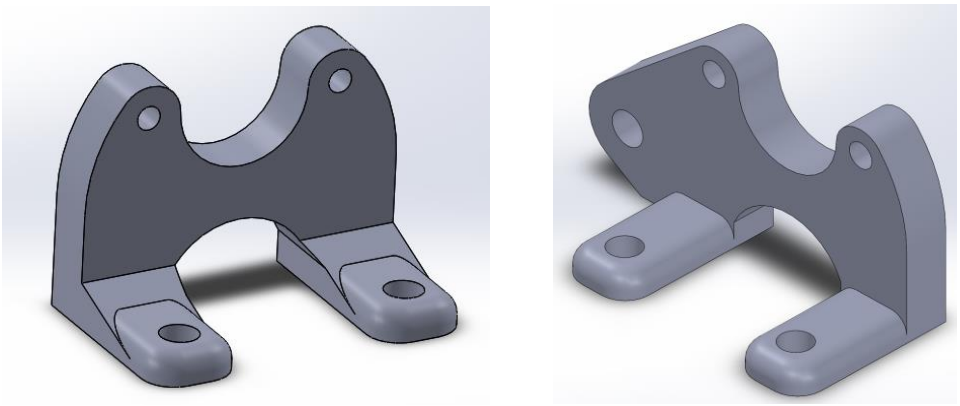

Figure 46: Encoder mounts: convergence (L) and pan (R)

6.6.3 Control Bar Joint & Convergence Slider

The control bar joint and convergence slider were simple in design and had very few design iterations. They were used to translate the motion from the control rod to the eyes. A D-Shaft was used in order to make sure that the motion is translated without slippage as well. The convergence slider was designed to attach to the flanged bearing and also mount to the pan bracket.

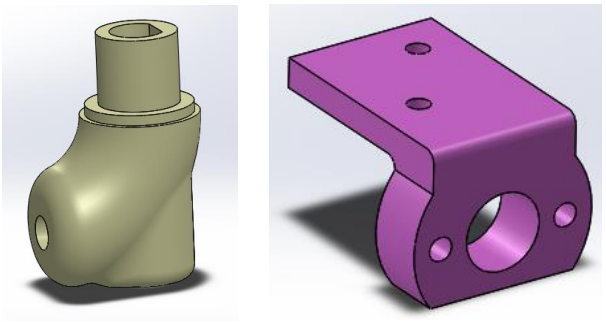

Figure 47: Control bar joint (Left) and convergence Slider (Right)

7 Development of Control Software

Control of the HSV System was split between an Arduino Mega and a PC, connected by USB. The Arduino handled all of the low-level mechanical control of the system, driving the motors and reading the encoders. Meanwhile the PC received images from the cameras, and was responsible for detecting the target face and sending appropriate control commands to the Arduino via serial communications. The basic loop structures of the two programs are shown in Figures 48 and 49 below.

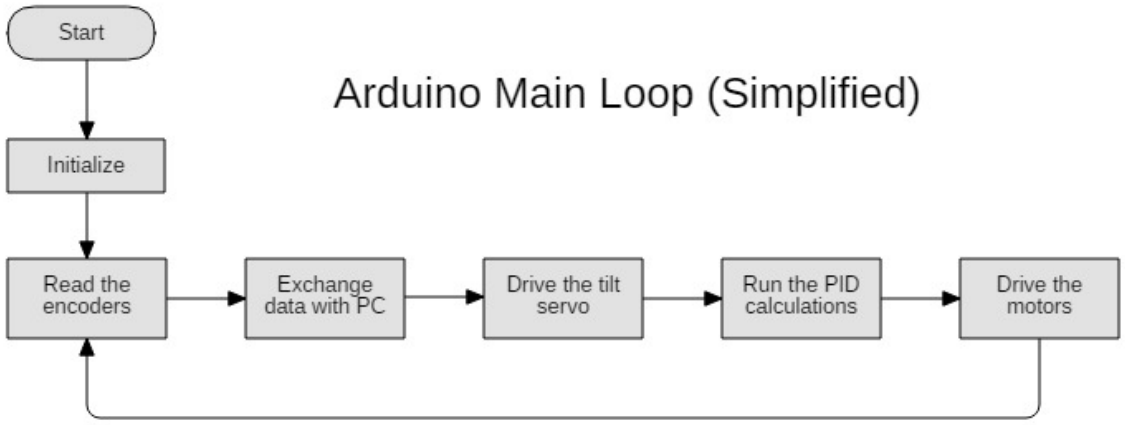

Figure 48: Main loop of Arduino control code

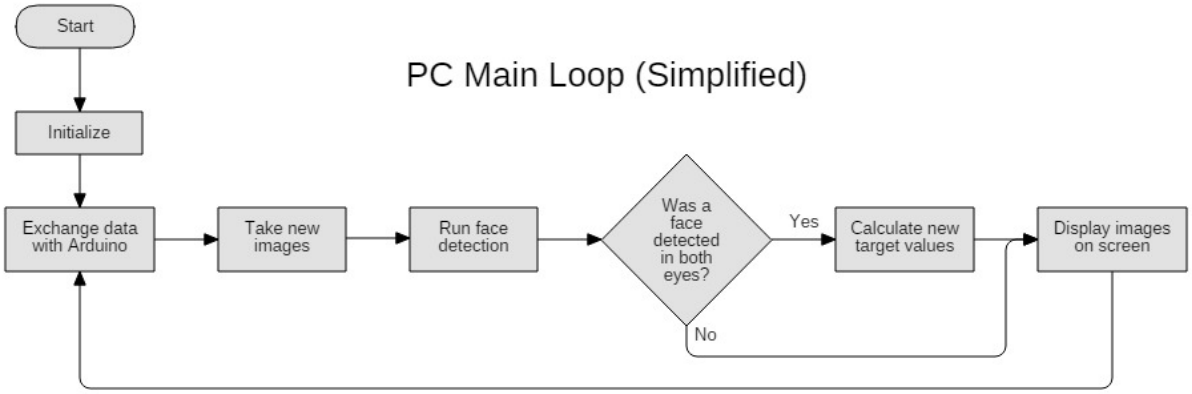

Figure 49: Main loop of PC image processing code

7.1 Arduino Code

The main loop of the Arduino control code was quite straightforward. The encoders are read, data is exchanged with the PC, the servo is driven directly, the PID calculations are updated, and finally the motors are driven. Most of the code lies within those functions.

The encoders were originally supposed to be absolute, so reading them would have been a simple SPI exchange, however an unresolvable fault in the SPI communications rendered that impossible. The encoders also feature an incremental output at the same 4096-count resolution, so instead that was tracked by a heavily optimized library written by Paul Stoffregen (2011).

Combined with a zeroing initialization procedure this library provided the same results as the absolute reading would have.

Serial communication using an Arduino is very straightforward, though a free library written by Thierry Schneider (2001) was used on the PC side, for simplicity. While it is easy to just send the current and target encoder counts back and forth directly, it was quickly realized that some kind of synchronization protocol would be needed in order to prevent errors such as the pan target being received as the convergence target. This protocol went through several inefficient iterations before settling on a much cleaner one. Since the Arduino code looped much faster than the PC code, which has to run the face detection software, the Arduino listened for a specific query character on the serial line and discarded everything else. This character was sent by the PC when it had new target data and thus needed new position data. Once the Arduino was queried, it would send the query character back as confirmation, before transmitting the current encoder positions and then receiving the new target values. Arduino serial transmissions are notoriously slow so this method minimized time spent communicating.

PID control is quite simple to implement at a base level, but another external library, written by Brett Beauregard (2011), was used. The primary advantage of this library was that it had internal timing handling, and timing is key to consistent PID control. The library was able to take in the current and target encoder counts and output a signal within the bounds of the motor drive commands (-255 to 255), with the two motors each handled by their own PID structure.

The motor shield added a small amount of complexity to driving the motors, but was fully described in the data sheet. For each motor two digital pins selected the direction (braked to power, clockwise, counterclockwise, or braked to ground), and then a PWM (Pulse Width Modulation) pin provided an analog signal for the motor power level.

7.2 Face Detection

As discussed in Section 2.4, the OpenCV library contains a function for detecting faces at multiple scales. For each eye this function generated a list of potential faces. These were filtered by size so that only the largest (presumably the closest) face was retained, to eliminate any false positives or background faces.

Initially the face detection software was running at a relatively low refresh rate, approximately 5 Hz. This was caused by two cameras being used at once, doubling the processing

time, as well as the fact that the default parameters of the OpenCV detection function were not ideal for this application. The primary improvement was increasing the scale factor by which the detection window changes after each pass, from a ten percent difference to twenty percent. The other key change was to increase the minimum detection window size from a thirty pixel square to a fifty pixel square, which would still detect faces at the farthest specified range. These two changes together greatly reduced the number of times the detection function passes through the image, bringing the refresh rate consistently above 10 Hz, sometimes as high as 15 Hz. Another potential change tested was the usage of a LBP (Local Binary Pattern) cascade, which uses integers instead of floating point numbers like a Haar cascade. Generally the use of integers should result in faster computation at the cost of precision, especially on lower-level hardware, but in this case there was no significant improvement in speed, so the LBP was not used.

7.3 Interpretation of Faces

It was simple to locate a face within the eye images, but the only location data about that face was pixel coordinates within images. Three different methods were considered for using those two-dimensional coordinates to focus the HSV System eyes on a three-dimensional point. In all cases the tilt of the eyes could be considered separately, since it was controlled directly by a servomotor and was just an independent angle, leaving most of the calculations in the pan-convergence plane.

7.3.1 Relative Positions

The simplest way to utilize the image coordinates was to view them relative to the center of each image. For each eye it could be determined if the face was to the left or right of the center, and the same with above or below. By creating cases for each combination of these relative positions, the motors could be driven in the correct directions without explicitly calculating a true three-dimensional point to be focused on.

The obvious downside to this method is that it was difficult to implement PID (Proportional-Integral-Derivative) control as no positional error could be directly calculated. While PID control could be implemented for a specific convergence depth, the more that depth changed the more sluggish or unstable the control would become. Instead an arbitrary increment would need to be added to the target values, but a constant increment still wouldn’t work. The

angular speed of the eyes had to be taken into account while tracking a face, as it was easy to overshoot a face by incrementing the target by too much, or lag behind too much if incrementing by too little. An increment tuned for a near convergence would be too slow at a far convergence, and vise versa. Despite these drawbacks this method was definitely the simplest of the three and was easy to implement as a back-up early in development.

7.3.2 Trigonometry

The second method was to calculate the three-dimensional focus point using trigonometry. For traditional fixed-camera systems this is a fairly simple task as the angles and positions of each eye are fixed and known, so the distance to an object can be calculated based on the difference between the horizontal position of a point in both images using the following equation:

$$z = \frac{bf}{x'_L - x'_R} \qquad \textit{(eq. 1)}$$

z = distance to target

b = separation of the eyes

f = focal length of camera

x'_L, x'_R = pixel distance of target from center of image

However, the above equation only works for fixed, parallel eyes, and the HSV System had eyes that rotated at different rates, so many of the traditional equations were not adequate on their own. First the eye angles had to be measured, in this case indirectly. The encoders on the pan and convergence motors provided the position of the focal point, which could then be used to calculate the eye angles by these equations and Figure 50 below:

$$\theta'_L = tan^{-1}(\frac{y}{b_L}), \theta'_R = tan^{-1}(\frac{y}{b_R}) \qquad \textit{(eq. 2)}$$

$$b_L = \frac{b}{2} + x, b_R = \frac{b}{2} - x \qquad \textit{(eq. 3)}$$

θ' = eye angle

x = pan of current focal point

y = distance of current focal point

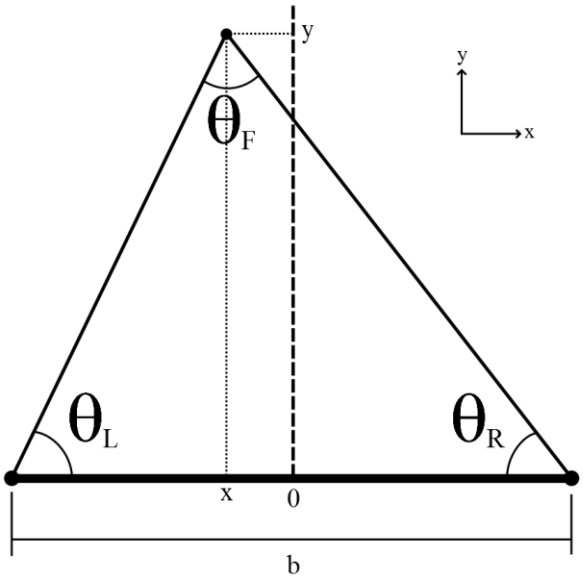

Figure 50: Diagram of eye angles and focal point

Once those angles were known, the angles to the target object from the eye axes could be calculated by mapping a pixel location to an angle with this equation:

$$\theta = \theta' + \tan^{-1}\left(\frac{2\,x\prime\, tan(\frac{HFOV}{2})}{w}\right) \quad \textit{(eq. 4)}$$

x' = pixel distance of face from center of image

$HFOV$ = horizontal angular field of view of the camera

w = pixel width of the image

Then the distance to the target object could be calculated based on the sine rule using this equation:

$$y = b\,\frac{sin(\theta_L)\,sin(\theta_R)}{sin(\theta_F)} \quad \textit{(eq. 5)}$$

$$\theta_F = 180 - \theta_L - \theta_R \quad \textit{(eq. 6)}$$

y = distance to target

b = separation of the eyes

Finally with the distance it was then easy to calculate the horizontal position of the target (since this can be calculated in two equivalent ways, both are just averaged):

$$x = \frac{-b}{2} + b_L = \frac{b}{2} - b_R \quad \textit{(eq. 7)}$$

$$b_L = \frac{y}{tan(\theta_L)}, b_R = \frac{y}{tan(\theta_R)} \quad \textit{(eq. 8)}$$

This method was the most computationally expensive of the three, with numerous trigonometric functions, but in theory would provide the most precise control, along with potentially useful feedback about the 3D location of a face. As such this method was the most promising of the three early on.

7.3.3 Intersection of Two Lines

The final method explored was to use the two target points to draw a line from each eye and calculate their intersection point. Originally the lines were assumed to be three dimensional, factoring in the tilt as well. Since these lines would likely not intersect perfectly it was necessary to calculate their closest approach. However, the HSV System could be considered as having a focal point in cylindrical coordinates, with pan as height, convergence as radius, and tilt as angle. Thus, any tilt discrepancy could be ignored as the two lines effectively projected onto the pan-convergence plane. This results in intersecting two dimensional lines, simplifying the calculations to a pair of determinant based equations for the focal point:

Line 1 described by (x_1, y_1) and (x_2, y_2)

Line 2 described by (x_3, y_3) and (x_4, y_4)

$$P_x = \frac{(x_1y_2 - y_1x_2)(x_3 - x_4) - (x_1 - x_2)(x_3y_4 - y_3x_4)}{(x_1 - x_2)(y_3 - y_4) - (y_1 - y_2)(x_3 - x_4)} \quad \textit{(eq.9)}$$

$$P_y = \frac{(x_1y_2 - y_1x_2)(y_3 - y_4) - (y_1 - y_2)(x_3y_4 - y_3x_4)}{(x_1 - x_2)(y_3 - y_4) - (y_1 - y_2)(x_3 - x_4)} \quad \textit{(eq.10)}$$

While this method seemed simpler than the trigonometric one, it was based entirely on the pixel coordinates of the target object, potentially limiting the accuracy of the system as the images were only 640x480 pixels in resolution. The unit vectors of the lines had to be calculated from the limited pixel count which restricted the angular resolution, and a small focal length which required precise measurement and calibration. As this method offered no considerable advantage over the other two, it was never explored further.

8 Assembly and Troubleshooting

While assembling and troubleshooting the mechanism, a number of problems were identified that had not been previously foreseen. These problems, described in detail in the section below, occurred with the mechanical system as well as with the controls system.

8.1 Mechanical System Problems

The majority of mechanical problems encountered during assembly were related to the alignment of various components. A recurring problem was that the 3D printed eyes were too big, which caused them to interfere with other parts at extremes of the pan, tilt, or convergence ranges. For example, the mechanism could not pan or tilt at all while at minimum convergence, because the eyes hit the bearing blocks used to support the servo shaft. This problem was also encountered when trying to pan all the way left or right while the eyes were tilted, at any convergence. The large size of the eyes also caused their bottom to hit the top of the pan bracket To remediate this problem somewhat, the eyes were sanded down where they were hitting the eye brackets, and the corners were sanded to allow a wider range of motion. By sanding the eyes' corners, the pan angle at the minimum allowable convergence (about 70 cm rather than 50 cm) was increased from about 35° to 42°. This angle could not be increased further because at that point the camera circuits were contacting the bearing blocks. If time (and budget) had permitted, it would have been possible to redesign the eyes to be smaller and find smaller cameras so that there would be no interferences. These are improvements that can be made in a future design.

Another problem encountered in the mechanism was the acrylic platform that holds the pan assembly. Initially, it was found that the center hole that opens space for the convergence nut was not wide enough, and it was causing the nut to produce a bending effect on the platform.

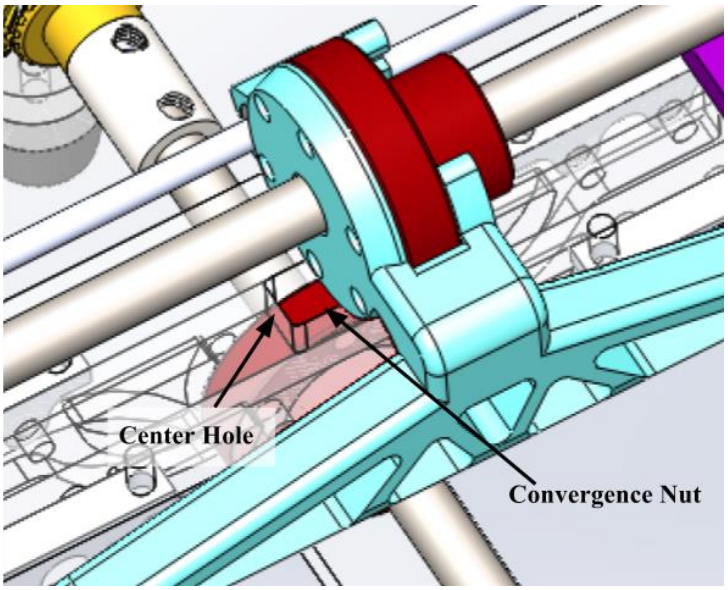

Figure 51: Pan mounting plate problem area

This effect produced interference because the leadscrew pushed upward, causing an upward radial force on the bearing. This misalignment caused friction in the bearing which made it harder to create pan movement. In addition, it was found that the motor shaft coupler was making contact with the bearing because of the reduced space between the motor and the bearing block, producing additional friction in the pan assembly when the pan motor was driving the lead screw. To fix those issues, it was decided to perform some minimal changes to the pan platform by increasing the size of the center hole. This allowed the nut to have enough space through the platform. Also, it was decided to reposition the fastener holes for the motor by moving them back approximately 5 mm. This provided enough space between the motor and the bearing block to eliminate any possible interference.

Upon initial testing of the mechanism, the 2737 rpm worked well enough to pan the eyes at high speeds, but did not work well at lower speeds. This is because to achieve lower speeds, less power was supplied to the motor, which then could not supply enough torque to move the pan movement bracket. A number of small adjustments were made to improve the alignment of pan components and reduce resistance to pan motion. These helped somewhat, but not significantly. The inability to move slowly did not pose a problem for position testing- in this case there was no

need for the eyes to move slowly. However, with face tracking, the motor needed to be able to move fairly slowly to achieve the desired smooth pursuit motion. When face tracking was attempted using the 2737 rpm motor, the movement was discontinuous. Ultimately it was determined that the best solution to this problem was to replace the 2737 rpm motor with a similar 730 rpm motor. This motor has about 3 times as much torque as the 2737 motor, and although it is about 4 times slower, it would still allow the mechanism to achieve the maximum speed specification at minimum convergence.

When connecting the encoder cables to their corresponding encoders, it was found that the pan nut would collide with the encoder connector since the encoder had been mounted facing the nut. Although the possibility of bending the cables was considered, it was decided that it was not the most optimal solution since it could cause damage in the cables. For this reason, it was decided that the best solution was to move the position of the encoder so the cable was facing the motor instead of the lead screw. The encoder mount was modified and repositioned in order to avoid any possible collision and further damage.

One problem encountered was that the 3D printed eye brackets, especially the one on the right, were not perfectly coupled with the d-shaft. Initially the d-channel on the eye bracket was too small to actually fit on the d-shaft, so it was dremeled out to allow the d-shaft to fit. This allowed slightly too much clearance, which allowed the bracket to move independently of the d-shaft. The brackets were reprinted with a channel so they could fit the d-shaft better. The d-shaft fit well in the new part with little to no clearance, but despite the fiberglass reinforcement in the eye bracket, the 3D printed part still allowed the d-shaft to move. As a result, they were able to move a small amount independently from the rest of the mechanism, even once a set screw was added. The free movement was small, but still caused some error in the focus point position. However, this misalignment does not cause any problems with face tracking because any error is accounted for by the camera's feedback.

When preparing the mechanism for final testing, a major problem encountered was a general misalignment in different parts. During initial troubleshooting, the mechanism was run to determine the overall performance, and the lasers did not remain horizontally aligned as expected. After checking the possible components causing the issue, it was found that some parts were slightly misaligned, and even if the misalignment was very small, this error accumulated over time. A major cause of misalignment was found in the universal joints. Since the universal joints are

responsible for providing a specific motion to the eyes, a minor misalignment in one of them could cause both eyes to be completely misaligned. Because there was no available way to make sure that the joints were properly aligned, they were aligned using visual inspection to a point such that they provided close to ideal results. Other parts that showed a general misalignment were the lead screw in the pan assembly. It was found that the lead-screw was not perfectly coaxial with the bearing blocks holding it, because some components were at a slightly higher position than others. In order to fix this issue, washers were added as thin spacers under certain components to raise them and keep everything coaxial as much as possible. Once this modification was made, the lead-screw showed a better performance and its motion was much smoother.

8.2 Control System Problems

The Encoders purchased for this project were originally going to be used as absolute encoders for tracking absolute location of the pan and convergence of the system. However, during troubleshooting, the Arduino was having trouble communicating to the encoders via SPI. Numbers received were random and had nothing to do with the actual location of the system. Due to this issue, the SPI was never implemented, and the encoders are not being used as absolute encoders. Instead, the Arduino is determining rotational position by reading the raw quadrature ticks from the encoder using. A limit switch is used on the pan and convergence motion to zero the system at the beginning of each use.

The cameras in the system were chosen for their small size and resolution. However, many issues were found with the cameras during testing. One of the major issues encountered was the field of view being very limited (26 degrees horizontally), so the display image was significantly smaller than expected. This caused issues with facial recognition; the facial movement had to be much slower so that it would not exit the field of view of the camera before being identified. Another major issue encountered with the cameras was the poor quality of the wires. The camera display would randomly stop responding, and could only be restored after moving or pinching the wires, or resetting the system entirely.

A small issue was encountered with the servo overdrawing the Arduino power supply whenever it started moving. The Arduino would continue operating but would sometimes read false signals from the encoders, leading to an accumulated positional error. This was solved by adding a capacitor to the servo power line in order to smooth out the current draw, but that was

only a quick fix. The issue could be more adequately resolved either with an independent five volt power supply or by routing the twelve volt motor supply through a five volt regulator.

8.3 Face Tracking Problems

The trigonometric approach for tracking faces was prioritized for most of the project, as it seemed to be the most accurate and complete of the three. However even after extensive debugging, the calculated results were still unacceptably inconsistent. The problem was one of sensitivity. A very small discrepancy in the eye angles results in a significant change in convergence. Even though the allowances on joints were fairly tight, there was still enough uncertainty in the system to produce significant errors in the actual eye angles, as compared to the ones calculated from the encoder values. Additionally the calculations were based heavily on precise measurements of the system, such as the separation of the eyes and range of motion of the focal point, which could vary enough to render exact measurements impossible. As a result of this, the code would often think that the eyes were looking at a very different point than they actually were, especially at extreme pan and tilt. The math behind the calculations was all verified extensively, but practically the physical limitations of the system generated large errors by amplifying small angular errors at the focal distance.

After trying numerous methods to fix the trigonometric code, it was finally decided to try the relative method instead. Even at the simplest implementation the resulting behavior of the system was much more consistent, though with a fixed increment of the target value it was quite slow. Work then focused on adding scaling to the incrementation, as well as smoothing out the motion. The first improvement was to base the increment on the average horizontal pixel error of the faces, where error is the distance from the center of the image. When multiplied by some coefficient, this provided a proportional response, though it was still either too slow at distant convergences or too fast close up. The next fix was then to have the coefficient scale along with the current convergence depth, as measured by the encoders. Since the encoders no longer needed to correspond to an exact physical range, they were much more useful. This scaling technique was then applied to pan, convergence, and tilt, resulting in a highly responsive and consistent system.

9 Final Testing and Results

Once the final mechanism was built, it was necessary to test its performance for different target specifications. Testing procedures were developed to measure the overall performance of the new mechanism. By doing this, it would be possible to know if the new design fulfilled the design specifications set at the beginning of the project. Tests conducted include focus point position precision and accuracy, maximum pan (saccadic) speed, and maximum face tracking (smooth-pursuit) speed. The mechanism's capabilities were also examined with regard to additional design specifications.

9.1 Specification 3.1.2: Focus Point Testing

A major goal of the HSV system was to have a final design that could precisely and accurately focus on a given point in space. As a result, focus point position testing was performed on the mechanism to determine positioning errors, and if these errors were consistent and repeatable.

9.1.1 Procedure

The same testing procedure was used for the HSV System as was used for the Motor Eyes mechanism. Please refer to Section 2.5.3.2 for the position testing procedure. The only modification made to the testing procedure was the distance between the white board and the eyes which changed to 50 cm for convenience in recording the points. Along with this, position testing was done with the cameras installed in order to further verify the positioning of the eyes. For testing done with the cameras, a point was placed at the center of the camera's display on the computer, and a dot drawn on the whiteboard exactly at the camera's center point.

9.1.2 Results and Analysis

When testing with the lasers, the mechanism's accuracy was not as good as expected. However, the points were very consistent, which confirms the precision of the mechanism. It was concluded that the lack of accuracy is due to minor mechanical misalignments, as discussed in Section 8.1. The results obtained from testing at the maximum convergence value are shown in

Figure 52. The red dots represent the focus point of the right eye, and the blue dots the left eye. The full sets of results for minimum and middle convergence are shown in Appendix G: HSVS Position Testing Results.

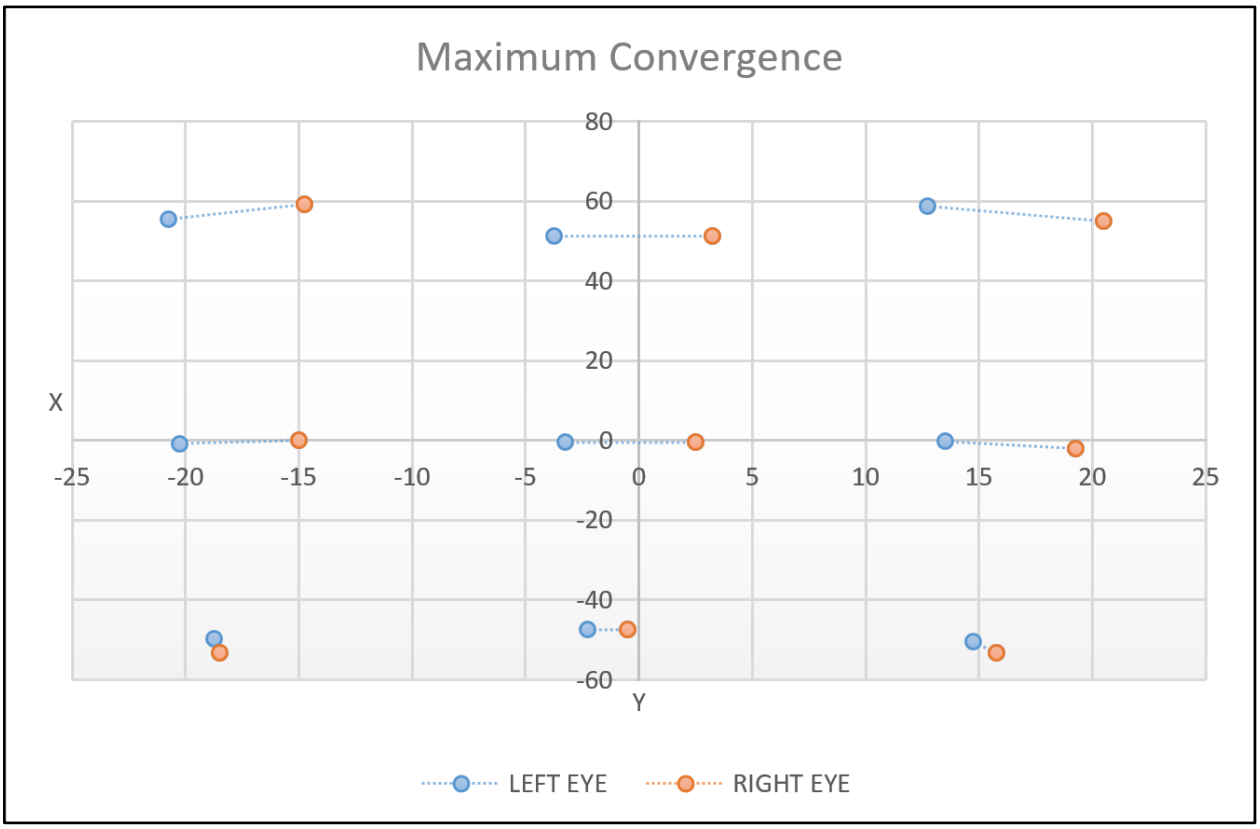

Figure 52: Plot of eye locations at maximum convergence using lasers

When testing was performed with the cameras, the accuracy was better than it was with the lasers. This indicates that the lasers themselves could have been misaligned, causing inaccuracies. Despite this, the system still was not as accurate as expected, but maintained its precision and repeatability. A plot showing the results from maximum convergence is shown in Figure 53. The rest of the results are shown in Appendix G.

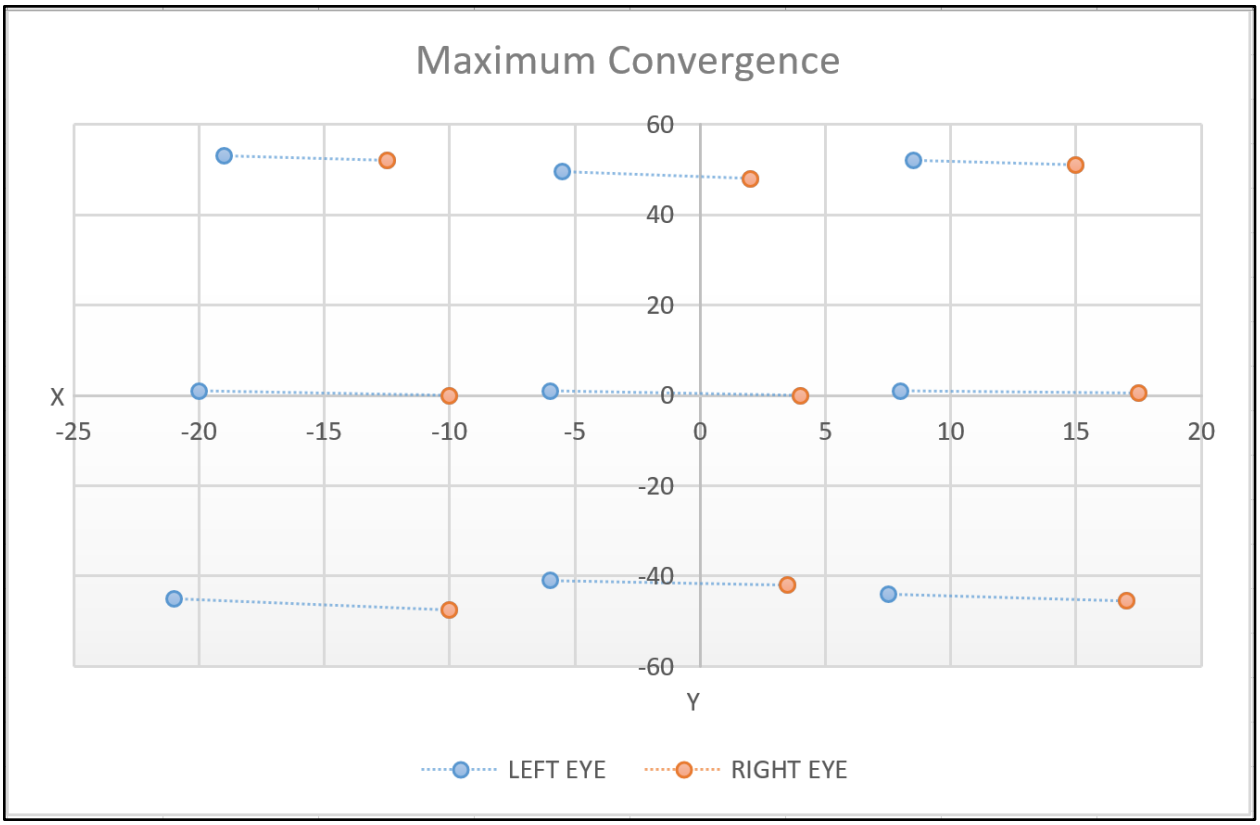

Figure 53: Plot of eye locations at maximum convergence using cameras

By performing different position testing, it was possible to verify the capabilities of the new mechanism when focusing on specific points. From both testing procedures, it was found that the mechanism was very precise, but lacked accuracy. As was the case with the Motor Eyes system, even the smallest misalignment in the eyes causes large errors in focus point position. When comparing the average results obtained using the HSV System and the Motor Eyes, it was observed that the HSVS was considerable more accurate than the Motor Eyes. The results obtained using the new mechanism were closer to the expected points. On the other hand, the results obtained using the Motor Eyes were fairly off from the expected points. When testing multiple times, the HSVS showed very close results repetitively, but the Motor Eyes did not. Refer to section 2.5.3.2 for the Motor Eyes testing results. The results obtained from doing a position testing exhibited the mechanical improvements achieved with the HSV System.

Overall, while it was not perfectly accurate, the HSV system showed improved accuracy over the Motor Eyes system. To gauge the accuracy of the system, the average percent errors were calculated for pan, convergence, and tilt, and compared with those of the Motor Eyes system. The

average percent error was calculated by subtracting the actual pan, convergence, or tilt from the ideal, and dividing by the maximum range value. In the Motor Eyes system, the average error in pan, convergence, and tilt were 76%, 93%, and 10%, respectively. By comparison, the HSV system had error values of 30%, 37%, and 4% for pan, convergence, and tilt when using the lasers pointers. When using the cameras, the average errors for pan, convergence, and tilt were 19%, 17%, and 4%. To gauge the precision of the system, the difference (in cm) between the x and y coordinates on the board for each trial was calculated. These calculations were performed for both the Motor Eyes system and the HSV system in order to compare them. In the Motor Eyes system, the average difference between points ranged from 1.38 cm (with a standard deviation of 2.82 cm) for the y-coordinate of the right eye to 3.57 cm (with a standard deviation of 7.54 cm) for the x-coordinate of the right eye. In the HSV system, the average difference between points ranged from 0.5 cm (with a standard deviation of 0.39 cm) for the x-coordinate of the left eye to 1.0 cm (with a standard deviation of 1.89 cm) for the y-coordinate of the right eye. Overall, the results obtained from doing a position testing exhibited significant system improvements in both position and accuracy of focus point positions.

9.2 Specification 3.1.3: Maximum Eye Velocity

One of the design specifications set for this mechanism was a maximum eye speed of 250 deg/s. This specification was chosen to mimic human saccadic eye motion. The maximum velocity of the eyes was tested, as described below, to determine if this specification was met. The results and the analysis discussed in the next sections show that the maximum eye speed specification was reached.

9.2.1 Procedure

To test the maximum velocity of the eyes, the Motion Capture System in WPI's Soft Robotics Lab was used. The Motion Capture System uses 4 infrared cameras to track any object within its field of vision that has at least 3 reflective markers on it. A group of markers can be grouped as a rigid object, with tracked position and orientation. In order to get more usable position and angle results the motion capture data was streamed to a MATLAB program that calculated and saved the appropriate information in text files.

Three markers were placed on the left eye of the HSV System, as shown in Figure 54 below. These 3 markers were added to the motion capture program as a single rigid body. The eyes were driven from leftmost to rightmost pan values while at minimum convergence. Minimum convergence was used because the angular velocity of the eyes is greatest here for a constant linear velocity of the pan nut. Further convergences were not tested as the slower angular speed is compensated for by the fact that a target moving at the same speed further away would require less rotation to track.

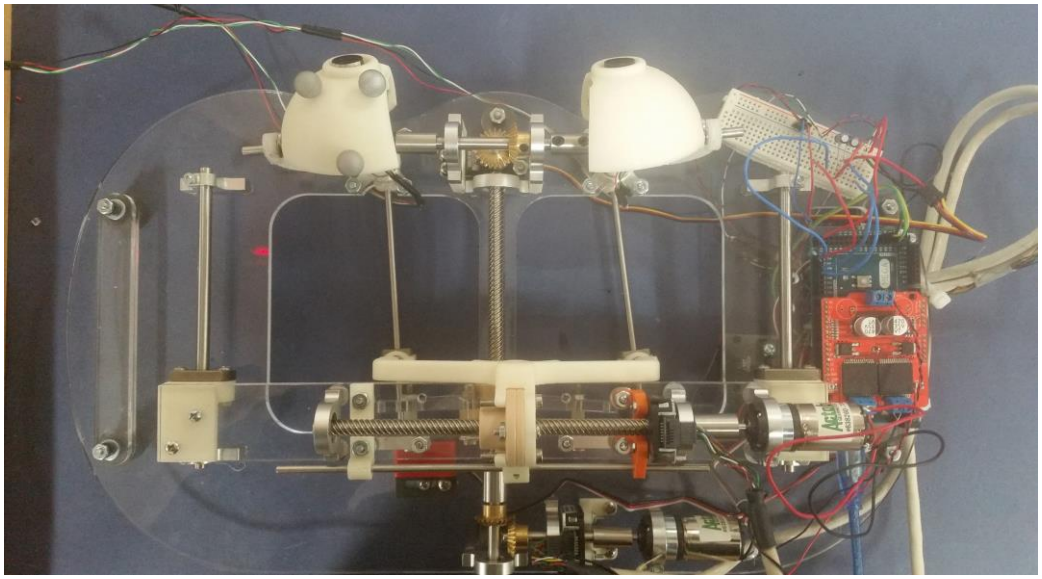

Figure 54: Motion capture setup

A pre-existing Matlab script was used in conjunction with the Motion Capture System to record and graph the angular position of the left eye as it panned from left to right and back at maximum speed. Using the recorded angular position data and the time data, the angular velocity of the eye was calculated. The results of the maximum velocity test are described in the next section.

9.2.2 Results and Analysis

Once the time and angular position data was recorded in Matlab, it was exported to a .csv file, and then plotted. The graph of angular position, in radians, versus time, in seconds, is shown in Figure 55 below.

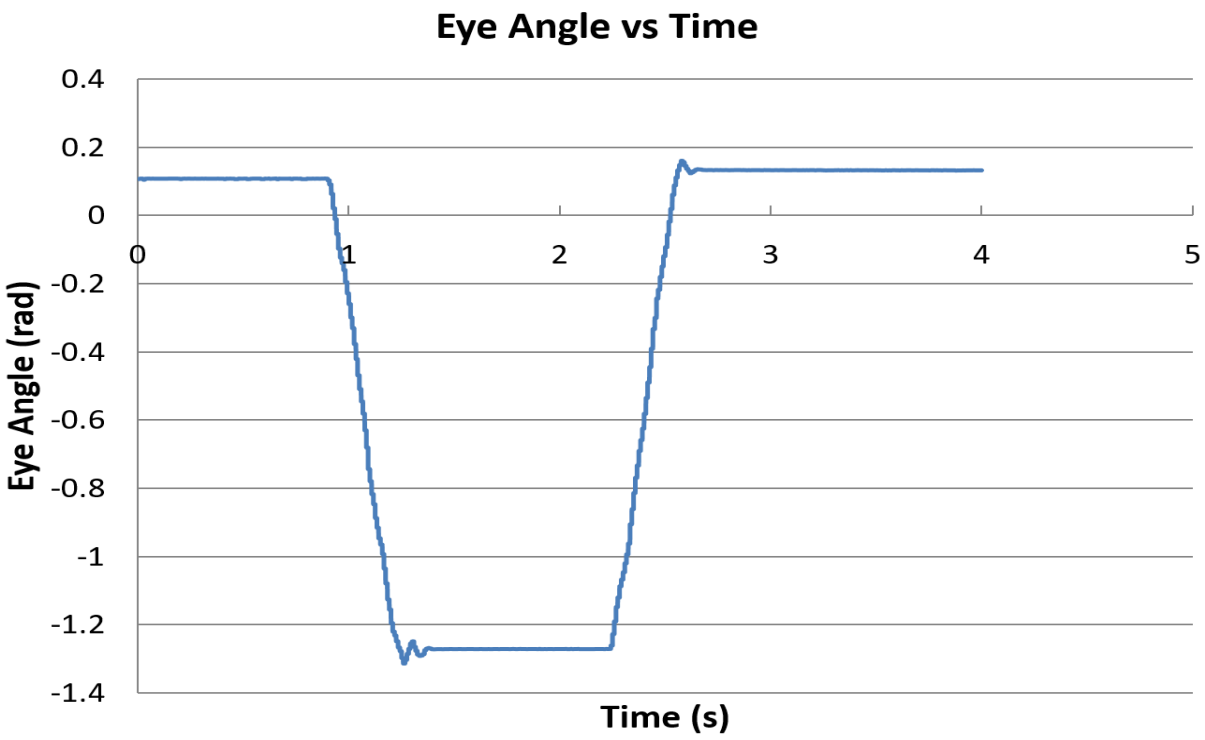

Figure 55: Angular position vs. time for maximum speed test

The average velocity of the eye was determined for both directions by finding the slope between 2 points on either side. For example, when finding the velocity of the eye as it moved left (the negative slope on the graph), the slope of the line between points at t=0.93s and t=1.20s was taken. This slope was calculated to be -4.45rad/s, which translates to an angular velocity of -254.9 deg/s. When moving the other way (to the right), the eye had an average velocity of 259.0 deg/s. The results obtained when moving in both directions confirm that the design specification of 250 deg/s was met.

9.3 Specification 3.5.1: Smooth Pursuit Face Tracking

Another goal for the mechanism was to be able to track a face with a smooth-pursuit speed of 30-100 deg/s. This speed corresponds to the smooth-pursuit speed of the human eye. However, it was largely limited by the quality of the cameras used.

9.3.1 Procedure

In order to complete testing for the smooth pursuit face tracking speed, the Motion Capture System was used again. The markers were put in the same positions on the eye as during maximum velocity testing. A life-sized image of a face was printed, and 3 markers were added to the face printout so that the face speed could later be calculated, if desired. From here, the program was run and the face was manually moved around within the Motion Capture space. The face was moved in such a way that the eyes panned, converged, and tilted. The x-y position of the face was recorded, as was the angle of the eye and the time.

Because the Motion Capture System had a limited field of view (about 1 m^2), the maximum convergence could not be tested. A smaller face, which was half the width and half the height of the original, was printed and moved around in the space at about 1m convergence. This emulated a convergence that was two times greater than the actual convergence. For both tests, the angular velocity was calculated. The results from these tests are described below.

9.3.2 Results and Analysis

The angular position versus time is graphed in Figure 56 below for the large face, which is moved around between about a 0.5m and 1m convergence.

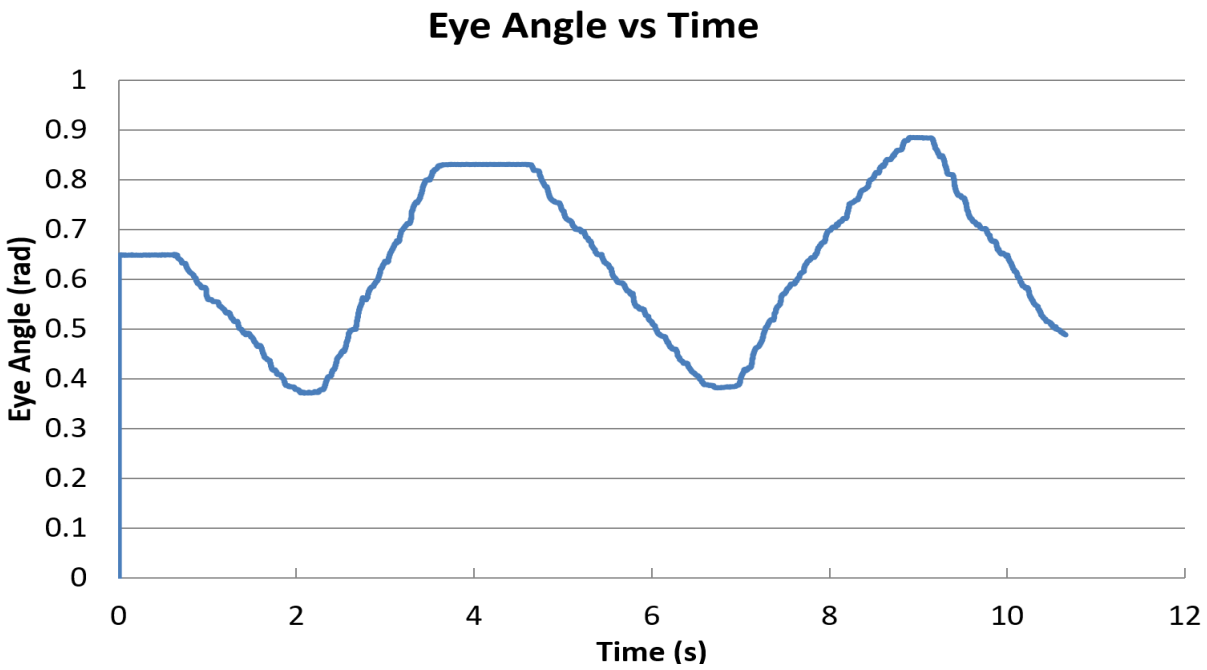

Figure 56: Angular position vs. time for maximum speed test

The slope of the line was calculated at multiple points to find the maximum value. Between t=7.12 and t=7.32, the average velocity was calculated to be 24.5 deg/s, which does not quite fall into the smooth-pursuit speed range. This is because the larger face takes up almost the entire field of vision of the camera, so if it moves a small amount, it is off the screen and not being detected by the camera. As a result, the face could not be moved quickly for this test.

Figure 57 below shows the graph for angular position versus time when tracking the smaller face, which emulates about a 2m convergence.

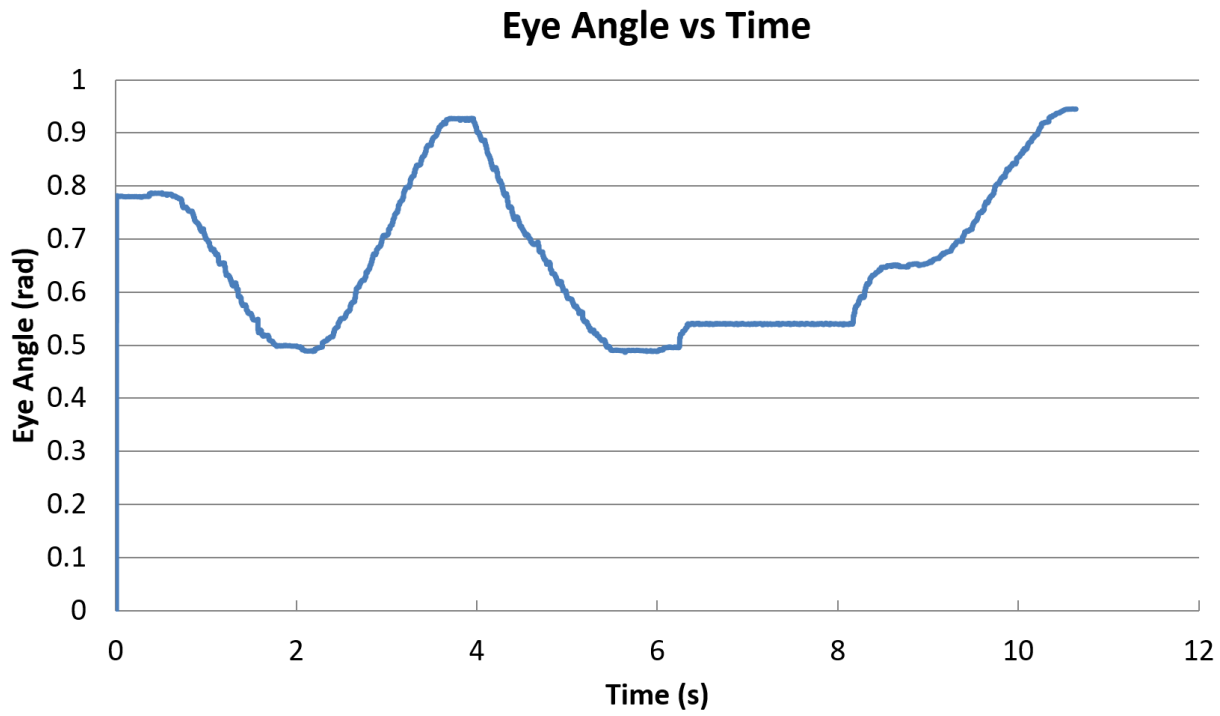

Figure 57: Angular position vs. time for smooth pursuit test

The same procedure was used as the one described above; multiple different slopes were calculated to determine the maximum. The maximum slope was found between t=4.09s and t=4.15s, and the speed was -31.2 deg/s. In this case, the face was allowed to move faster before the system lost track of it, although it still could not move very fast because the camera's refresh rate was still fairly slow. However, it moved slightly faster than with the large face, and this speed falls within the desired smooth-pursuit range. The smaller face could move further in the limited field of view before no longer being detected, which combined with the slow refresh rate of the system meant that higher speeds could be achieved.

9.4 Additional Design Specifications

A number of other design specifications were set that did not require formal testing to verify. One design specification (3.3.2) was to have a convergence range of 0.5 to 2.5m. In the final mechanism, the convergence range was 0.7 to 2.5m. The mechanism was technically able to reach the minimum convergence of 0.5m, but it could not pan very far because the circuit boards of the cameras would collide with the bearing blocks being used to support the tilt shaft. Another design specification (3.3.3) was to be able to pan 45^o left and right. The mechanism should have been able to do this at zero tilt and minimum convergence. However, when the eyes were tilted up or down at minimum convergence, they could only pan to 42^o because once again the eyes would collide with the bearing blocks. Finally, according to the design specifications (3.3.1) the eyes should have been able to tilt 45^o up and down. In the final mechanism, they were able to easily tilt this much or more, if desired. Thus, the system met the tilt specifications, and almost met the pan and convergence specifications. If the eyes are redesigned to be smaller, the system can meet all three specifications.

Another design specification (3.4.2) was that the new system should not increase the overall footprint or size of the old system. The old system was 43.18 x 35.56 x 12.09cm (L x W x H), and the new system is 25.76 x 45.21 x 11.40cm (L x W x H). The overall height of the system was about the same. The total area taken up by the new system (1165 cm^2) was 76% of that of the old system (1535 cm^2). The width of the new system, which was its largest dimension, was only slightly larger than the largest dimension of the old system (the length). By comparison the length of the new system was considerably less than the width of the old system. Overall, this design specification was met.

The mechanism had a design specification (3.2.2) for desired resolution for all three movements, meaning smallest amount of movement achievable by the system. The desired convergence resolution was 5 cm, the pan was 2 cm, and the tilt was 1 deg. It was determined based on the encoder resolution and lead screw lead amount that both pan and convergence had a resolution of 0.35cm. Based on the Servo range and Arduino resolution, the tilt resolution was about 0.1 deg. Hence these specifications were met.

A final specification (3.2.3) was that the eyes' control system should be able to calculate the focus position within 1 deg of accuracy. This means that the system should have been able to achieve the desired focus point position to within 1 deg for tilt and 1 deg for pan and convergence

combined. To measure this, angular error values were calculated based on the position testing data. The angular error in tilt was simply calculated by subtracting the actual (calculated) tilt angle of the eyes from their ideal (target) tilt angle. The average tilt error was determined to be 1.40 deg. The angular error for pan and convergence were calculated together using a similar method, by subtracting the actual angle of each eye from the ideal angle of each eye. The average error for the left eye was 1.05 deg, and the average error for the right eye was 2.01 deg. None of these results met the desired specification for position accuracy. However, this did not cause a problem when face tracking using the relative method because the eyes are driven until they are actually focused on the face, rather than being told to focus on a particular point in space where the face is thought to be located.

Table 2 below lists all quantifiable specifications for mechanism performance along with the physical mechanism's corresponding measured or tested values.

	Specification Number	**Design Specification**	**Mechanism capability**
Maximum (saccadic) velocity	3.1.3	250 deg/s	259.0 deg/s
Maximum (smooth-pursuit) velocity	3.5.1	30-100 deg/s	31.2 deg/s
Maximum size	3.4.2	43.18 x 35.56 x 12.09 cm	25.76 x 45.21 x 11.40 cm
Resolution	3.2.2	Pan 2 cm Convergence 5 cm Tilt 1 deg	Pan 0.35 cm Convergence 0.35 cm Tilt 0.1 deg
Focus position accuracy	3.2.3	Tilt 1 deg Pan/ convergence: Left eye 1 deg Right eye 1 deg	Tilt 1.40 deg Pan/ convergence: Left eye 1.05 deg Right eye 2.01 deg
Field of vision	3.3.3 3.3.2 3.3.1	Pan ± 45 deg Convergence 0.5-2.5 m Tilt ± 45 deg	Pan ± 42 deg Convergence 0.7-2.5 m Tilt ± 45 deg

Table 2: Mechanism Capabilities

10 Conclusion

The HSV System was designed based on the earlier Motor Eyes mechanism (2014) in order to create a robotic system capable of mimicking the motion of human eyes. By using a pair of cameras resembling human eyes, a refined linkage mechanism, closed loop control, and image processing algorithms, the HSV System was able to smoothly and responsively tracking a face in front of it. This ability provides the possibility for social robotics applications in the future. Figures 58 and 59 below show the mechanism in operation tracking a face as well as the face detection in use.

Figure 58: HSV System tracking a face

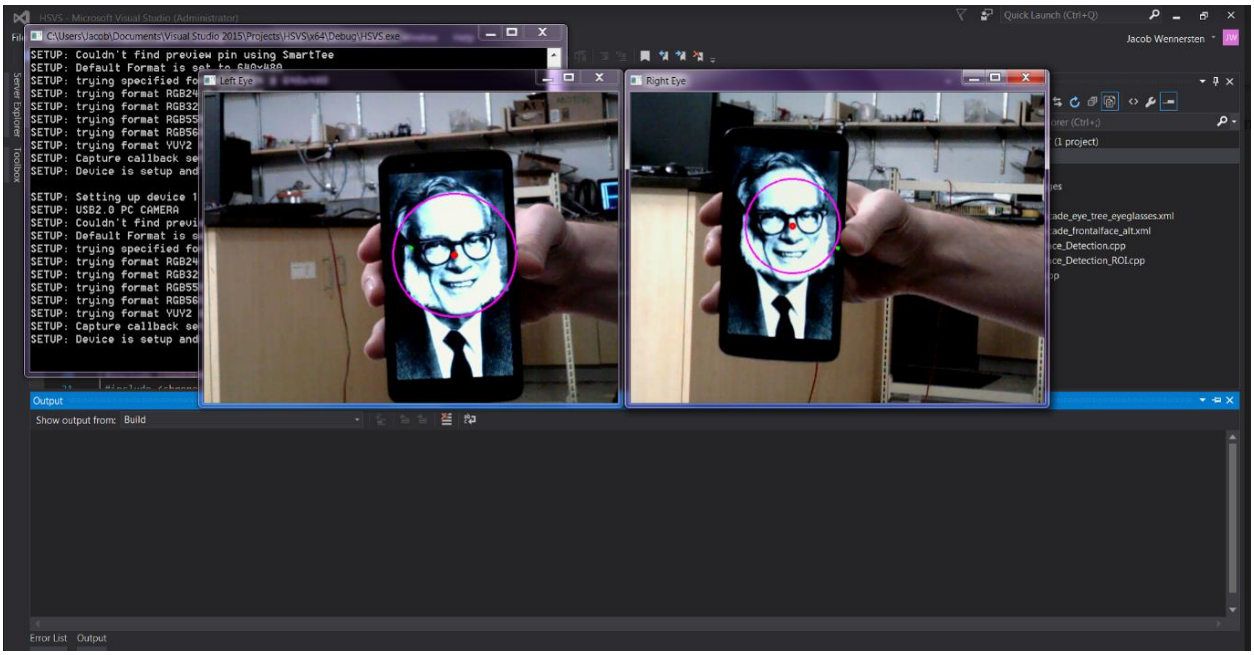

Figure 59: HSV System face detection

The HSV mechanism was built using a combination of purchased and custom-made components aiming to obtain the most satisfactory results obtainable within the resource limits of the project. The new design was tested comprehensively to determine the overall performance of the mechanism. Testing results showed the overall mechanism's capabilities satisfy almost all of the initial specifications set for the project. For specifications not satisfied, the mechanism came close, indicating that small modifications will be sufficient to meet them in the future, if desired.

The HSV System overall has proven to be extremely precise and repeatable. Although the mechanism is not completely accurate all the time, the image processing and control software compensate for any error in pan, convergence, or tilt during face tracking. In addition, the specifications for maximum eye velocity and smooth pursuit speed were met, and smooth pursuit speed can be increased significantly in the future with better cameras.

Two of the major problems found with the HSV system were the camera's tight field of view and the low processing rate of the face detection, which severely limited the mechanism's face tracking abilities. Although the issues mentioned before and the tracking velocity can be greatly improved by obtaining more appropriate cameras, the chosen components still provided the desired results. Additionally, the mechanism showed a very smooth motion during operation, reducing possible vibrations that might affect the image of the cameras and thus limit the success of face tracking. Overall, the performance of the HSV System is satisfactory, and is a significant

improvement over the Motor Eyes mechanism. Although there is always a possibility for improvement, the chosen components and the analyses performed produced a final mechanism that proved that the final goals for this project were achieved. Some recommendations for future work and improvements are included in the section below.

10.1 Recommendations

While this project was completed successfully, there are still many points that can be improved.

1. *Reduce the size of the eyes.* This will reduce potential interferences at extreme convergence, pan, and tilt values, which will result in a larger range of vision for the system.
2. *Increase PC processing power and study efficiency improvements in image processing.* This will improve the performance of the face tracking to allow for a more optimized performance and faster facial recognition.
3. *Obtain smaller cameras with a larger resolution and field of view.* Cameras with a wider field of view would be more successful in face tracking, because the face would remain in view for a longer time, so the face will not get lost by the eyes as easily. Also a faster shutter speed would help reduce motion blur of the face, improving retention when the face is moving erratically.
4. *Get the encoders to work as absolute encoders.* This will allow the absolute position of the eyes to be known at all times so that they do not need to be zeroed with every use, as well as eliminating the possibility of accumulated position error.
5. *Possible future social application.* A possible future application for this mechanism is in providing therapy for children with autism. Research has found that social robots can potentially interact with children with autism since their actions are perfectly repeatable and can be modified to meet the requirements of different children. Currently, social robots can be used as tools for children with autism to play and to elicit certain desired behaviors from them (MIT Technology Review, 2013). Autistic children also have difficulty making eye contact with people. A more sociable external appearance could be designed and added to the HSV system, and the eyes specifically could be used to help children with autism feel more comfortable making eye contact.

Work Cited

Alexander, E. (June, 2011). Affordable Compact Humanoid Robot For Autism Spectrum Disorder in Children (Project Number: MQP GSF M112). Retrieved from https://web.wpi.edu/Pubs/E-project/Available/E-project-060111-155513/unrestricted/AutismRobotMQP_FinalReport.pdf

Atta, T. (March, 2014). Advantages & disadvantages of different types of gears. Retrieved from http://www.green-mechanic.com/2014/05/advantages-and disadvantages-of_7.html

Beauregard, B. (2011). *Arduino PID Library* (Version 1.1.1) [Computer program]. Retrieved from http://playground.arduino.cc/Code/PIDLibrary

British Heart Foundation. (n.d.). *Walks and treks- FAQs.* Retrieved from https://www.bhf.org.uk/get-involved/events/training-zone/walking-training-zone/walking-faqs

Brown University. (n.d.). Smooth Pursuit. Retrieved from http://www.brown.edu/Departments/Engineering/Courses/122JDD/Lcturs/SPlec03.htm

Buildmedia. (n.d.) Field of View. Retrieved from http://buildmedia.com/portfolio-items/what-are-survey-accurate-visual-simulations/

Changing Minds. (n.d.). Social Distance Retrieved from http://changingminds.org/techniques/body/social_distance.htm

Chen, C. (August, 2011). Personal Website and blog about Robot. Retrieved from http://chienpinchen.blogspot.com/2011/08/robotic-eye-mechanism-design.html

Chilson, L. (2013). The Difference Between ABS and PLA for 3D Printing. Retrieved from http://www.protoparadigm.com/news-updates/the-difference-between-abs-and-pla-for-3d-printing/

Csanyi, E. (November, 2013). Few Words About Stepper Motor (Advantages, Disadvantages and Classification). Retrieved from http://electrical-engineering-portal.com/few-words-about-stepper-motor-advantages-disadvantages-and-classification

Cyro. (n.d.). Physical Properties of Acrylite FF. Retrieved from http://www.sdplastics.com/acryliteliterature/1121DFFPhysicalProperties%5B1%5D.pdf

Dautenhahn, K. (April, 2007). Social Intelligent Robots. Retrieved from http://rstb.royalsocietypublishing.org/content/362/1480/679

Engineers Edge. (n.d.). Common Plastic Molding Design Material Specification. Retrieved from http://www.engineersedge.com/plastic/materials_common_plastic.htm

Ford, C. , Bugmann, C, Culverhouse, P. (March, 2010). Eye Movement & Facial Expression in Human-Robot Communication. Retrieved from http://www.tech.plym.ac.uk/soc/staff/GuidBugm/pub/KEER2010_paper_FINAL.pdf

Gere, J. (n.d.).Moduli of Elasticity and Poisson's Ratio. Retrieved from http://www.essom.com/upload/eng_data/23.pdf

IntoRobotics. (March, 2013). Overview of Robotic Vision - Object Tracking and Image processing Software. Retrieved from https://www.intorobotics.com/overview-of-robotic-vision-object-tracking-and-image-processing-software/

Kiely, W. , Yee, W. , Rappoli, O. , Strobel, B. , Walcott, R. (April 2014). Motor Eyes (Project Number: MQP ME-CDO-1301/1302). Retrieved from https://web.wpi.edu/Pubs/E-project/Available/E-project-042814-233707/unrestricted/MotorEyes_MQP_Final_Report.pdf

Leadshine Technology Co, Ltd. (n.d.). Motor Torque Calculation. Retrieved from http://www.leadshine.com/pdf/calculation.pdf

Lim, A. (April, 2014). What Robot Behavior Makes People Feel Uncomfortable? Retrieved from http://spectrum.ieee.org/automaton/robotics/artificial-intelligence/what-robot-behavior-makes-people-feel-uncomfortable

MakerBot. (n.d.). PLA and ABS strength data. Retrieved from https://eu.makerbot.com/fileadmin/Inhalte/Support/Datenblatt/MakerBot_R__PLA_and_ABS_Strength_Data.pdf

Markforged. (n.d.). Mechanical properties of Continuous Fibers. Retrieved from https://markforged.com/materials/

Microsoft Cognitive Services. (n.d.) Face API. Retrieved from https://www.microsoft.com/cognitive-services/en-us/face-api/documentation/overview

Owen-Hill, A. (July, 2016). Robot Vision vs Computer Vision: What's the Difference? Retrieved from http://www.roboticstomorrow.com/article/2016/07/robot-vision-vs-computer-vision-whats-the-difference/8484

Plexiglas (n.d.). Average Physical Properties of Plexiglas. Retrieved from http://www.associatedplastics.com/forms/acrylic_plastics_data.pdf

Prospector. (n.d.). Acrylic Typical Properties Generic Acrylic. Retrieved from https://plastics.ulprospector.com/generics/3/c/t/acrylic-properties-processing

Rebuild Your Vision LLC. (n.d.). What is depth perception and how important is it?. Retrieved from http://www.rebuildyourvision.com/blog/interesting-vision-facts/depth-perception-important/

Reed, F. (March, 2013). How Do Servo Motors Work. Retrieved from http://www.jameco.com/jameco/workshop/howitworks/how-servo-motors-work.html

RobotWorks. (n.d.). What is robot vision? Retrieved from https://www.robots.com/faq/show/what-is-robot-vision

Rommelse, N., Van Der Stigchel, S., Sergeant, J. (December, 2008). A review on eye movement studies in childhood and adolescent psychiatry. Retrieved from http://www.sciencedirect.com/science/article/pii/S0278262608002704

Rosebrock, A. (January, 2016). Real-time panorama and image stitching with OpenCV. Retrieved from http://www.pyimagesearch.com/2016/01/25/real-time-panorama-and-image-stitching-with-opencv/

Schneider, T. (April 8, 2001). *Serial Communication for WIN32*. Retrieved from http://www.tetraedre.com/advanced/serial/

Stoffregen, P. (2011). *Encoder Library* (Version 1.2). Retrieved from https://www.pjrc.com/teensy/td_libs_Encoder.html

SubsTech, (n.d.). Estimations of Composite Materials Properties. Retrieved from http://www.substech.com/dokuwiki/doku.php?id=estimations_of_composite_materials_properties

Tearle, M. (May, 2009). Animatronics. Retrieved from http://marshalltearle.wix.com/props#!contact/c16fm

The Engineering ToolBox. (n.d.). Properties of common Solids. Retrieved from http://www.engineeringtoolbox.com/density-solids-d_1265.html

Viola, P. , Jones, M. (2004). Robust Real-Time Face Detection. Retrieved from http://www.vision.caltech.edu/html-files/EE148-2005-Spring/pprs/viola04ijcv.pdf

Appendix A: Theoretical Sensitivity Analysis of Motor Eyes Mechanism

A basic sensitivity analysis was performed on different parts of the mechanism to determine how the potential error in certain parts, or unwanted movement caused by clearance in joints, would theoretically affect the focus point of the mechanism.

The figures below are screenshots of the Matlab script used to calculate the error in the focus point. The x- and z- coordinates, or pan and convergence, of the focus point were calculated by finding the intersection of the two lines parallel to the control arm sliders and coincident to the eyes themselves. This is shown in Figure 60 below.

```
function [ xfocusr, zfocusr ] = FocusError( b,lc,p,c,sideOff,degOff )
%calculates focus point for a number of input parameters
    %b: distance between eyes
    %lc: effective control bar length
    %p: input pan discance-- offert of pan slider from center
    %c: input convergence distance-- offset of convergence slider from eyes
    %sideOff: linear offset of eyes
    %degOff: angular offset of right eye


distRighttoCenter= (abs(p-(lc/2)))-sideOff;
distLefttoCenter= lc-distRighttoCenter;

syms x
slopeRth=(c/((distRighttoCenter-b/2))); %slope of line through right eye, no angular error
thetar=atan(slopeRth); %angle (in rad) of this slope relative to the horizontal
mlr=tan(thetar-degOff*pi/180); %slope of line through right eye eith angular error included
mrr=(c/(b/2-prr)); %slope of line through left eye

zlxr=mlr*(x+b/2); %equation of the line representing the "laser" from the right eye (in x-z plane)
zrxr=mrr*(x-b/2); %equation of hte line representing the "laser" from the left eye

xfocusr=double(solve(zlxr==zrxr));
zfocusr=double(subs(zlxr,xfocusr)); %calculates the intersection of these 2 lines, [pan, convergence]

end
```

Figure 60: Matlab function used to calculate focus point position.

The error was calculated by keeping most parameters constant and set at an ideal value, and varying a single parameter over a specified range. In the script there were 3 very similar loops, each of which varied a different parameter while keeping all other parameters constant. The ranges used for each varied parameter is shown in Figure 61 below. Pan and convergence were kept constant for each loop, but error was calculated and plotted for a number of different pan-convergence combinations were. The first loop, used for calculating and plotting error due to changing distance between the eyes, is shown in Figure 62 below. This loop kept angular offset of

the laser mount/ L-bracket and the effective control bar length constant, and varied the distance between the eyes from 12.4 cm to 12.6 cm.

```
b=12.4:.01:12.6; %distance between eyes
lc=13:.01:13.2;  %effective control bar length
degOffset=[-.35:.05:.35]; %angular offset of single L-bracket

p=5;    %input pan discance
c=13.1; %input convergence distance

%FocusError(b,lc,p,c,sideOff,degOff) is a function that calculates focus point for these inputs :
           %distange between eyes,
           %control bar length, pan
           %input pan distance,
           %input convergence distance,
           %angular offset of left  eye (in deg)
           %linear offset of eyes
```

Figure 61: Input ranges for Matlab script error calculations.

```
figure
for i=1:1:length(b)
    [XF, ZF]=FocusError(b(i),13.1,p,c,0,0); %calcuates focus point; only distance b/w eyes changes
    xerr=(abs(XF-XFI)/104)*100; %error relative to maximum range
    zerr=(abs(ZF-ZFI)/273)*100;
    scatter (b(i)-12.5,xerr,'*','r') %plots error vs change in control bar length
    hold on
    scatter (b(i)-12.5,zerr,'b')
    hold on
    title('Relative Percent Error caused by Separation in Eye Joints, Max-Pan Max-Convergence')
    xlabel('Movement of Eyes relative to eachother (cm)')
    ylabel('Relative Error (error/ Max focal point)')
    legend('Pan', 'Convergence')
end
```

Figure 62: Matlab script used to calculate focus point error.

It was determined that for any varied parameter, the maximum error occured at the maximum convergence and maximum absolute pan. Scatter plots of Error vs Varied Parameter were consequently generated for the maximum convergence and pan in order to display the maximum error. These plots are displayed throughout the remainder of this section.

The type of error first analyzed was a variation in the distance between the eyes due to the clearance between the eye axles and their plastic bearings (joint shown in Figure 63).

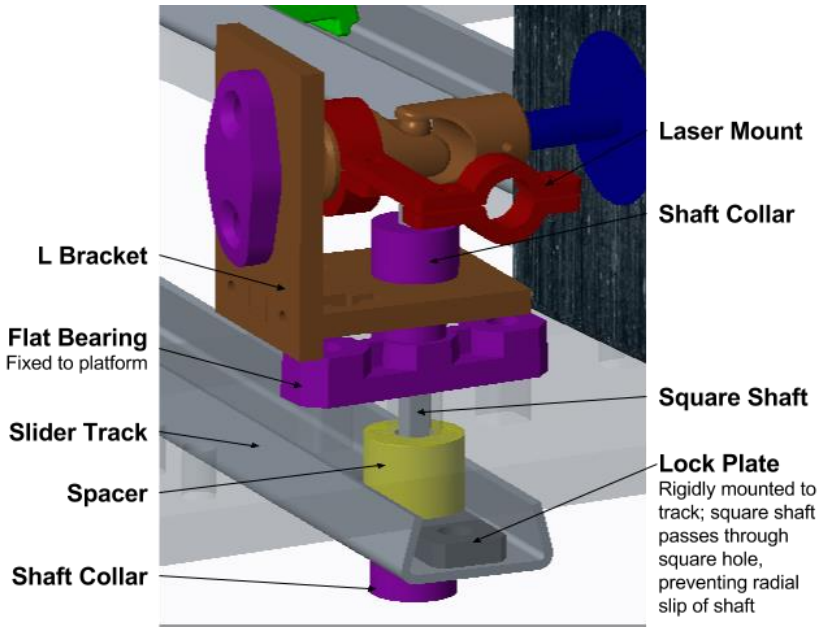

Figure 63: Laser mount and components.

Based on measurements taken of VEX axles and plastic bearings, which were used in the previous mechanism, it was determined that the distance between the eyes could change by up to 1 mm in either direction. A Matlab script was used to calculate the actual x (pan) and z (convergence) coordinates for a set of input eye distances while keeping all other inputs constant. The focus point error was calculated and plotted for a number of different target focus points and for movements of the eyes relative to each other ranging from -1 mm to +1 mm.

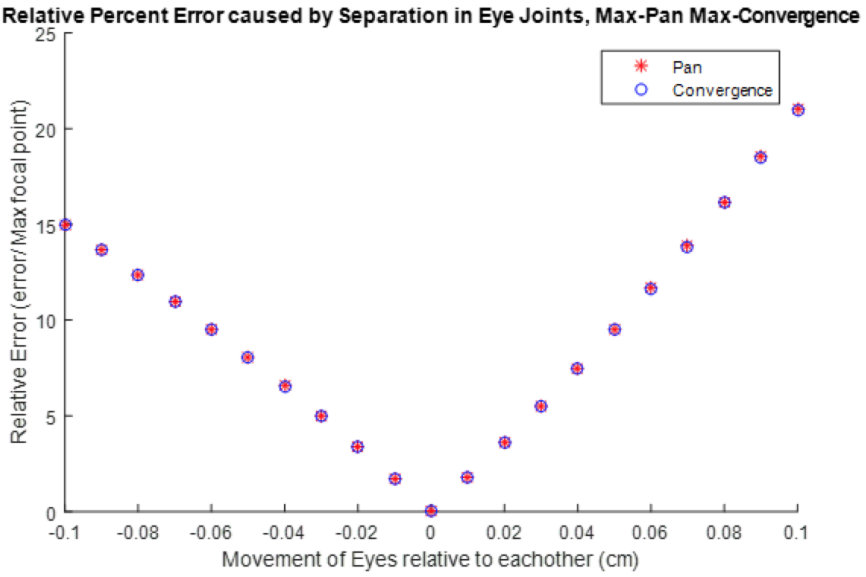

Figure 64: Error caused by change in distance between eyes.

The percent error was calculated by subtracting the error coordinates from the target coordinates and dividing the absolute value of that discrepancy by the maximum pan (104 cm) or convergence (273 cm) values of the system. The maximum percent error in focus point was found to be about 22% for both pan and convergence.

The source of error examined was the consequence of changes in the effective control bar length. This could be caused by clearance between the control arm slider and slider-track, as well as the movement present in the connection between the control bar and the control arm sliders shown in Figure 65. Error in focus position was determined for a change in effective control bar length ranging from -1 mm to +1 mm.

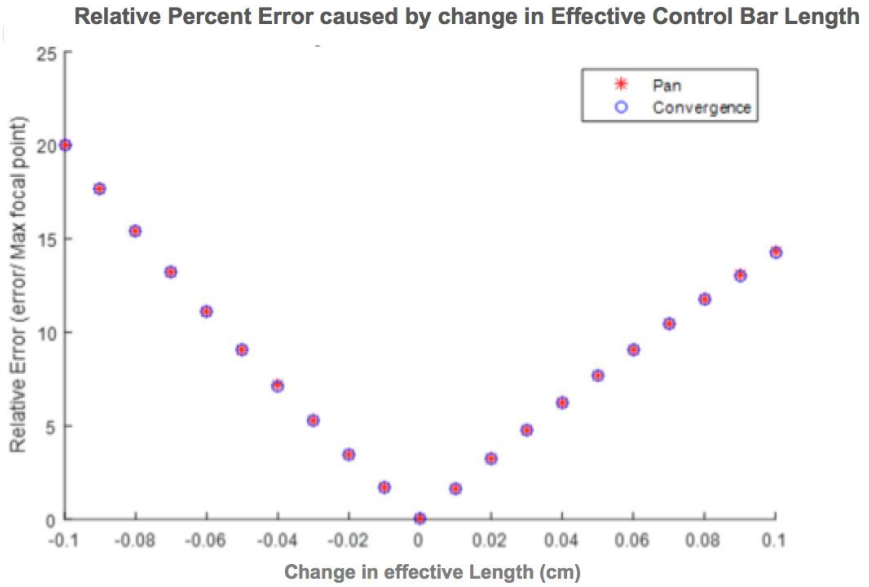

Figure 65: Error caused by change in effective control bar length.

The maximum error found for this scenario was 20% for both pan and convergence which is less than the error caused by movement in the eye joints. However, it should be noted that the movement in this joint is much less predictable in direction and magnitude than in any other on the mechanism, potentially allowing for much more error than what was calculated.

Finally, the error was calculated for misaligned eye rotation up to 1 degree in either direction. This is a problem that was encountered by the previous team, and could be caused by a misalignment between the L-bracket holding the eyes in position as discussed above.

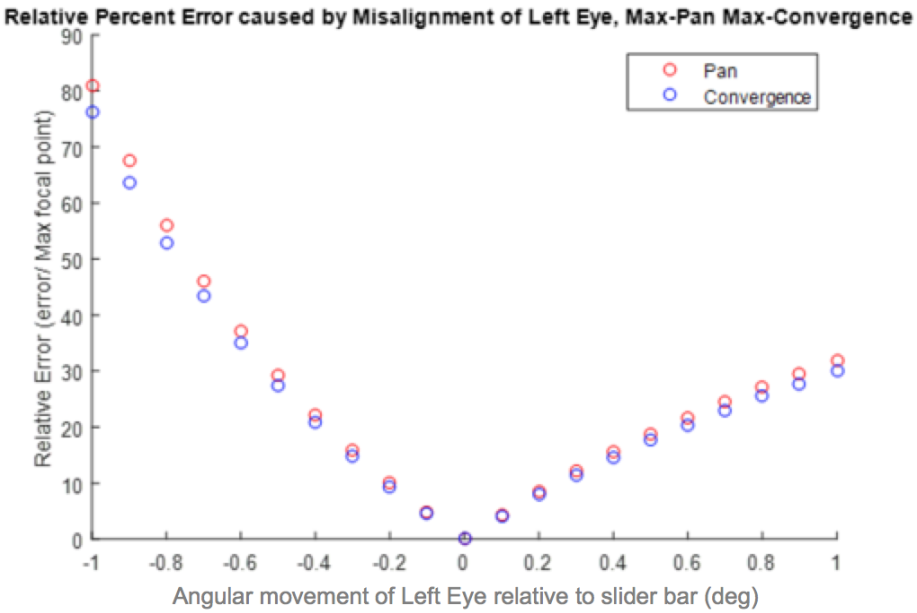

Figure 66: Error caused by angular misalignment of left eye.

The error was calculated using the same method as for the previous two scenarios, and the maximum error was found to be 81% for pan and 76% for convergence. This is considerably larger than the error caused by allowances in the joints, thus it can be concluded that maintaining the alignment of the eyes relative to the control arm sliders is crucial to achieving an accurate focus position, and should be a primary goal in the redesign.

From the above analysis, it was determined that even small errors in the inputs tested would result in very large focus point position error. Hence, it was determined that the mechanism would need to be redesigned with components with smaller clearances to allow fewer opportunities for error.

Appendix B: Motor Eyes Testing Results

The initial testing of the mechanism created by the past MQP group was performed by using a wide writing board. This was done in order to have enough space to visualize the results since some of the points could potentially take place in unmeasurable areas such as floor, ceiling, etc. if a wide range of space was not being used. There were 27 points to be tested a total of two times each by using different determined values for convergence, pan, and tilt for which the final output had been previously calculated by the previous group. The coordinate positions of each laser pointer, right and left, were recorded, and the target and actual positions for all points were plotted in a Cartesian coordinate system in order to understand and visualize the discrepancy between the target and actual positions. The plotted results are shown in Figures 67 and 68. It is readily apparent that the mechanism had fairly accurate tilt control, but never panned as far as it should and could not retain eye alignment.

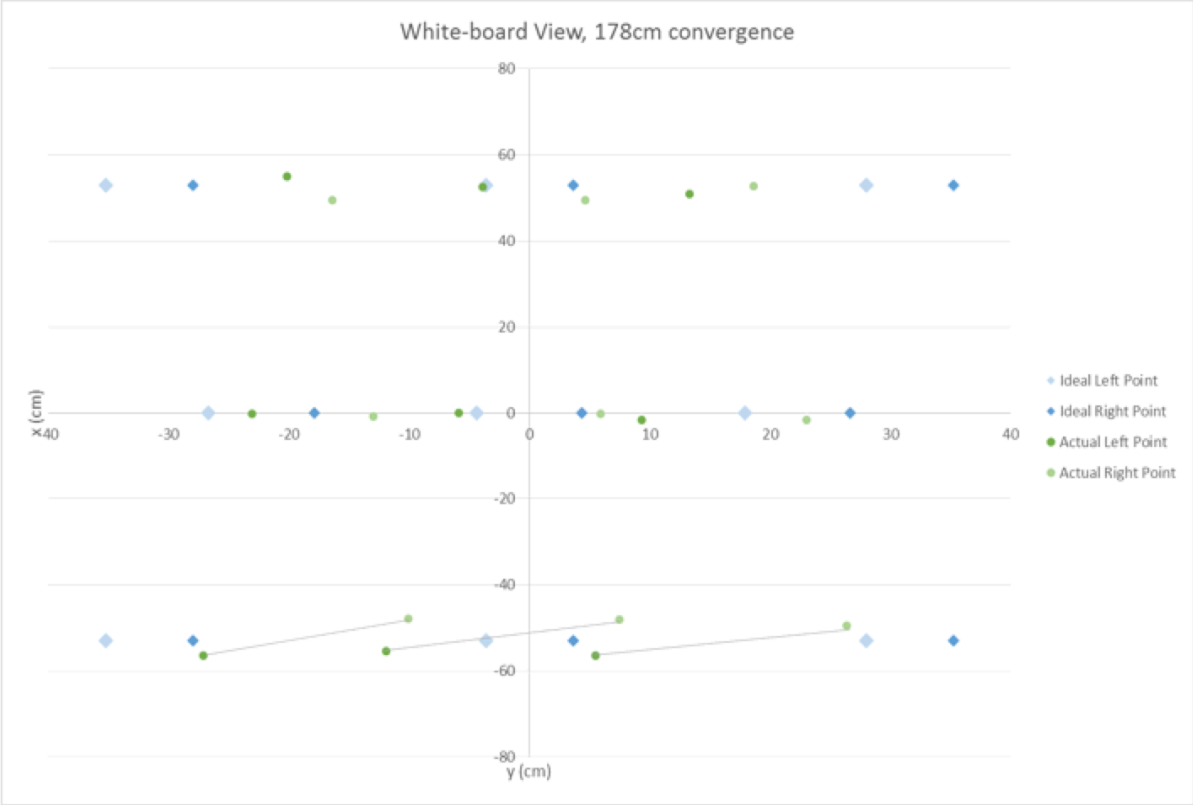

Figure 67: Theoretical positions vs actual positions plot for 178 cm convergence.

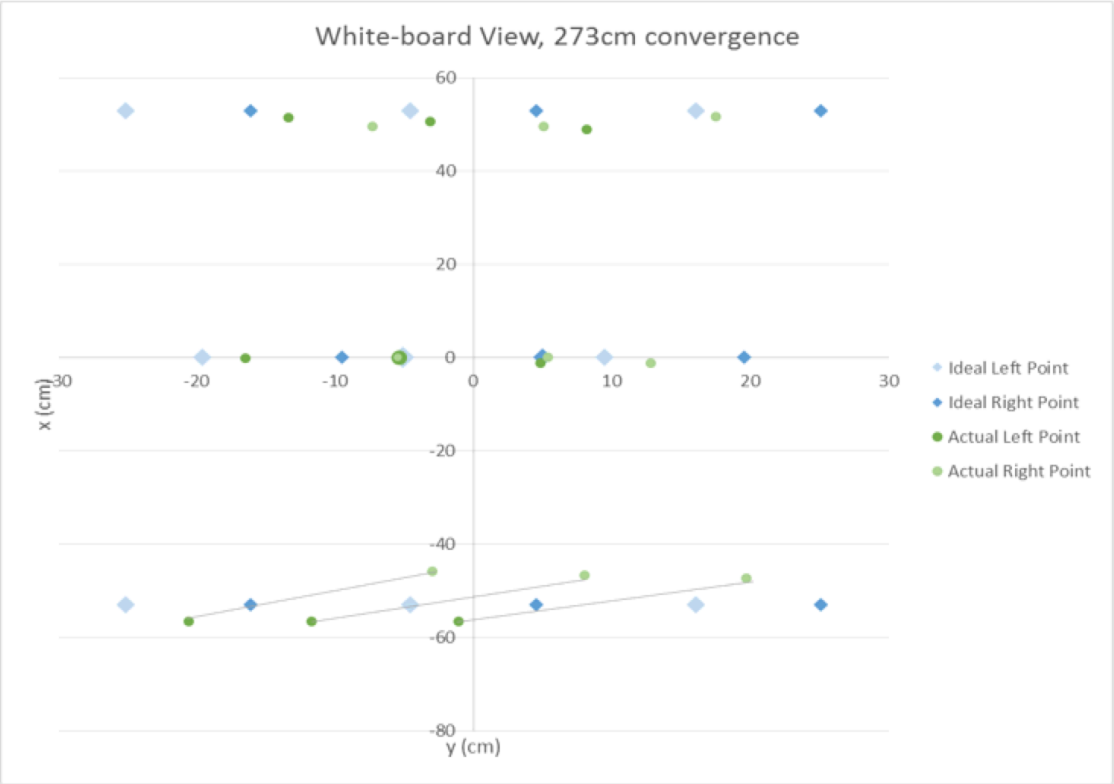

Figure 68: Theoretical positions vs actual positions plot for 273 cm convergence.

In order to keep all data organized, an average result was calculated for each actual points in order to compare the results to the ideal values. This was done in order to ensure to obtain a correct value since values can vary slightly every time they are tested. Then, the error of the actual values with respect to the ideal ones was calculated by subtracting the actual value from the ideal one and then obtaining the absolute value of the result. Some of the points were very close to the ideal ones, but the majority were far off from them. This was because of the different mechanical issues encountered in the mechanism as discussed in Section 2.3.5.1 (Motor Eyes Problems). The ideal values, average calculated values, and the error between them are shown in Table 3.

Goal Values			Left		Right		Calculated			Error			Percent Error		
Pan (cm)	Converence (cm)	Tilt (deg)	x	y	x	y	pan	conv	tilt	pan (cm)	conv (cm)	tilt (deg)	pan	conv	tilt
0	75	0	-4.2	0.5	3	0.5	-1.4	117.9	0.6	-1.4	42.9	0.6	1.9%	17.2%	1.3%
-75	75	0	-44	1.1	-43.3	-1.1	-47.1	53.9	0.0	28	-21.1	0.0	37.1%	8.4%	0.0%
75	75	0	46	-3.5	54	-2.5	138.9	138.9	-2.4	64	63.9	-2.4	85.2%	25.6%	5.4%
0	75	45	-1	53.5	2	51.5	0.9	62.5	46.3	1	-12.5	1.3	1.3%	5.0%	2.8%
-75	75	45	-46	60.7	-58.5	52.8	-26.1	25.0	37.9	49	-50.0	-7.1	65.2%	20.0%	15.7%
75	75	45	46	53.5	52	60.2	90.3	91.9	39.0	15	16.9	-6.0	20.5%	6.8%	13.3%
0	75	-45	-55	-54.2	-45	-49.8	-222.5	223.2	-36.4	-223	148.2	8.6	296.7%	59.3%	19.2%
-75	75	-45	-8	-49.3	5	-44.3	58.3	-2083.3	-43.1	133	-2158.3	1.9	177.8%	863.3%	4.2%
75	75	-45	-23	-35.7	-21	-48	-24.7	56.8	-37.4	-100	-18.2	7.6	133.0%	7.3%	16.9%
0	178	0	-5	0.5	6.5	0.2	10.7	892.9	0.4	11	714.9	0.4	14.3%	285.9%	0.9%
-75	178	0	-22	0.3	-12.5	-0.6	-83.9	240.4	-0.2	-9	62.4	-0.2	11.9%	25.0%	0.4%
75	178	0	10	-0.6	23.7	-0.6	-130.1	-390.6	-0.7	-205	-568.6	-0.7	273.4%	227.5%	1.4%
0	178	45	-3	54.5	5.8	50	4.6	178.6	46.2	5	0.6	1.2	6.2%	0.2%	2.7%
-75	178	45	-20	57.2	-15.7	50.1	-26.4	74.4	45.2	49	-103.6	0.2	64.8%	41.4%	0.5%
75	178	45	14	52.4	14.1	53.5	14.4	52.1	45.4	-61	-125.9	0.4	80.8%	50.4%	0.9%
0	178	-45	-12	-54.5	7.7	-47.1	3.5	-93.3	-45.4	4	-271.3	-0.4	4.7%	108.5%	0.8%
-75	178	-45	-27	-55.5	-8.9	-46.9	43.4	-122.5	-44.0	118	-300.5	1.0	157.8%	120.2%	2.3%
75	178	-45	6	-55.5	27.3	-49.6	-24.7	-73.5	-44.8	-100	-251.5	0.2	132.9%	100.6%	0.4%
0	273	0	-5	0	5.5	0	1.0	347.2	0.0	1	74.2	0.0	1.4%	29.7%	0.0%
-75	273	0	-16	0	-5.2	0	-96.0	446.4	0.0	-21	173.4	0.0	28.0%	69.4%	0.0%
75	273	0	4	-1.1	7.3	-1	7.6	65.1	-1.2	-67	-207.9	-1.2	89.8%	83.2%	2.6%
0	273	45	-3	50.8	5.3	49.7	3.5	145.3	45.1	3	-127.7	0.1	4.7%	51.1%	0.2%
-75	273	45	-13	51.6	-7.2	49.2	-20.0	97.7	44.6	55	-175.3	-0.4	73.3%	70.1%	0.9%
75	273	45	8	49.4	17.7	51.9	52.4	201.6	44.4	-23	-71.4	-0.6	30.1%	28.6%	1.3%
0	273	-45	-11	-56.5	8.3	46	2.7	-86.8	-6.0	3	-359.8	39.0	3.6%	143.9%	86.7%
-75	273	-45	-20	-56.5	-2.5	-45.9	27.7	-122.5	-44.9	103	-395.5	0.1	136.9%	158.2%	0.2%
75	273	-45	-1	-56.5	20.2	47.3	-14.8	-75.3	-5.1	-90	-348.3	39.9	119.7%	139.3%	88.6%

Table 3: Average calculated values and error

Appendix C: Final Parts List

PART #	PART NAME	DESCRIPTION	QTY	Vendor	Individual Cost	Total Cost
Stock Parts						
NA	Camera	HDE Portable 5 Megapixel Webcam Clip On Video Chat USBCamera	3	Amazon	$8.99	$26.97
NA	Plastic Sheet	Platform (1/4" x 18" x 24")	1	CollabLab	$25.00	$25.00
2650	ArduinoMega2650	Microcontroller	1	Adafruit	$45.95	$45.95
102-2050-ND	Absolute Encoder	AMT203-V Absolute/Quadrature Encoder Kit	2	Digi-Key	$48.65	$97.30
901418842	Motor Driver Shield	30A High Current Dual Motor Module Full-bridge Driver for Arduino	2	DXSOUL	$12.83	$25.66
DS-LS-8X15-R	Pan Lead Screw	8x15mm Lead Screw @ 178mm	1	IGUS	$17.80	$17.80
DS-LS-8x15-R	Conv Lead Screw	8x15mm Lead Screw @ 159mm	1	IGUS	$16.77	$16.77
DST-JFRM-006	IGUS Lead Screw Nut	dryspin - Flange lead screw nut (type f) iglide J material	2	IGUS	$18.31	$36.62
61205K72	61205K72	4mm Non Flanged Linear Ball Bearing	1	McMaster-Carr	$17.02	$17.02
9540K737	Rubber Feet	Round Bumper, 9/64 hole, 3/4 dia (10pk)	6	McMaster-Carr	$6.48	$38.88
Cable Tie Mounts	7566K73	Adhesive/Fastener Mount, 4 Way, 0.20" Tie Width, 3/4" Long 25pk	1	McMaster-Carr	$3.53	$3.53
PSCS4-8	Pan Alignment Shaft Collar	4mm ID Shaft Collar w/ Slit	2	Misumi	$3.52	$7.04
SLHFCS4	Flanged Bearing	Flanged Linear Bushing	2	Misumi	$18.22	$36.44
U-LHFC0.25	Flanged Linear Bearing	Flanged Linear Bushings - Single Bushing	2	Misumi	$15.35	$30.70
31225S	Tilt Motor	HS-225BB Servo	1	ServoCity	$17.99	$17.99

535018	Pan Rotary Bearing	1/4" ID x 3/8" OD Non-Flanged Ball Bearing (2 pack)	1	ServoCity	$1.99	$1.99
535038	Eye Bearing	3/16" ID x 5/16" OD Flanged Ball Bearing (2 pack)	1	ServoCity	$2.49	$2.49
535104	Lead Screw Bearing Block	8mm Bore Bottom Tapped Pillow Block	3	ServoCity	$6.49	$19.47
535114	Eye Bearing Block	3/8" Bore, Face Thru-Hole Pillow Block	2	ServoCity	$6.49	$12.98
535150	Lead Screw End Support	1/4" Bore Bottom Tapped Pillow Block	4	ServoCity	$5.99	$23.96
545584	Eye Shaft Lock	Face Tapped Clamping Hub, 0.77" Pattern, .1875" Shaft	2	ServoCity	$5.99	$11.98
585504	Convergence Pan Mount	90 deg Dual Side Mount	4	ServoCity	$3.99	$15.96
585542	585542	1/4" Bore Bottom Tapped Clamping Mount	4	ServoCity	$5.99	$23.96
585642	Motor Mount	22mm Bore Bottom Tapper Clamping Mount	2	ServoCity	$5.99	$11.98
615398	TiltLead Screw Bevel Gear	1/4" Bore Bevel Gear, 24T	4	ServoCity	$5.99	$23.96
625110	_25-.1875 coupler	1/4" to 3/16" coupler	2	ServoCity	$4.99	$9.98
625118	Pan Motor Shaft Coupler	1/4in to 4mm	1	ServoCity	$4.99	$4.99
625182	8mm-.25in Shaft Coupler	8mm to .25" Set Screw Shaft Coupler	1	ServoCity	$4.99	$4.99
625222	Pan Motor-Lead Screw Coupler	4mm to 8mm Set Screw Shaft Coupler	1	ServoCity	$4.99	$4.99
633130	MountingPin	6-32 Thread, 1/4" OD Round Aluminum Standoffs, 1" L	2	ServoCity	$2.49	$4.98
634064	Eye Drive D Shaft	1/4" Stainless Steel D-Shafting 1.5" L	2	ServoCity	$1.29	$2.58

634138	.1875Eye Shaft Connector	2" x .1875" Shaft	4	ServoCity	$0.69	$2.76
634158	_25x1 Shaft	1" x .25" Shaft	1	ServoCity	$0.59	$0.59
634160	Bevel Gear Conv Drive Shaft	1/4" Stainless Steel Precision Shafting, 2" Length	2	ServoCity	$0.89	$1.78
634162	Tilt Drive Shaft	2.91"(3") x.25" Shaft	1	ServoCity	$1.19	$1.19
634168	.25in shaft 6in length	6" x .25" Shaft	2	ServoCity	$2.09	$4.18
634266	Linear Drive Shaft	150mm x 4mm Shaft	2	ServoCity	$0.99	$1.98
634268	Pan Alignment Shaft	200mm x 4mm Shaft	1	ServoCity	$1.09	$1.09
638262	PanMotor	2737 RPM Planetary Gear Motor	1	ServoCity	$27.99	$27.99
638260	PanMotor	730 RPM Planetary Gear Motor	1	ServoCity	$27.99	$27.99
638368	ConvMotor	416 RPM Premium Planetary Gear Motor	1	ServoCity	$27.99	$27.99
6435K12	Conv Shaft Collar	.25" Steel Clamp Collar	1	ServoCity	$4.80	$4.80
AGB-A2-4	Eye Bushing	.1875" Flanged Bushing, .375" L	4	ServoCity	$1.35	$5.40
HSA125	Servo Coupler	24T Spline Servo to 1/4" Shaft Coupler	1	ServoCity	$12.99	$12.99
SAM8831-ND	Connector	14 Position Rectangular Housing Connector Black 0.050" (1.27mm)	2	Digi-Key	$0.98	$1.96
SAM9030CT-ND	Crimp Pins	Contact Crimp Socket 28-30 AWG Gold	28	Digi-Key	$0.23	$6.44
CP-AMT-14C-0-036-1-ND	Encoder Cables	AMT CABLE 14C 203/303 36" STAND	2	Digi-Key	$55.53	$111.06
					Total Stock Part Cost	$865.10
3D Printed Parts						
5	Eye Connector	High Density	2	Dimension	$1.92	$3.84

6	LinearBearingPanSliderHousing	Low Density	2	Dimension	$1.76	$3.52
7	Pan Movement Bracket	High Density	1	Dimension	$19.36	$19.36
8	Convergence Side Rail Bracket	Low Density	2	Dimension	$5.12	$10.24
9	Eye Bracket L	100% Density	2	MarkForge	$4.79	$9.58
10	Eye Bracket R	100% Density	2	MarkForge	$4.79	$9.58
11	Eye	Solid Density	2	Dimension	$15.60	$31.20
12	Bearing Mounting Block	Low Density	2	Dimension	$2.08	$4.16
13	Encoder Mount	Low Density	1	Dimension	$2.08	$2.08
14	Pan Encoder Mount	Low Density	1	Dimension	$2.32	$2.32
17	Alignment Shaft Bracket	Low Density	1	Dimension	$1.60	$1.60
18	Laser Adapter	Low Density	2	Dimension	$2.00	$4.00
				Total 3D Print Cost	$101.48	
Acrylic Parts						
1	Base Platform	Base Platform	1	Laser Cutter		
2	Pan Mounting Plate	Pan Mounting Plate	1	Laser Cutter		
3	Conv-Pan Mech Support Inside Fixed	Conv-Pan Mech Support Inside Fixed	1	Laser Cutter		
4	Conv-Pan Mech Support	Conv-Pan Mech Support	1	Laser Cutter		
15	Acrylic Spacer	Acrylic Spacer	4	Laser Cutter		
16	Standoff Support	Standoff Support	4	Laser Cutter		
Hardware						

91772A148	Screw	6-32 Screw .5" L	30	ServoCity	$0.17	$5.10
91772A151	Screw	6-32 Screw .75" L	15	ServoCity	$0.17	$2.55
91772A155	Screw	6-32 Screw 1.25" L	8	ServoCity	$0.17	$1.36
91772A157	Screw	6-32 Screw 1.5" L	6	ServoCity	$0.26	$1.56
91772A106	Screw	4-40 Screw .25" L	6	ServoCity	$0.09	$0.54
92855A422	Screw	Lead Screw Nut Mounting Screws M4 x 25mm, 25 pk	1	McMaster-Carr	$5.48	$5.48
91772A081	Screw	Servo Mounting Screws 2-56 x .5" L	5	ServoCity	$0.10	$0.50
90480A007	Nut	6-32 Nuts	59	ServoCity	$0.05	$2.95
94000A035	Nut	M4 Nuts 25 pk	1	McMaster-Carr	$3.90	$3.90
90480A003	Nut	2-56 Nuts	5	ServoCity	$0.02	$0.10
90126A009	Washer	#8 Washer for 6-32 & M4 Screws	59	ServoCity	$0.05	$2.95
90126A304	Washer	#3 Washer for 2-56 Screws	5	ServoCity	$0.05	$0.25
				Hardware Total	$26.99	
				HSVS Cost	$993.57	

Table 4: List of purchased parts

**For 3D printed parts, the vendor column is the machine on which the part was printed*

Appendix D: 3D Printer Specification Table

	Dimension SST 1200es	Objet 260 Connex	Markforged Mark Two
Materials	ABS	see range of resins	Nylon
Build envelope	10 x 10 x 12 inches	10 x 9.9 x 7.9 inches	12.6 x 5.2 x 6 inches
Layer thickness	0.01 inches	0.001 inches	0.004 inches
Error range	0.006 inches	0.0008 - 0.0078 inches	
Minimum recommended feature thickness	0.06 inches	0.01 inches	0.06 inches
Density settings	Low Density High Density Solid	N/A	0% - 100%
Other options	Color: ivory, black, red, orange, yellow, blue	Shelling Surface finish Coating	Reinforcement: Fiberglass, Carbon Fiber, or Kevlar
Approximate Costs (per unit material used)	$8/inch^3	$20-30/inch^3	Model: $7/inch^3 Reinforcement: $25-50/inch^3
Benefits	Relatively high HDT, strength & stability Dissolvable support material	Smaller features Smoother surface finish Multiple material properties	High strength to weight ratio Smooth, scratch-free material

Table 5: WPI Rapid Prototyping Lab 3D printer specifications

Appendix E: Determination of Dynamic Loads for Analysis

Determination of loads on Pan Movement Bracket:

In order to calculate the loads on the pan movement bracket, a number of other reaction forces needed to be calculated. In order to determine these reaction forces, the linear acceleration due to the pan and convergence motors needed to be calculated. To determine acceleration, the motor torque corresponding to the highest motor efficiency was used. In addition, the moment of inertia of each lead screw and its load were calculated, and this used in conjunction with the motor torque to calculate the angular acceleration of the motor, and from this, the linear acceleration of the pan and convergence nuts.

From here, the moment of inertia of the eyes about their axis of rotation during pan/ convergence movement was determined, and this used to calculate the angular acceleration of the eyes at minimum convergence based on the linear pan acceleration. These values were used to determine the torque required to move the eyes at the calculated angular acceleration, and from there the force needed to achieve that torque at minimum convergence. This force is the approximate force from the control arm sliders on the control arm slider bearing, and was used in a simple ANSYS analysis to find the force and moment from the control arm slider bearing on the pan movement bracket. Finally, the ANSYS analysis described in Section 6.3 (Analysis of Pan Movement Bracket) was performed to ensure that the pan movement bracket would not break.

Weight and mass on convergence nut:

$W_{onConvNut} := 7.24N$

$m_{onConvNut} := \frac{W_{onConvNut}}{g} = 0.738\,kg$

Calculate the total moment of inertia on convergence screw nut:

$lead := 15mm$ Linear motion per revolution

$J_{leadScrew} := 0.000002472kg \cdot m^2$ Moment of inertia of lead screw, given on lead screw website for 8mm OD screw

$J_{convLoad} := m_{onConvNut} \cdot \left(\frac{lead}{2 \cdot \pi}\right)^2 = 4.208 \times 10^{-6}\, m^2 \cdot kg$ Moment of inertia of convergence load

$J_{total} := J_{leadScrew} + J_{convLoad} = 6.68 \times 10^{-6}\, m^2 \cdot kg$ Total moment of inertia

Calculate acceleration based on total moment of ienrtia and motor torque:

$T_{convMotor} := 6.2ozf \cdot in$ Torque of convergence motor at maximum efficiency

$\alpha_{motor} := \frac{T_{convMotor}}{J_{total}} = 1.043 \times 10^3 \cdot \frac{rev}{s^2}$ Angular acceleration of convergence motor

$a_{linLeadScrew} := \alpha_{motor} \cdot 15 \frac{mm}{rev} = 15.648 \frac{m}{s^2}$ **Linear acceleration of convergence lead screw**

Weight and mass on convergence nut:

$W_{onPanNut} := 2.243N$

$m_{onPanNut} := \frac{W_{onPanNut}}{g} = 0.229\,kg$

Calculate total moment of inertia on pan screw nut:

$lead := 15mm$

$J_{leadScrew} := 0.000002472kg \cdot m^2$ Given on lead screw website for 8mm OD lead screw

$J_{panLoad} := m_{onPanNut} \cdot \left(\frac{lead}{2 \cdot \pi}\right)^2 = 1.304 \times 10^{-6}\, m^2 \cdot kg$ Moment of inertia from load on pan screw

$J_{total} := J_{leadScrew} + J_{panLoad} = 3.776 \times 10^{-6}\, m^2 \cdot kg$ Total moment of inertia on pan screw

We chose an input torque based on when the motor has the highest efficiency

$T_{panMotor} := 1.6ozf \cdot in$ Torque of pan motor at maximum efficiency

$\alpha_{motor} := \frac{T_{panMotor}}{J_{total}} = 476.276 \cdot \frac{rev}{s^2}$ Angular acceleration of pan motor

$a_{linLeadScrew} := \alpha_{motor} \cdot 15 \frac{mm}{rev} = 7.144 \frac{m}{s^2}$ **Linear acceleration of pan lead screw**

SOLIDWORKS was used to determine the moments of inertia of relevant parts about the eye's vertical axis of rotation

$$I_{total\_eye} := I_{elbow} + I_{bracket} + I_{eye} + I_{support} + I_{rod} = 6.13 \times 10^{-5}\,m^2 \cdot kg$$

Caluclate the angular acceleration of the eye using the pan linear acceleration and the distance between the control arm slider bearing and the eye's axis of rotation

$$r_{eye\_bearing} := 2.4cm$$

$$\alpha_{eye} := \frac{a_{linLeadScrew}}{r_{eye\_bearing}} = 297.673 \cdot \frac{rad}{s^2}$$

Calculate the torque required to move the eyes at this acceleration, and the force required to create this torque when the mechanism is at zero pan and minimum convergence

$$T_{move\_eye} := I_{total\_eye} \cdot \alpha_{eye} = 0.018 \cdot N \cdot m$$

$$F_{move\_eye} := \frac{T_{move\_eye}}{r_{eye\_bearing}} = 0.76N$$

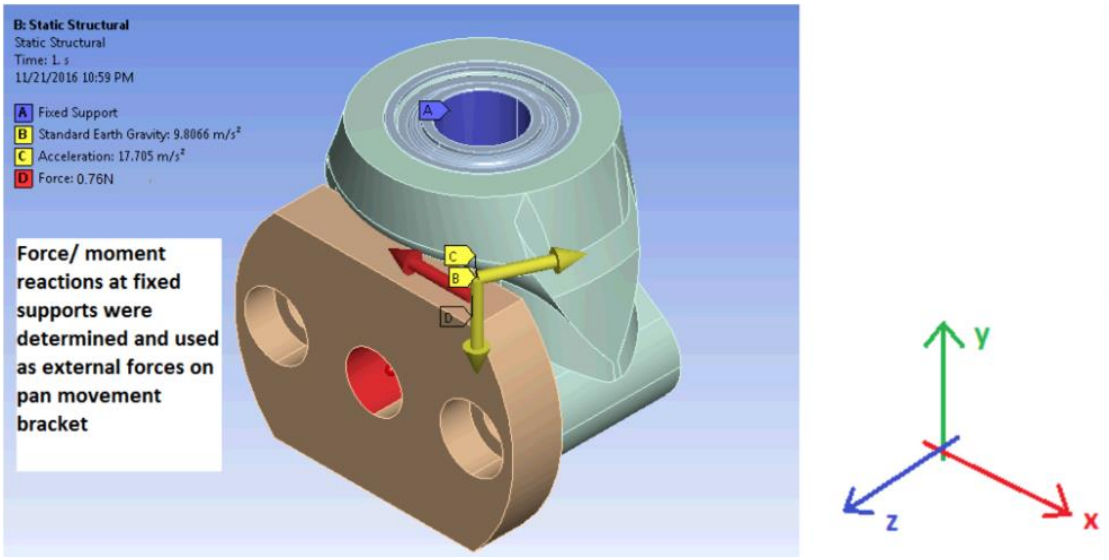

Figure 69: ANSYS setup for analysis to determine loads on pan movement bracket

In the above analysis, acceleration from the pan and convergence movement were applied. Structural steel was the material chosen for the flanged bearing (brown), and material properties of ABS were used for the housing (green). The design of the housing was changed slightly after

this analysis was performed to allow a set screw to be inserted on the top "neck," but because the majority of the mass is in the flanged bearing, this will not drastically change the results of the analysis.

Determination of loads on Eye Bracket:

In order to determine the forces on the eye bracket, a partial CAD model was imported into Creo and is seen in Figure 70. An acceleration was applied on the rod sticking out of the Linear Bearing Pan Slider Housing as seen in Figure 71. This acceleration was representative of the mechanism's pan acceleration, so the value inputted to the model was the linear pan acceleration ($7.144 m/s^2$). The final resultant force and moment are shown in Figure 72. These numbers were used to create a more accurate interpretation of the force applied to the eye bracket.

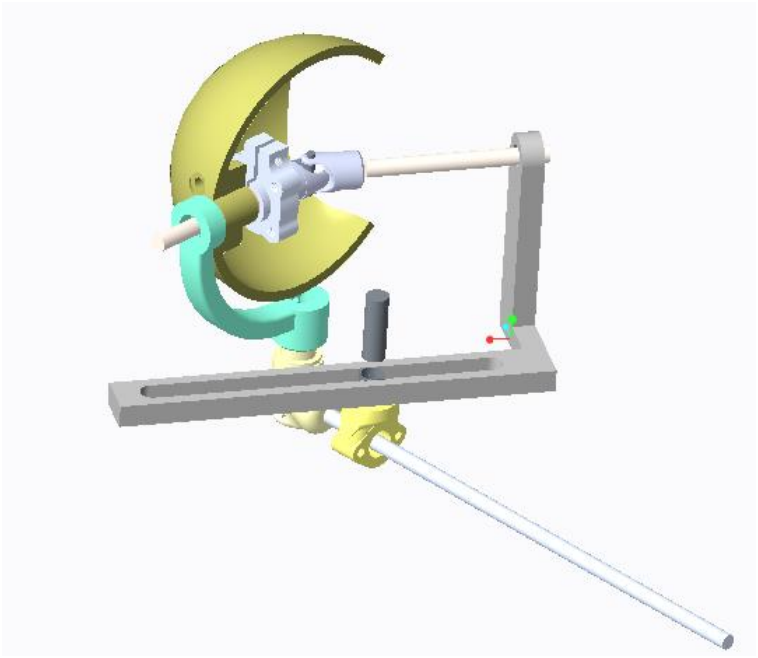

Figure 70: Test model

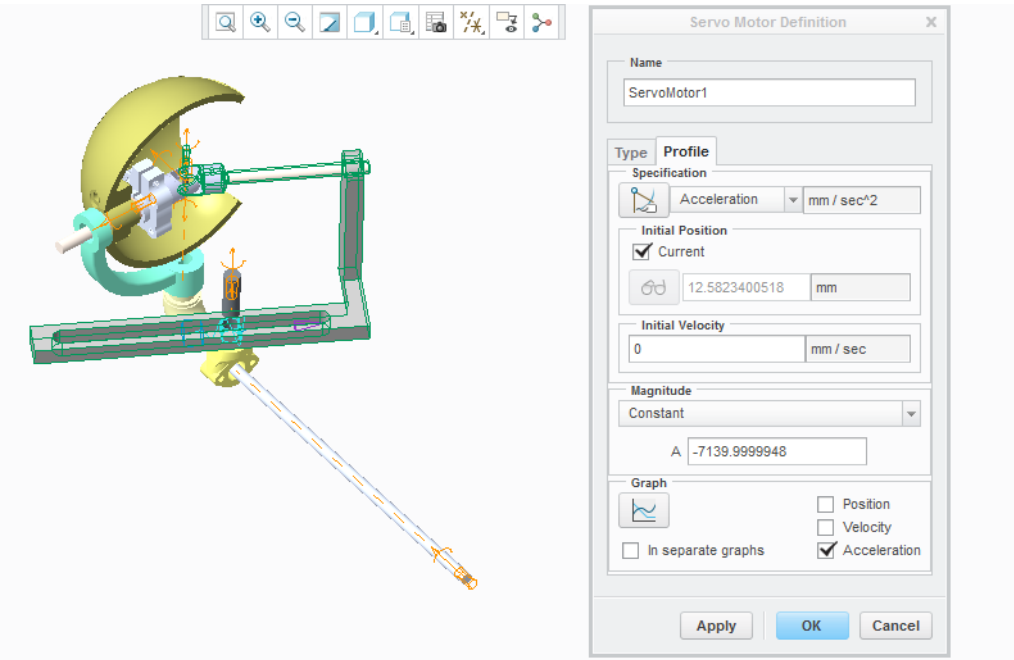

Figure 71: Input parameters to obtain values

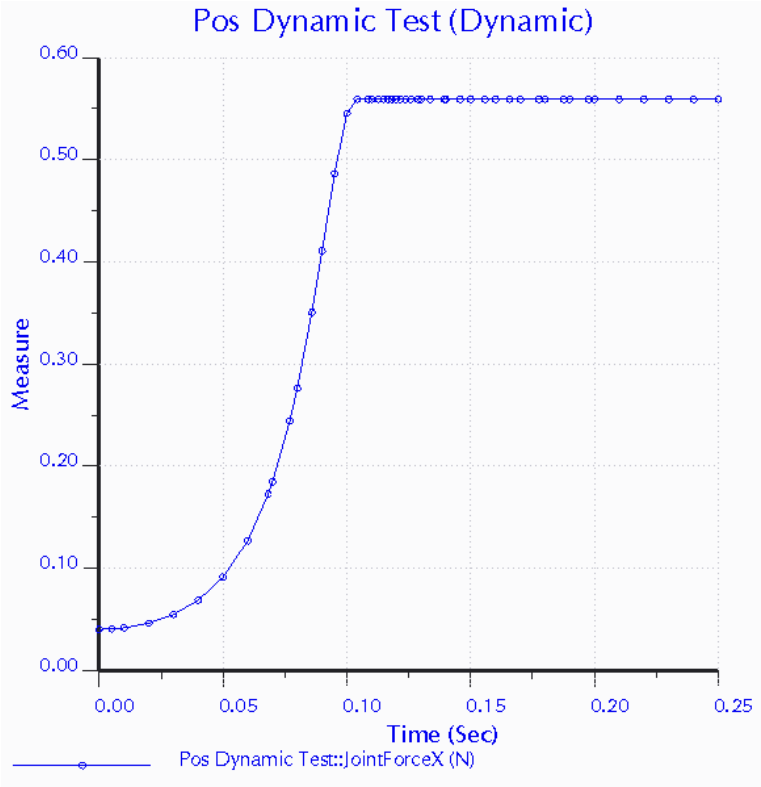

Figure 72: Reaction force on eye bracket, X

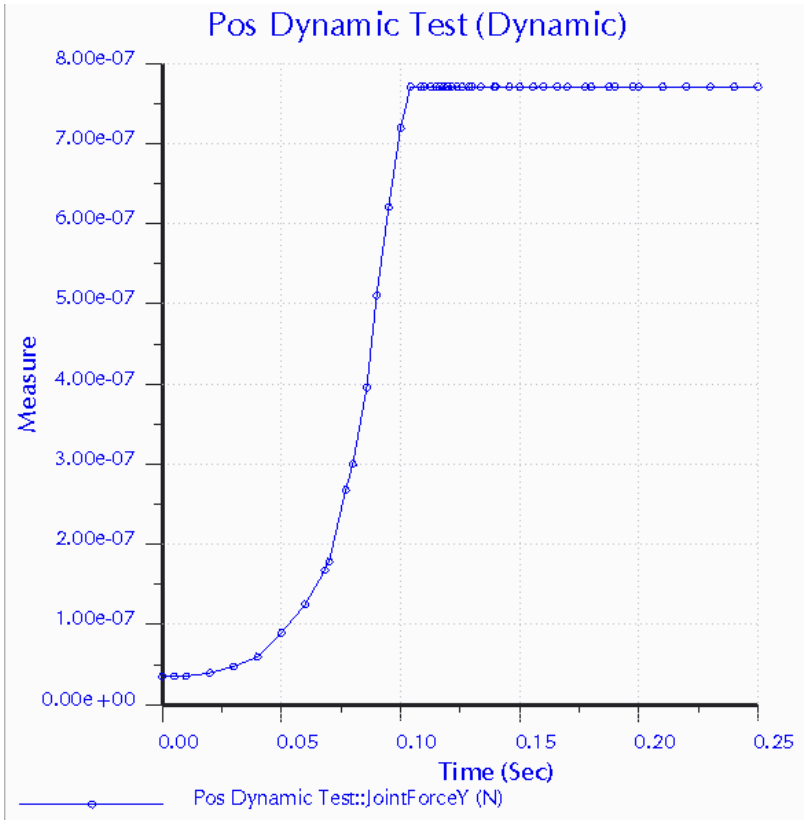

Figure 73: Reaction force on eye bracket, Y

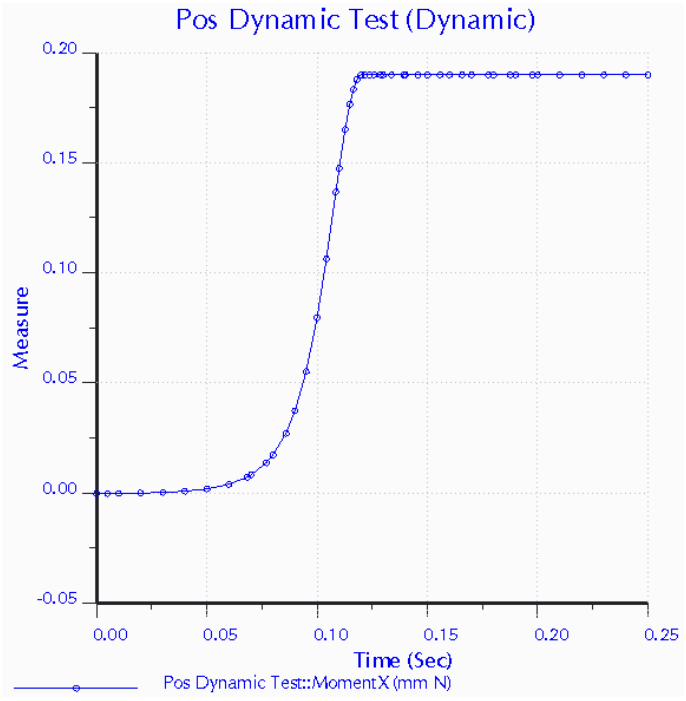

Figure 74: Reaction moment on eye bracket, X

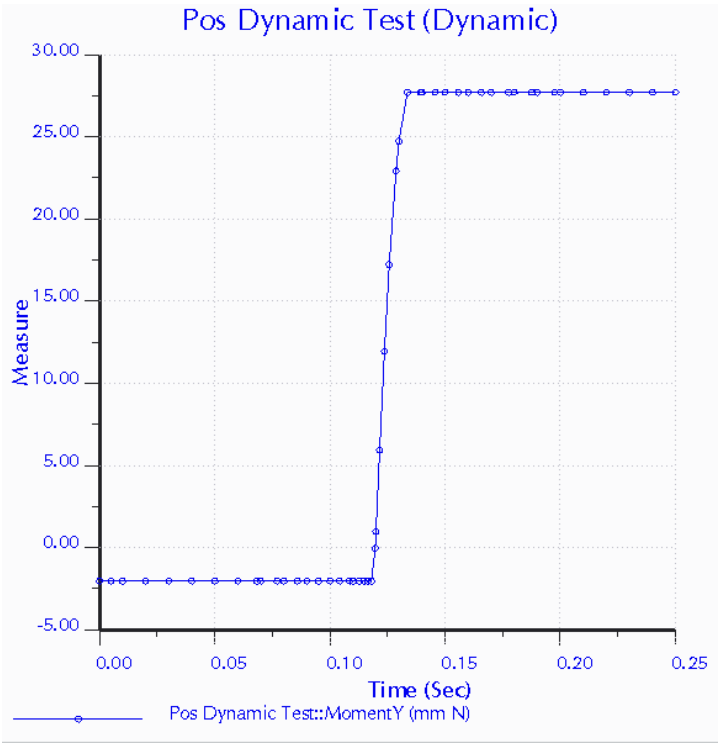

Figure 75: Reaction moment on eye bracket, Y

Appendix F: Material Properties used for Analysis

MATERIAL PROPERTIES		
Acrylic	**Metric**	**English**
Young Modulus of Elasticity	2800 MPa	400,000 psi
Tensile Strength	69 MPa	10,000 psi
Density	1.19*10³ Kg/m³	74 lb/ft³
Poisson's Ratio	0.35	0.35
Shear Modulus	1151.42 MPa	167000 psi
Yield Strength	37 - 73 MPa	5420 - 10700 psi
Nylon	**Metric**	**English**
Young Modulus of Elasticity	2.1 - 3.4 GPa	300 - 500 Ksi
Tensile Strength	45 MPa	8.122 Ksi
Density	1150 Kg/m³	70 - 73 lb/ft³
Poisson's Ratio	0.4	0.4
Shear Modulus	4.1 GPa	0.59 * 10^6 psi
Yield Strength	56 MPa	8122 psi
ABS	**Metric**	**English**
Young Modulus of Elasticity	2 GPa	290 ksi
Tensile Strength	30 MPa	4351 psi
Density	1020 Kg/m³	64 lb/ft³
Poisson's Ratio	0.39	0.39
Shear Modulus	96 MPa	14000 psi
Yield Strength	18.5	2683 psi

Table 6: Material properties used for analysis

Appendix G: HSVS Position Testing Results

The following data summarize the results obtained when testing the new mechanism.

MECHANISM FOCUS POSITION TESTING

THEORETICAL POSITIONS				TESTING RESULTS																							
				1st Trial								2nd Trial						Average						Ideal		Error	
				Red/left		black/right		Angle		Left		Right		Angle		Left		Right		Angle		Angle		Angle			
Distance to Board (cm)	Pan (cm)	Convergence fz (cm)	Tilt (deg)	x	y	x	y	Angle Left	Angle Right	x	y	x	y	Angle Left	Angle Right	x	y	x	y	Angle Left	Angle Right	Angle Left	Angle Right	Error Left	Error Right
50	0	70	0	0.0	0.0	0.0	0.0	7.1	-7.1	0.0	0.0	0.0	0.0	7.1	-7.1	*0.0*	*0.0*	*0.0*	*0.0*	7.1	-7.1	5.1	-5.1	2.0	2.0
50	-63	70	0	-50.0	-1.0	-52.5	1.8	-41.2	-8.3	-50.5	-2.0	-52.0	1.0	-41.5	-49.4	-50.3	*-1.5*	*-52.3*	*1.4*	-41.3	-49.5	-39.0	-44.7	2.3	4.8
50	63	70	0	51.0	3.0	49.5	-7.0	48.9	-3.7	50.5	2.0	49.5	-7.5	48.6	40.9	50.8	*2.5*	*49.5*	*-7.3*	48.7	40.9	44.7	39.0	4.1	1.8
50	0	70	-45	1.0	-48.5	-2.0	-48.0	8.3	-47.6	0.0	-47.0	-3.0	-47.0	7.1	-10.5	*0.5*	*-47.8*	*-2.5*	*-47.5*	7.7	-9.9	5.1	-5.1	2.6	4.8
50	-63	70	-45	-46.5	-68.0	-62.0	-90.0	-38.8	-56.0	-46.0	-68.0	-61.5	-86.0	-38.5	-53.6	*-46.3*	*-68.0*	*-61.8*	*-88.0*	-38.7	-53.7	-39.0	-44.7	0.4	9.0
50	63	70	-45	52.5	-75.5	42.0	-62.5	49.6	-58.5	53.0	-74.0	42.0	-61.5	49.8	35.6	*52.8*	*-74.8*	*42.0*	*-62.0*	49.7	35.6	44.7	39.0	5.0	3.5
50	0	70	45	-0.5	51.0	0.5	50.8	6.6	41.8	-2.0	52.0	-0.5	52.0	4.9	-7.7	*-1.3*	*51.5*	*0.0*	*51.4*	5.7	-7.1	5.1	-5.1	0.6	2.0
50	-63	70	45	-54.0	84.5	-49.0	102.0	-43.7	57.4	-54.5	85.0	-49.0	102.5	-44.0	-47.9	*-54.3*	*84.8*	*-49.0*	*102.3*	-43.8	-47.9	-39.0	-44.7	4.8	3.2
50	63	70	45	50.0	110.0	54.0	86.0	48.4	64.3	50.0	110.0	54.5	86.5	48.4	44.0	*50.0*	*110.0*	*54.3*	*86.3*	48.4	43.8	44.7	39.0	3.7	4.8
50	0	160	0	-3.0	-0.5	1.5	-0.5	3.7	-7.7	-2.0	-0.5	2.0	-0.5	4.9	-4.9	*-2.5*	*-0.5*	*1.8*	*-0.5*	4.3	-5.1	2.2	-2.2	2.1	2.9
50	-63	160	0	-28.0	-0.5	-24.0	0.5	-23.5	-7.7	-28.0	-1.0	-24.0	0.5	-23.5	-31.2	*-28.0*	*-0.8*	*-24.0*	*0.5*	-23.5	-31.2	-19.5	-23.4	4.0	7.8
50	63	160	0	23.5	0.0	27.0	-3.0	30.8	-7.1	24.0	0.5	28.0	-2.5	31.2	23.5	*23.8*	*0.3*	*27.5*	*-2.8*	31.0	23.0	23.4	19.5	7.6	3.5
50	0	160	-45	-2.0	-46.5	-1.0	-46.5	4.9	-46.5	-1.5	-48.0	0.5	-48.0	5.4	-6.6	*-1.8*	*-47.3*	*-0.3*	*-47.3*	5.1	-7.4	2.2	-2.2	2.9	5.2
50	-63	160	-45	-26.0	-54.0	-28.0	-59.5	-21.6	-50.3	-26.0	-53.0	-28.0	-58.0	-21.6	-34.4	*-26.0*	*-53.5*	*-28.0*	*-58.8*	-21.6	-34.4	-19.5	-23.4	2.0	11.0
50	63	160	-45	24.5	-54.0	23.0	-50.0	31.6	-50.3	26.0	-56.0	23.5	-50.0	32.8	19.0	*25.3*	*-55.0*	*23.3*	*-50.0*	32.2	18.8	23.4	19.5	8.8	0.8
50	0	160	45	-3.0	52.0	2.5	52.0	3.7	42.5	-2.5	52.5	3.0	52.5	4.3	-3.7	*-2.8*	*52.3*	*2.8*	*52.3*	4.0	-4.0	2.2	-2.2	1.8	1.8
50	-63	160	45	-29.0	60.0	-23.0	67.0	-24.5	47.1	-29.0	60.0	-23.5	67.0	-24.5	-30.8	*-29.0*	*60.0*	*-23.3*	*67.0*	-24.5	-30.5	-19.5	-23.4	4.9	7.1
50	63	160	45	22.5	68.0	29.5	61.0	29.9	51.0	23.0	69.0	30.0	61.0	30.3	25.4	*22.8*	*68.5*	*29.8*	*61.0*	30.1	25.2	23.4	19.5	6.7	5.6
50	0	250	0	-3.0	-0.5	2.5	-0.5	3.7	-7.7	-3.5	-0.5	2.5	-0.5	3.1	-4.3	*-3.3*	*-0.5*	*2.5*	*-0.5*	3.4	-4.3	1.4	-1.4	2.0	2.9
50	-63	250	0	-20.5	-0.5	-15.0	0.0	-15.9	-7.7	-20.0	-1.0	-15.0	0.0	-15.4	-23.0	*-20.3*	*-0.8*	*-15.0*	*0.0*	-15.6	-23.0	-12.8	-15.5	2.9	7.5
50	63	250	0	13.5	-0.5	19.0	-2.0	21.6	-7.7	13.5	0.0	19.5	-2.0	21.6	14.8	*13.5*	*-0.3*	*19.3*	*-2.0*	21.6	14.6	15.5	12.8	6.1	1.8
50	0	250	-45	-2.5	-47.0	-0.5	-47.0	4.3	-46.8	-2.0	-48.0	-0.5	-48.0	4.9	-7.7	*-2.3*	*-47.5*	*-0.5*	*-47.5*	4.6	-7.7	1.4	-1.4	3.1	6.3
50	-63	250	-45	-18.5	-49.5	-18.0	-52.5	-13.8	-48.1	-19.0	-50.0	-19.0	-54.0	-14.3	-26.8	*-18.8*	*-49.8*	*-18.5*	*-53.3*	-14.0	-26.3	-12.8	-15.5	1.2	10.9
50	63	250	-45	15.0	-51.0	16.0	-58.0	23.0	-48.9	14.5	-50.0	15.5	-48.5	22.5	10.5	*14.8*	*-50.5*	*15.8*	*-53.3*	22.8	10.8	15.5	12.8	7.3	2.0
50	0	250	45	-3.5	51.5	3.5	51.5	3.1	42.1	-4.0	51.0	3.0	51.0	2.6	-3.7	*-3.8*	*51.3*	*3.3*	*51.3*	2.9	-3.4	1.4	-1.4	1.4	2.0
50	-63	250	45	-20.5	56.0	-15.5	59.5	-15.9	44.9	-21.0	55.0	-14.0	59.0	-16.4	-22.0	*-20.8*	*55.5*	*-14.8*	*59.3*	-16.2	-22.8	-12.8	-15.5	3.4	7.3
50	63	250	45	13.0	59.5	21.0	55.5	21.1	46.8	12.5	58.0	20.0	54.5	20.6	15.4	*12.8*	*58.8*	*20.5*	*55.0*	20.8	15.9	15.5	12.8	5.3	3.1

Table 7: Position testing results

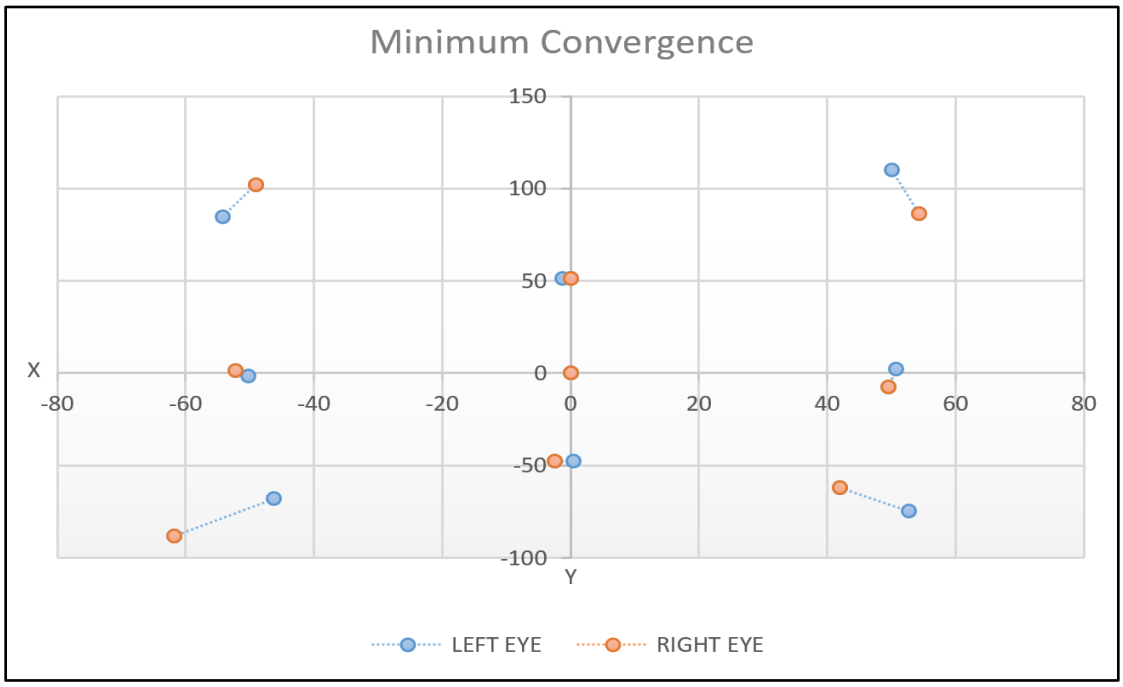

Figure 76: Plot of eye locations at minimum convergence

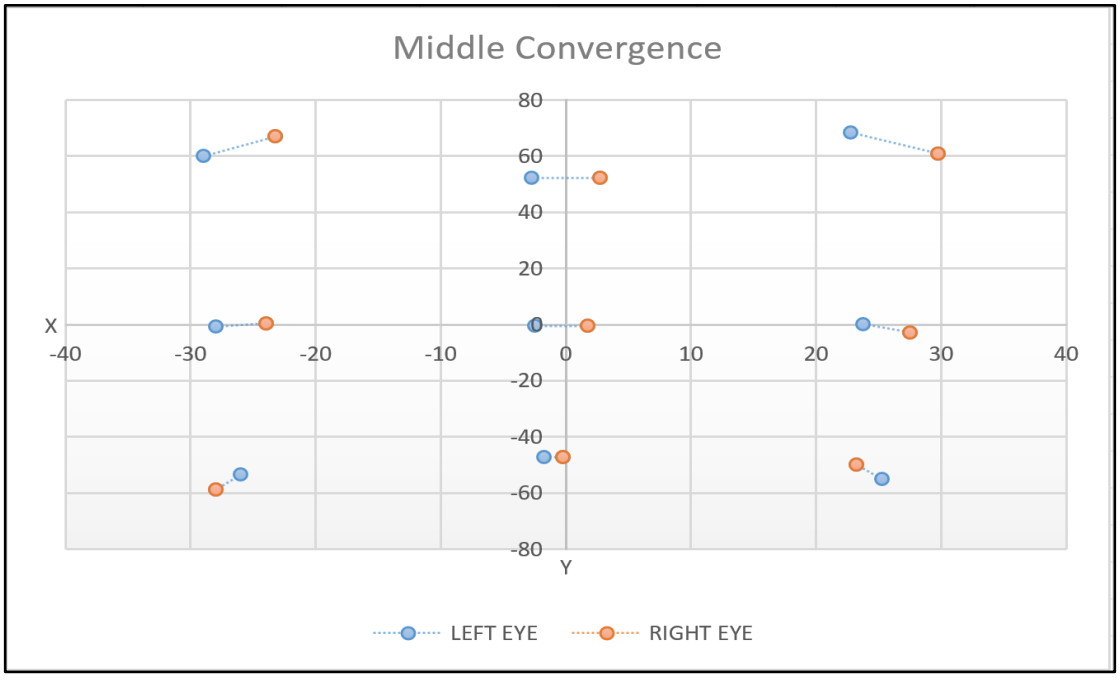

Figure 77: Plot of eye locations at middle convergence

MECHANISM FOCUS POSITION TESTING															
THEORETICAL POSITIONS				TESTING RESULTS											
				1st Trial											
				blue/left		red/right		Angle		Ideal		Error			
Distance to Board (cm)	Pan (cm)	Convergence fz (cm)	Tilt (deg)	x	y	x	y	Angle Left	Angle Right	Angle Left	Angle Right	Error Left	Error Right	% error left	% error right
50	0	70	0	-1.5	0	1.5	0	84.57	84.57	84.90	84.90	0.32	0.32	0.38%	0.38%
50	-63	70	0	-47.5	1	-43.5	-1.5	129.52	45.14	129.03	45.31	0.49	0.16	0.38%	0.36%
50	63	70	0	43.5	1	45.5	1	45.14	128.13	45.31	129.03	0.16	0.90	0.36%	0.70%
50	0	70	-45	-2	-43.5	1.5	-42.5	85.14	84.57	84.90	84.90	0.24	0.32	0.29%	0.38%
50	-63	70	-45	-47.5	-71	-43.5	-73	129.52	45.14	129.03	45.31	0.49	0.16	0.38%	0.36%
50	63	70	-45	42.5	-73	43	-61.5	45.73	126.32	45.31	129.03	0.42	2.72	0.92%	2.11%
50	0	70	45	-2	47.5	-1.5	49	85.14	81.19	84.90	84.90	0.24	3.71	0.29%	4.37%
50	-63	70	45	-49	79	-51	89	130.53	41.13	129.03	45.31	1.50	4.18	1.16%	9.22%
50	63	70	45	44.5	83	42.5	75.5	44.57	125.94	45.31	129.03	0.74	3.09	1.62%	2.39%
50	0	160	0	-4	1	4.5	0.5	87.42	88.00	87.76	87.76	0.34	0.23	0.39%	0.26%
50	-63	160	0	-25.5	1.5	-17	0	111.06	65.06	109.53	66.60	1.53	1.53	1.39%	2.30%
50	63	160	0	17.5	1	25	1	64.59	110.56	66.60	109.53	2.00	1.03	3.01%	0.94%
50	0	160	-45	-4.5	-42	3.5	-43	88.00	86.85	87.76	87.76	0.23	0.91	0.26%	1.04%
50	-63	160	-45	-25.5	-50	-16.5	-50	111.06	65.53	109.53	66.60	1.53	1.06	1.39%	1.59%
50	63	160	-45	16.5	-49	24	-47.5	65.53	109.54	66.60	109.53	1.06	0.02	1.59%	0.01%
50	0	160	45	-3.5	49	2	49	86.85	85.14	87.76	87.76	0.91	2.62	1.04%	2.99%
50	-63	160	45	-25.5	56	-27	56	111.06	56.38	109.53	66.60	1.53	10.22	1.39%	15.35%
50	63	160	45	18	56	23	54	64.13	108.52	66.60	109.53	2.47	1.01	3.71%	0.92%
50	0	250	0	-6	1	4	0	89.71	87.42	88.57	88.57	1.15	1.14	1.29%	1.29%
50	-63	250	0	-20	1	-10	0	105.38	72.00	102.79	74.52	2.59	2.52	2.52%	3.38%
50	63	250	0	8	1	17.5	0.5	74.09	102.68	74.52	102.79	0.42	0.11	0.57%	0.11%
50	0	250	-45	-6	-41	3.5	-42	89.71	86.85	88.57	88.57	1.15	1.72	1.29%	1.94%
50	-63	250	-45	-21	-45	-10	-47.5	106.44	72.00	102.79	74.52	3.65	2.52	3.55%	3.38%
50	63	250	-45	7.5	-44	17	-45.5	74.62	102.13	74.52	102.79	0.11	0.66	0.14%	0.64%
50	0	250	45	-5.5	49.5	2	48	89.14	85.14	88.57	88.57	0.57	3.43	0.65%	3.87%
50	-63	250	45	-19	53	-12.5	52	104.31	69.44	102.79	74.52	1.52	5.07	1.48%	6.81%
50	63	250	45	8.5	52	15	51	73.56	99.93	74.52	102.79	0.95	2.86	1.28%	2.79%

Table 8: Position testing results using cameras

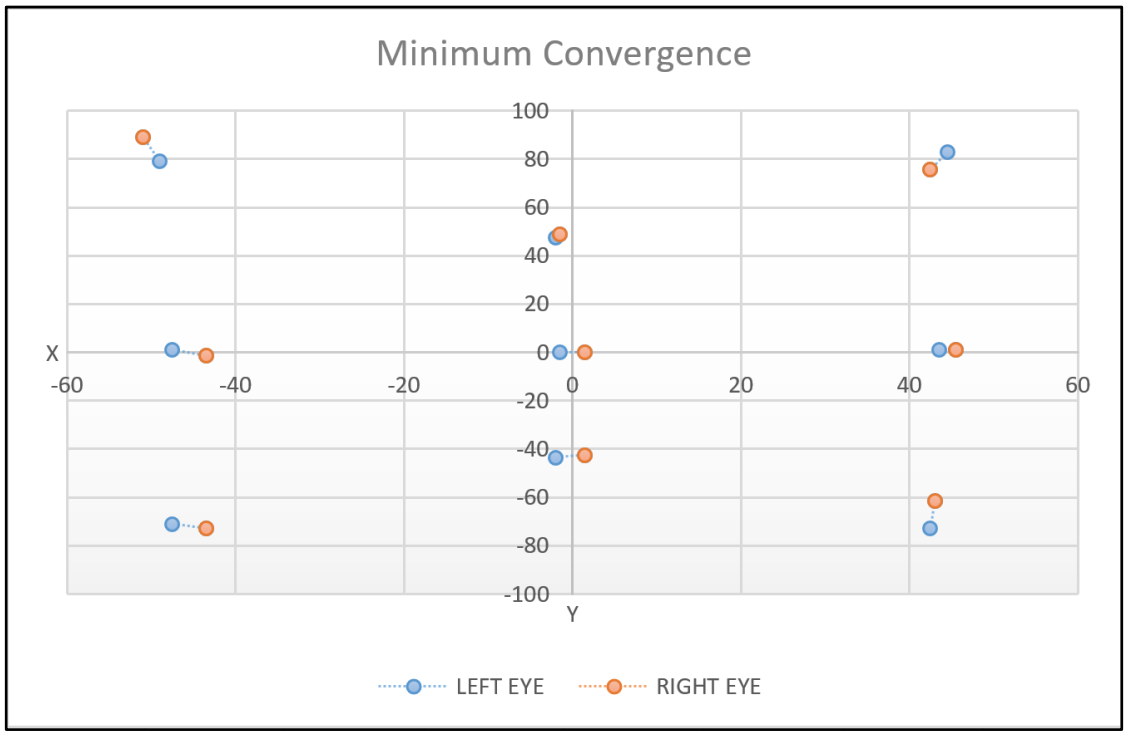

Figure 78: Plot of eye locations at minimum convergence when using cameras

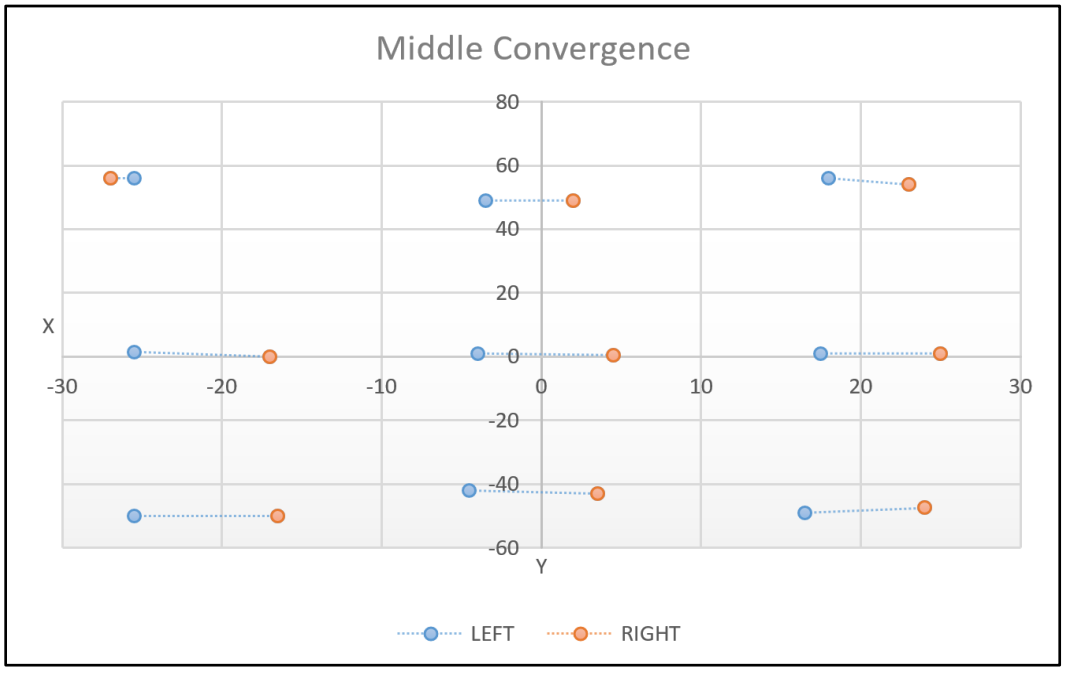

Figure 79: Plot of eye locations at minimum convergence when using cameras

Appendix H: Custom Part Drawings

Base Platform Front

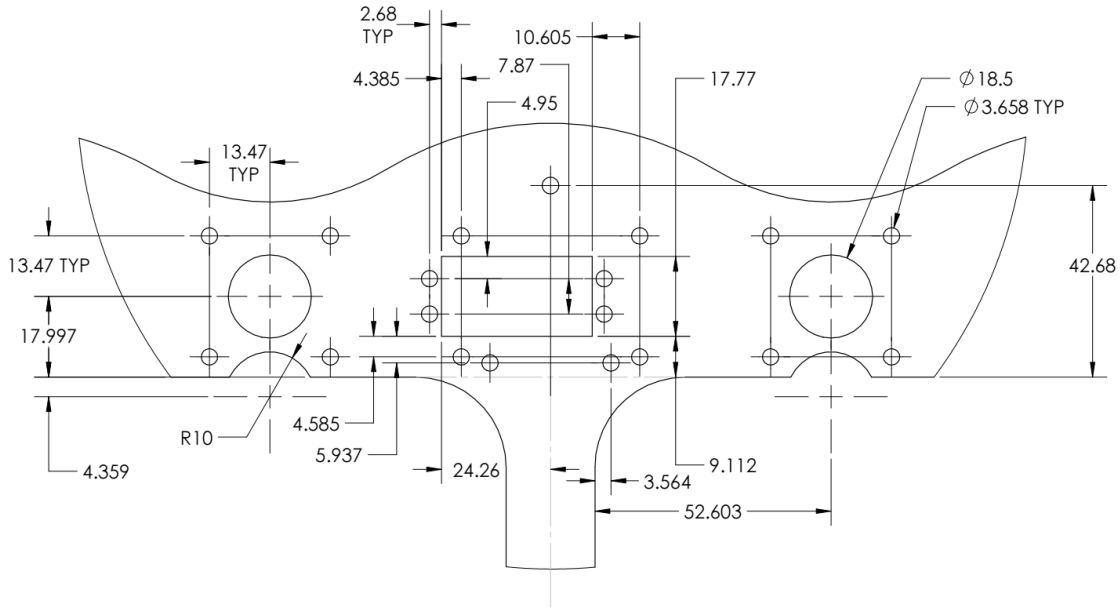

DETAIL D
SCALE 1 : 1

COSMETIC FILLETS OMMITTED FOR DRAWING CLARITY

WORCESTER POLYTECHNIC INSTITUTE
HUMANOID STEREOSCOPIC VISION SYSTEM

TITLE:
BASE PLATFORM FRONT

MATERIAL ACRYLIC

SCALE: 1:1	UNITS: MM	SHEET 2 OF 18

Base Platform Holes

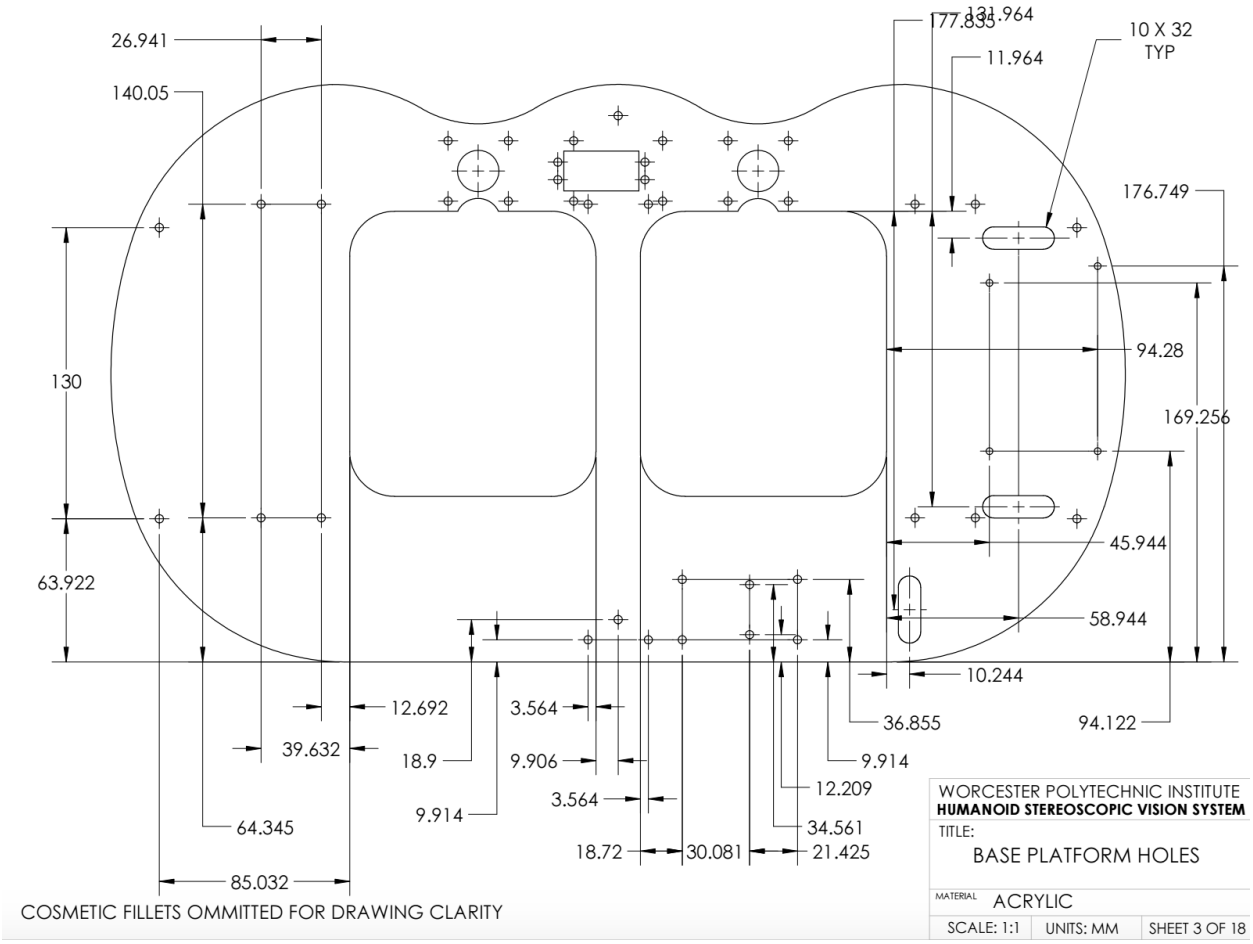

Pan Mounting Plate

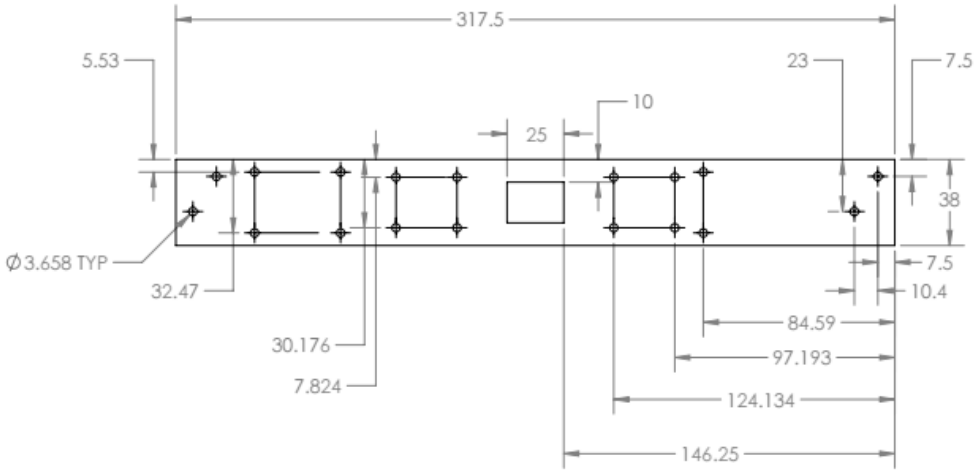

COSMETIC FILLETS OMMITTED FOR DRAWING CLARITY

WORCESTER POLYTECHNIC INSTITUTE **HUMANOID STEREOSCOPIC VISION SYSTEM**		
TITLE: PAN MOUNTING PLATE		
MATERIAL ACRYLIC		
SCALE: 1:2	UNITS: MM	SHEET 4 OF 18

Rear Convergence Bracket

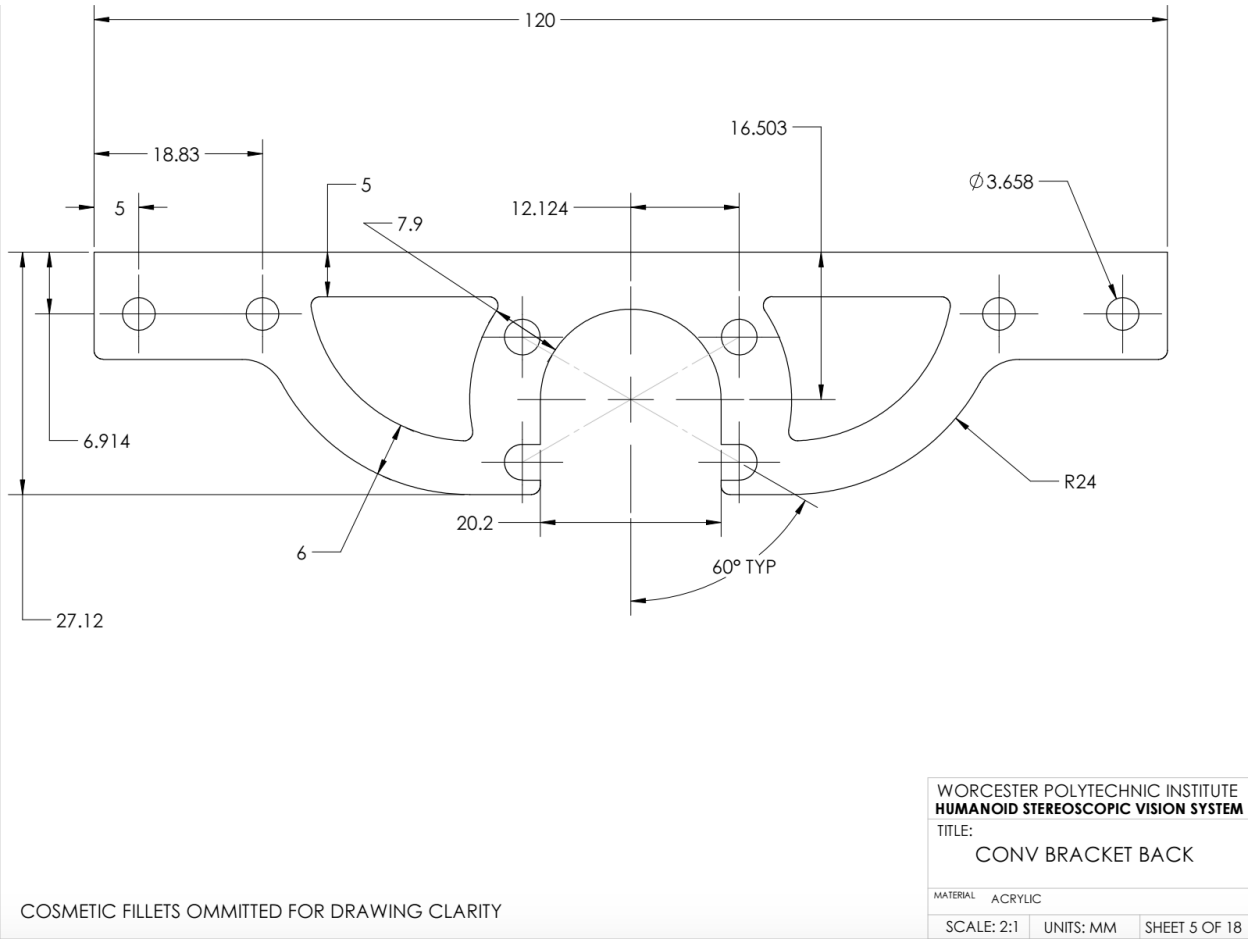

Front Convergence Bracket

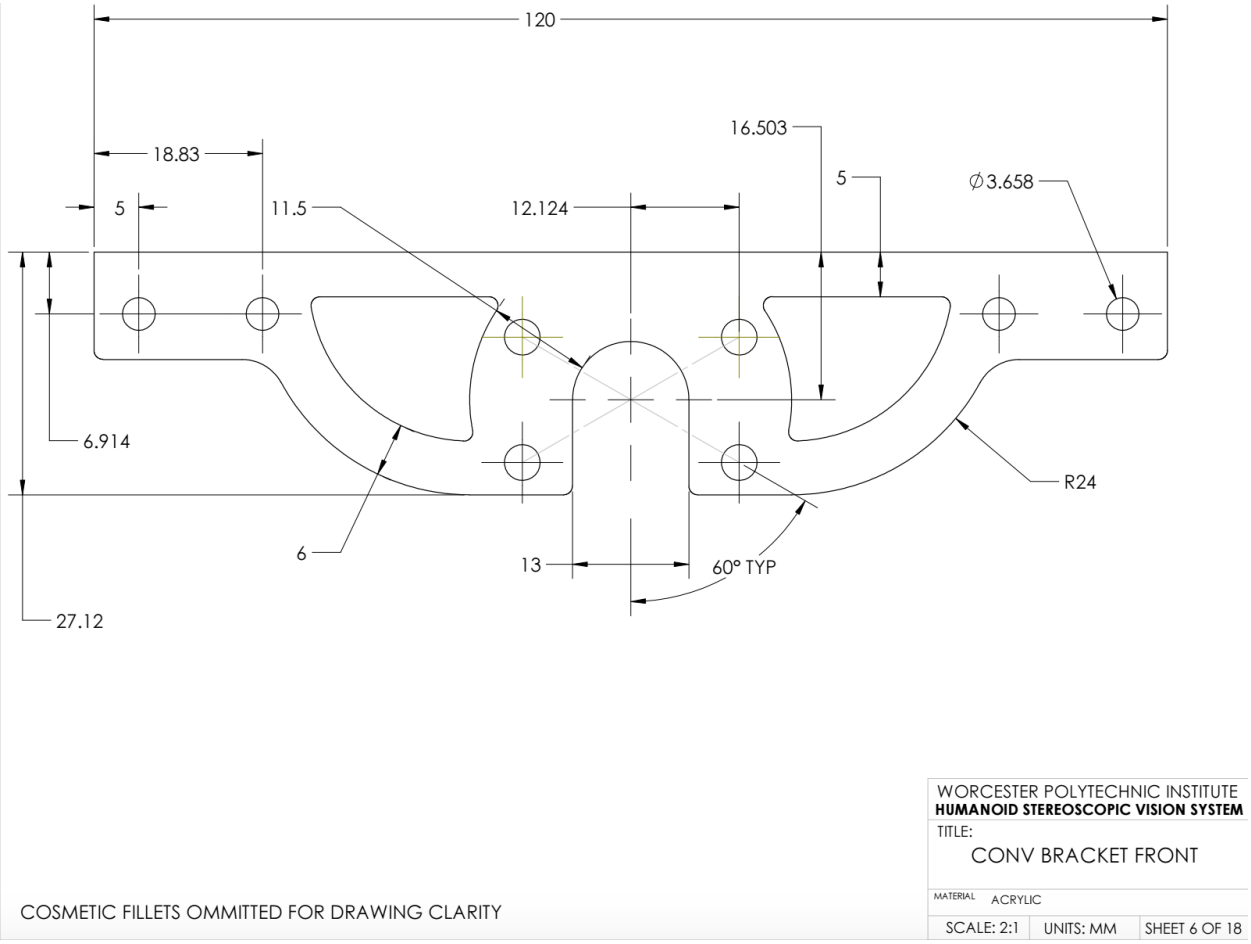

Eye Connector

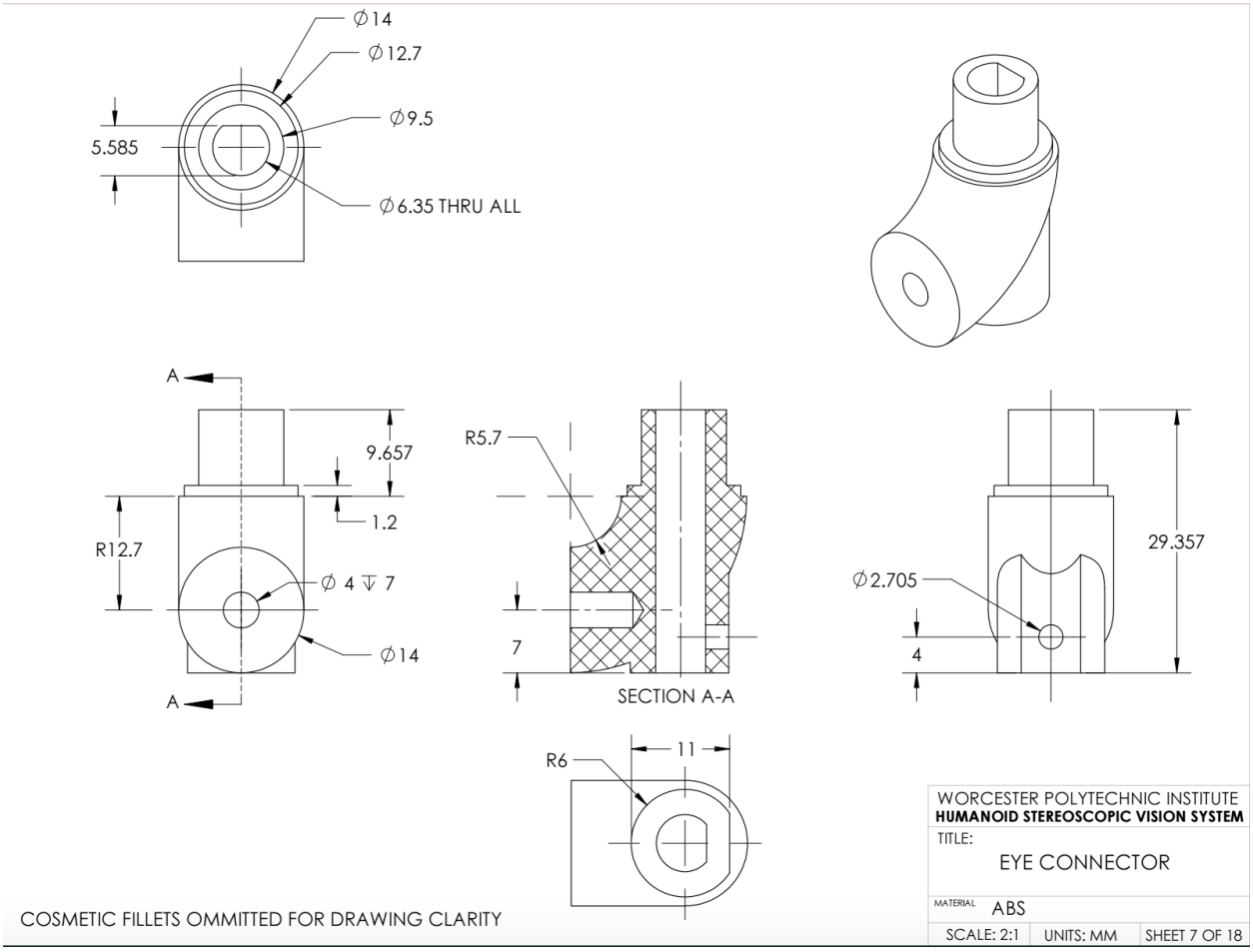

Slide Bearing Housing

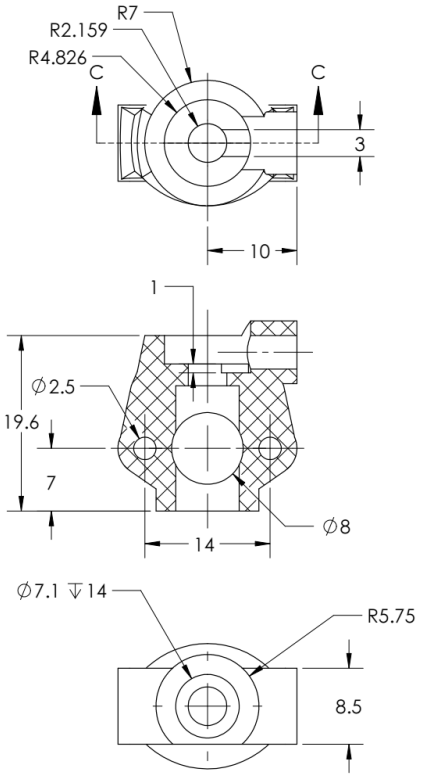

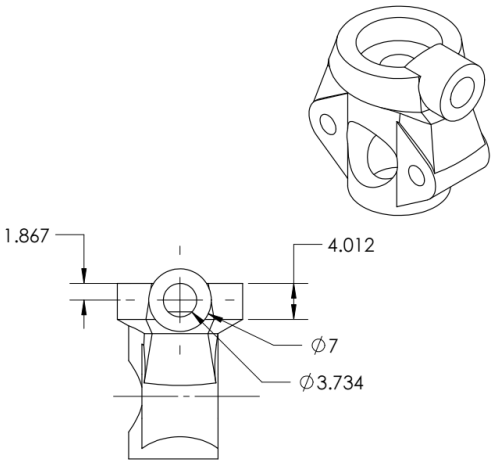

COSMETIC FILLETS OMMITTED FOR DRAWING CLARITY

WORCESTER POLYTECHNIC INSTITUTE **HUMANOID STEREOSCOPIC VISION SYSTEM**		
TITLE: SLIDE BEARING HOUSING		
MATERIAL ABS		
SCALE: 2:1	UNITS: MM	SHEET 8 OF 18

Pan Movement Bracket

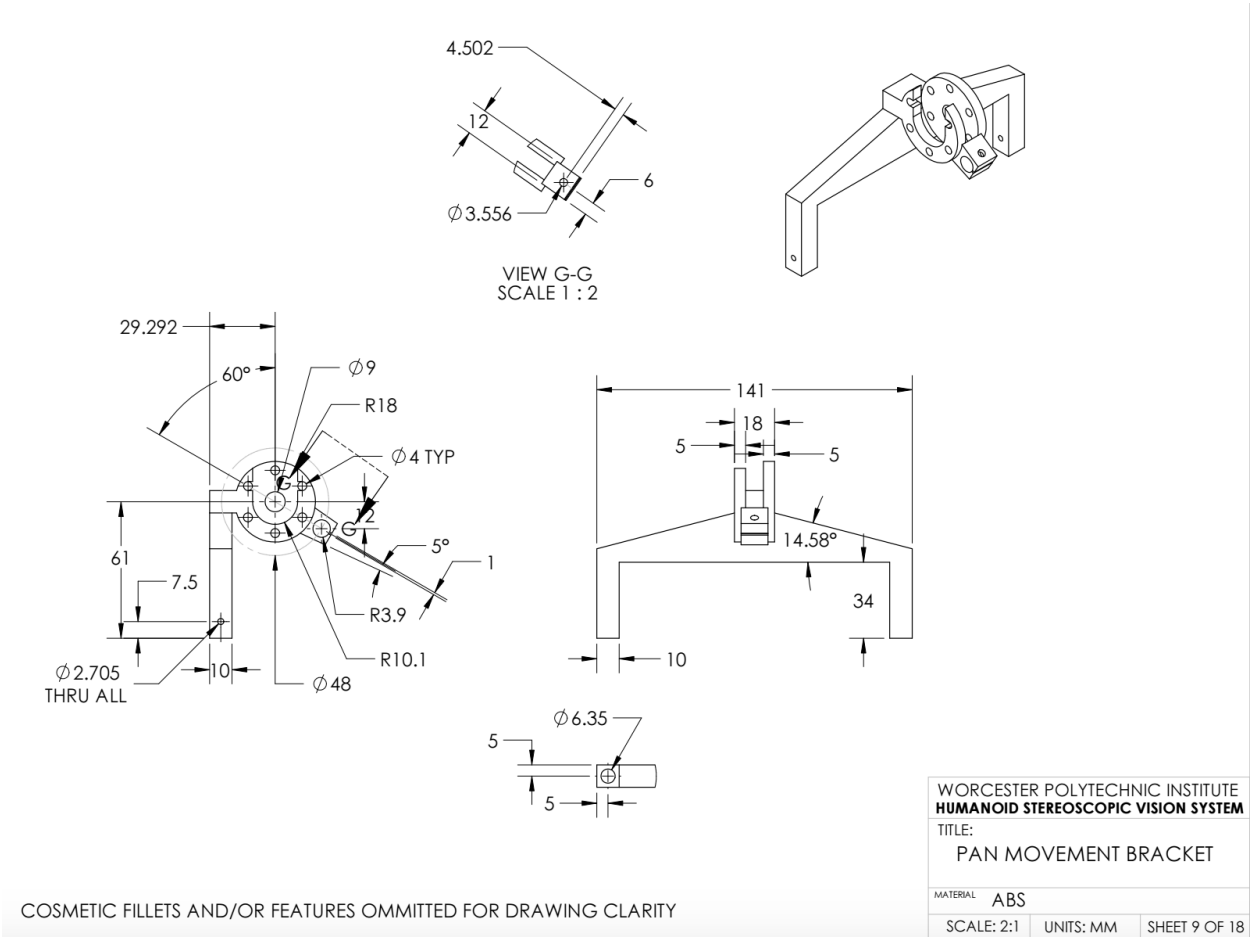

Convergence Rail Bracket

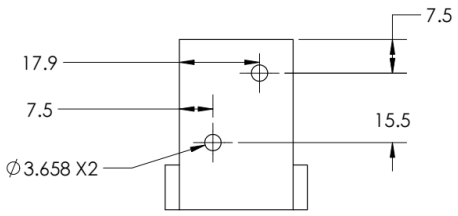

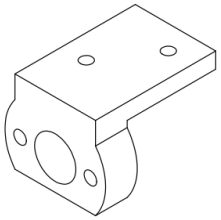

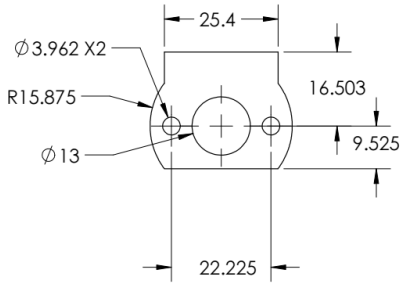

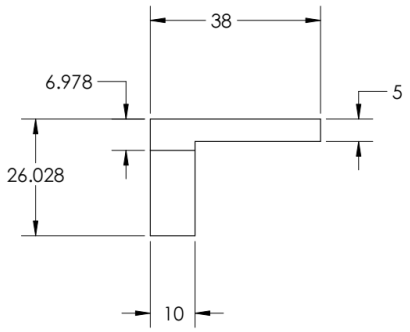

COSMETIC FILLETS AND/OR FEATURES OMMITTED FOR DRAWING CLARITY

WORCESTER POLYTECHNIC INSTITUTE **HUMANOID STEREOSCOPIC VISION SYSTEM**		
TITLE: CONVERGENCE RAIL BRACKET		
MATERIAL ABS		
SCALE: 1:1	UNITS: MM	SHEET 10 OF 18

Eye Bracket L&R

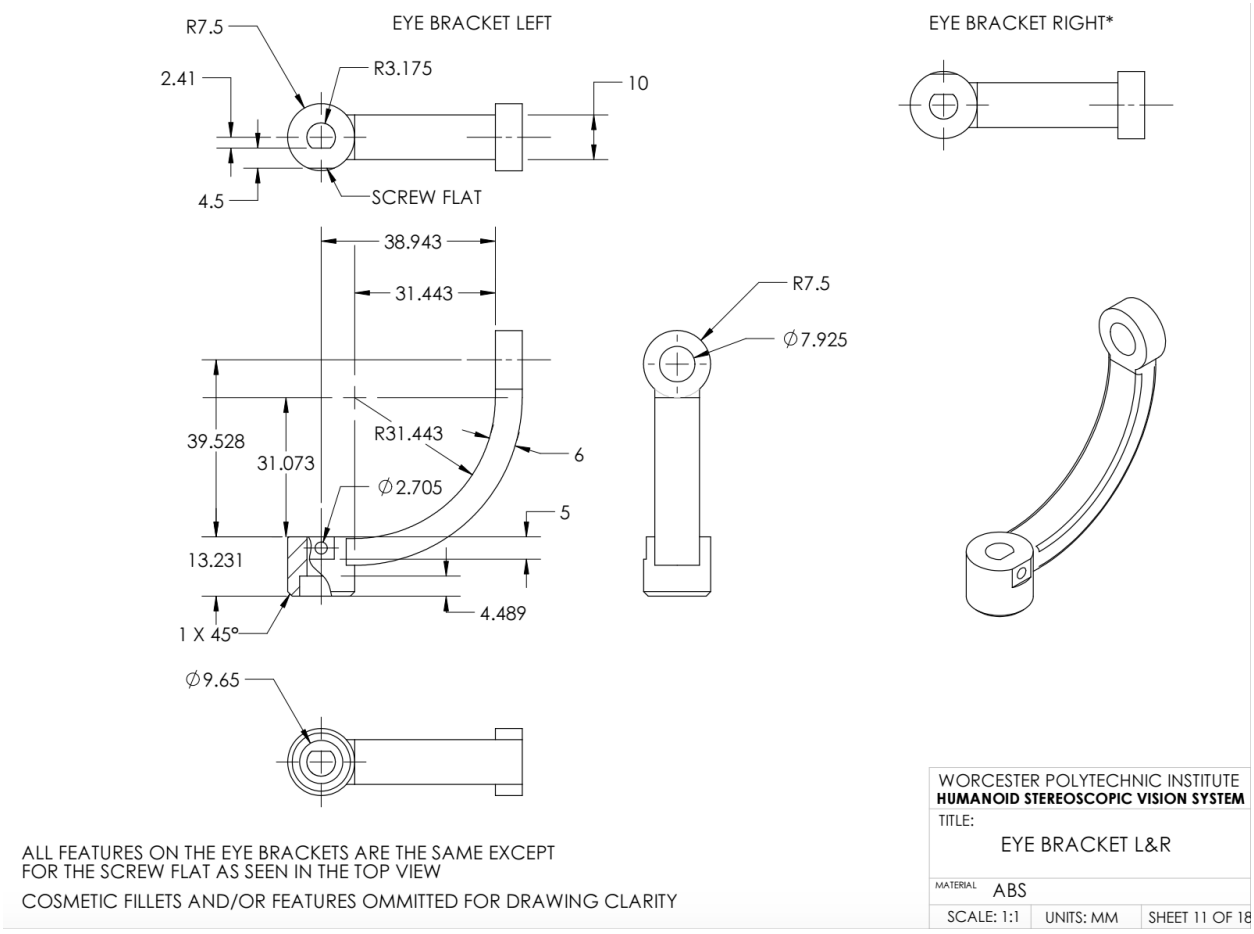

Eye

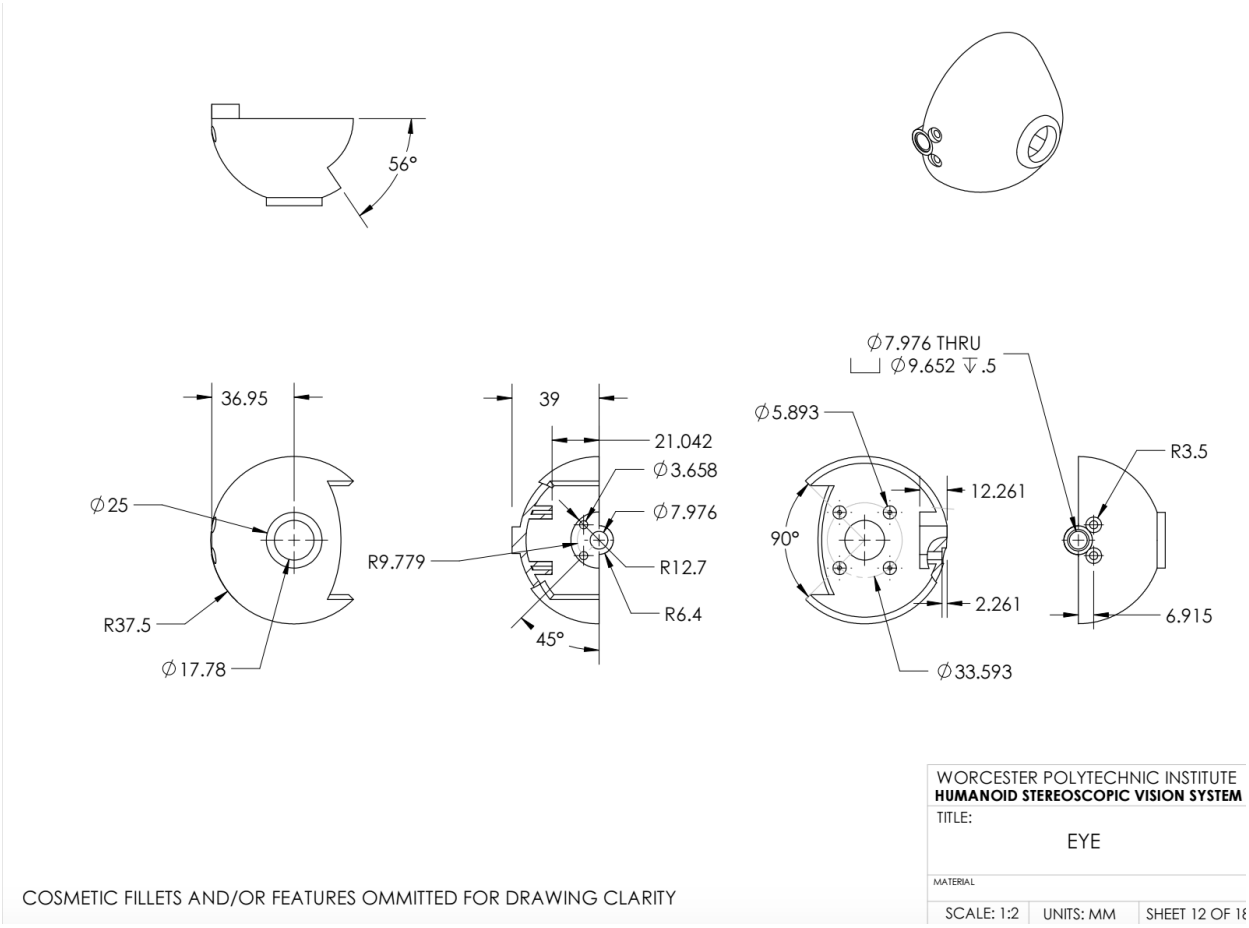
56°
36.95
39
21.042
∅3.658
∅7.976
R12.7
R6.4
45°
R9.779
∅25
R37.5
∅17.78
∅7.976 THRU
⌴ ∅9.652 ↧.5
∅5.893
90°
12.261
2.261
∅33.593
R3.5
6.915
COSMETIC FILLETS AND/OR FEATURES OMMITTED FOR DRAWING CLARITY
WORCESTER POLYTECHNIC INSTITUTE
HUMANOID STEREOSCOPIC VISION SYSTEM
TITLE:
EYE
MATERIAL
SCALE: 1:2
UNITS: MM
SHEET 12 OF 18

Bearing Mounting Block

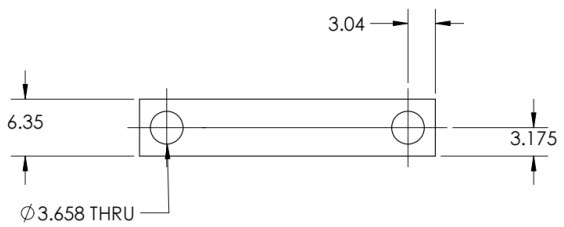

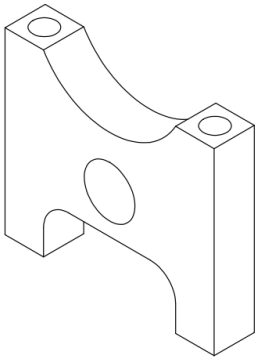

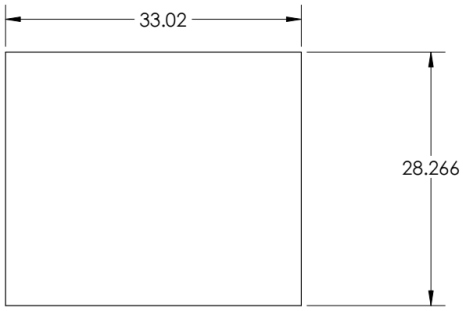

COSMETIC FILLETS AND/OR FEATURES OMMITTED FOR DRAWING CLARITY

WORCESTER POLYTECHNIC INSTITUTE
HUMANOID STEREOSCOPIC VISION SYSTEM
TITLE:
BEARING MOUNTING BLOCK
MATERIAL
SCALE: 2:1 | UNITS: MM | SHEET 13 OF 18

Encoder Mount

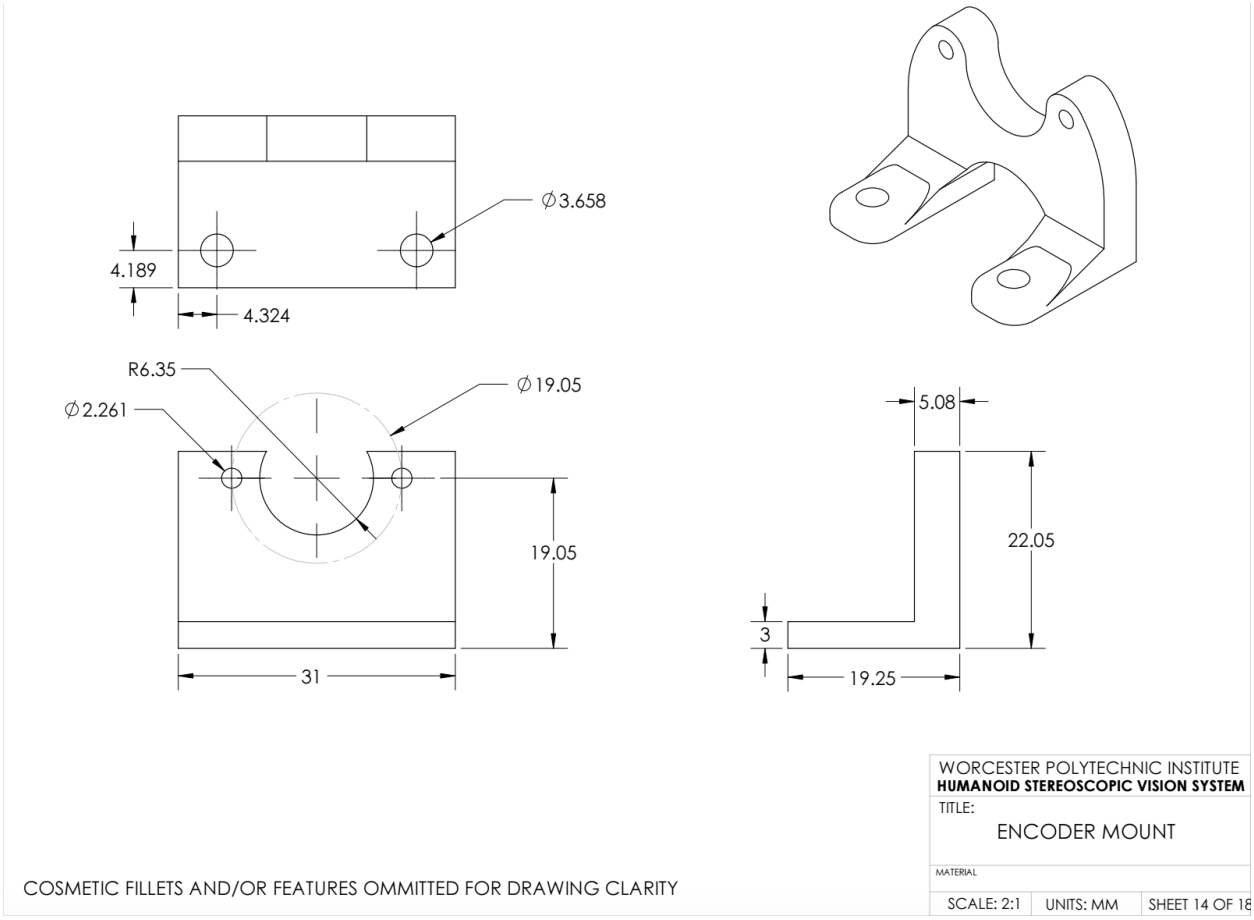

Pan Encoder Mount

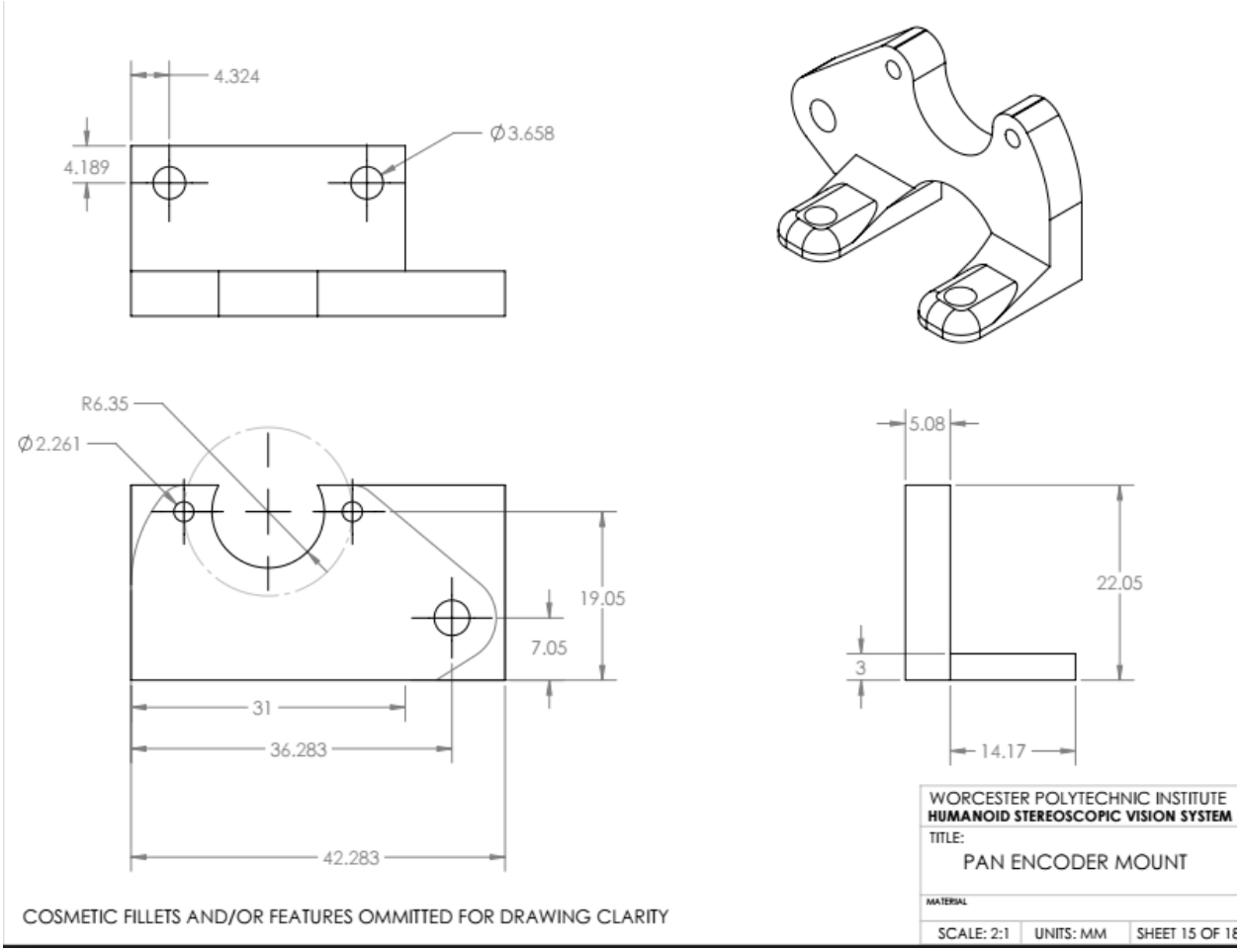

Acrylic Spacer

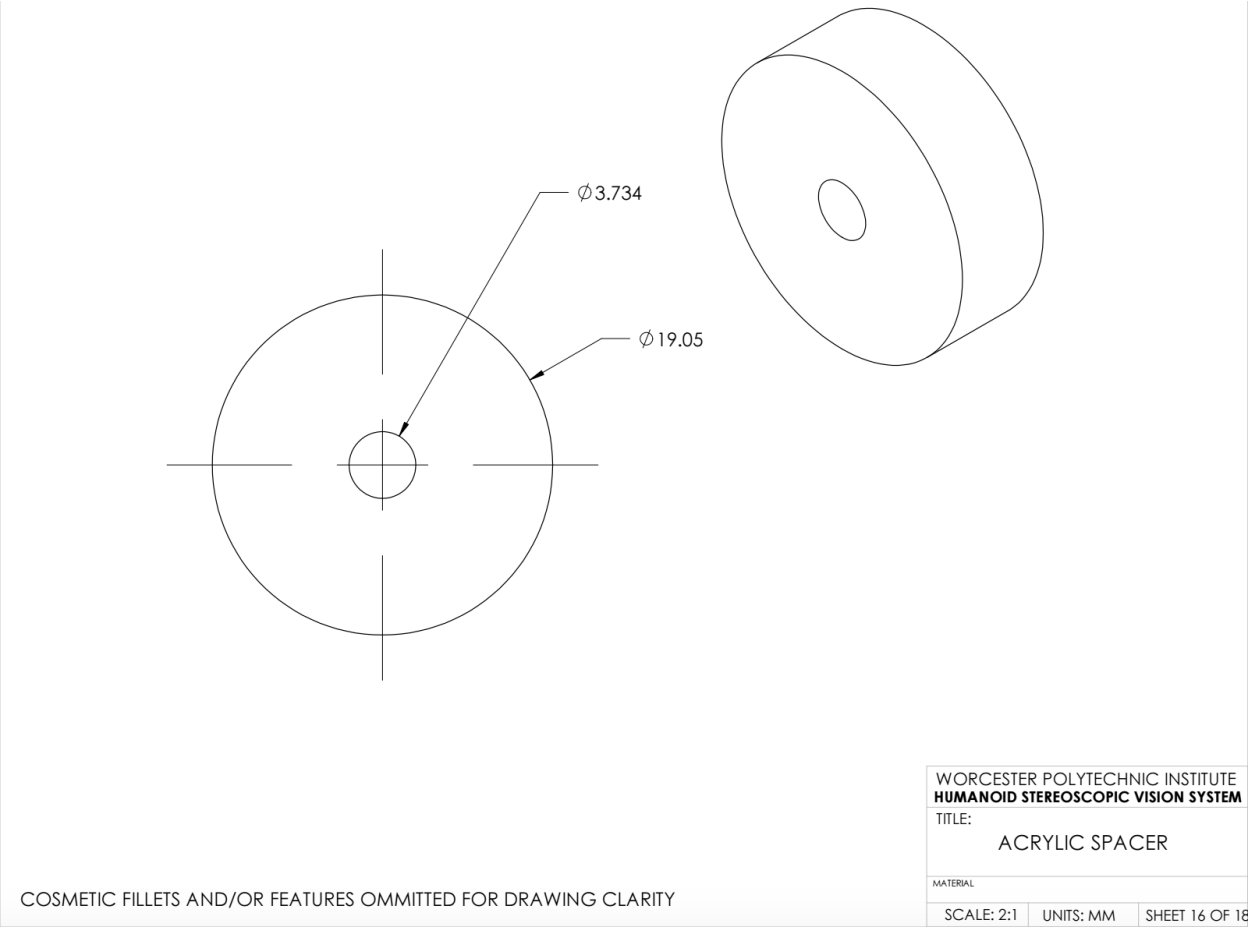

Standoff Support

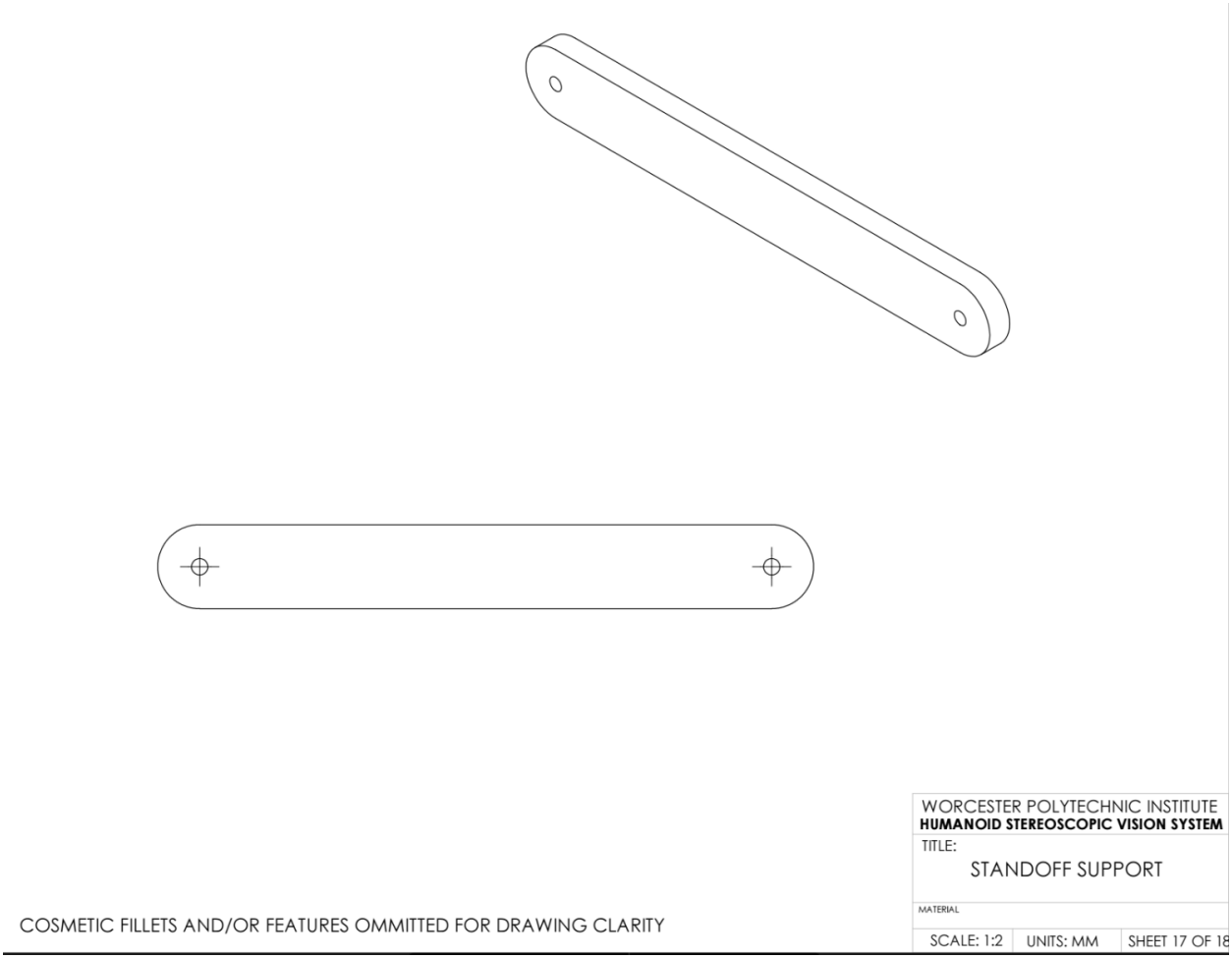

COSMETIC FILLETS AND/OR FEATURES OMMITTED FOR DRAWING CLARITY

WORCESTER POLYTECHNIC INSTITUTE
HUMANOID STEREOSCOPIC VISION SYSTEM
TITLE:
STANDOFF SUPPORT
MATERIAL
SCALE: 1:2 | UNITS: MM | SHEET 17 OF 18

Alignment Shaft Bracket

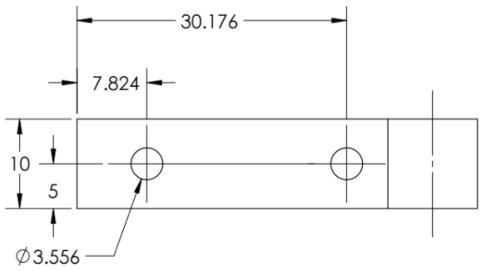

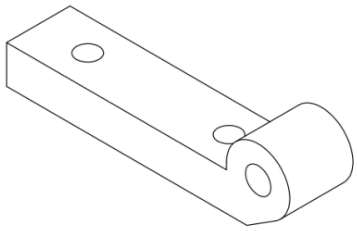

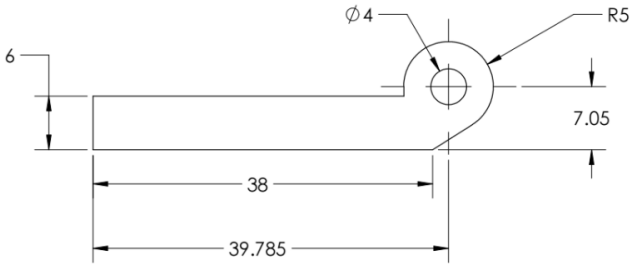

COSMETIC FILLETS AND/OR FEATURES OMMITTED FOR DRAWING CLARITY

WORCESTER POLYTECHNIC INSTITUTE
HUMANOID STEREOSCOPIC VISION SYSTEM
TITLE:
ALIGNMENT SHAFT BRACKET
MATERIAL
SCALE: 2:1 | UNITS: MM | SHEET 18 OF 18